# 3

# About the Nature of the Structural Glass Transition: An Experimental Approach

J. K. Krüger[1,2], P. Alnot[1,3], J. Baller[1,2], R. Bactavatchalou[1,2,3,4], S. Dorosz[1,3], M. Henkel[1,3], M. Kolle[1,4], S. P. Krüger[1,3], U. Müller[1,2,4], M. Philipp[1,2,4], W. Possart[1,5], R. Sanctuary[1,2], Ch. Vergnat[1,4]

[1] Laboratoire Européen de Recherche, Universitaire Sarre-Lorraine-(Luxembourg) jan.krueger@uni.lu
[2] Université du Luxembourg, Laboratoire de Physique des Matériaux, 162a, avenue de la Faïencerie, L-1511 Luxembourg, Luxembourg
[3] Université Henri Poincaré, Nancy 1, Boulevard des Aiguillettes, Nancy, France
[4] Universität des Saarlandes, Experimentalphysik, POB 151150, D-66041 Saarbrücken, Germany
[5] Universität des Saarlandes, Werkstoffwissenschaften, POB 151150, D-66041 Saarbrücken, Germany

**Abstract.** The nature of the glassy state and of the glass transition of structural glasses is still a matter of debate. This debate stems predominantly from the kinetic features of the thermal glass transition. However the glass transition has at least two faces: the kinetic one which becomes apparent in the regime of low relaxation frequencies and a static one observed in static or frequency-clamped linear and non-linear susceptibilities. New results concerning the so-called $\alpha$-relaxation process show that the historical view of an unavoidable cross-over of this relaxation time with the experimental time scale is probably wrong and support instead the existence of an intrinsic glass transition. In order to prove this, three different experimental strategies have been applied: studying the glass transition at extremely long time scales, the investigation of properties which are not sensitive to the kinetics of the glass transition and studying glass transitions which do not depend at all on a forced external time scale.

## 3.1 Introduction

Synthetic glassy materials are known for more than 8000 years. Nevertheless, the question about the nature of the glassy state and of the thermal glass transition (TGT) of structural (or canonical) glasses is still open [1–26]. Usually, synthetic glasses belong to the class of structural (canonical) glasses which behave mechanically as solids, but which have an amorphous, that means a liquid-like, structure. In other words, glasses are hybrids which have similarities as well with solids as with liquids. This hybrid nature also becomes obvious in the course of the transformation from the liquid to the

J.K. Krüger et al.: *About the Nature of the Structural Glass Transition: An Experimental Approach*, Lect. Notes Phys. **716**, 61–159 (2007)
DOI 10.1007/3-540-69684-9_3 

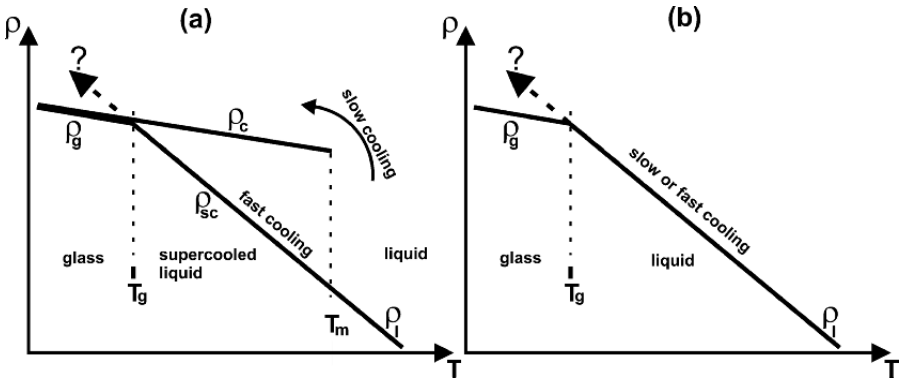


**Fig. 3.1.** Schematic drawing of the effect of slow and fast cooling on the mass density $\rho$ of (**a**) a crystallisable and (**b**) a non-crystallisable liquid. $\rho_l$: mass density of the equilibrium liquid, $\rho_c$: mass density of the crystalline state, $\rho_{sc}$: mass density of the under-cooled liquid, $\rho_g$: mass density of the glassy state

glassy state. On cooling the glass-forming liquid, the transition from the liquid to the glassy state is accompanied by experimental features which may be attributed to phase transitions as well as to under-cooling effects (Figs. 3.1a,b, 3.2).

Under-cooling means that the temperature of the liquid sample can be decreased faster than certain of its physical properties do respond. For instance, crystallization of a liquid may be prevented by fast cooling if the viscosity of the liquid increases much faster than nucleation takes place. As a result a super-cooled liquid is obtained. Figure 3.1a shows schematically this situation for the mass density $\rho$ for slow and fast cooling. Below the melting temperature $T_m$ the liquid becomes super-cooled and is therefore out of equilibrium. The degree of metastability of the super-cooled state depends amongst other parameters on the glass-forming liquid itself and on the temperature deviation $\Delta T = (T_m - T)$. As a matter of fact the mass density curve of the super-cooled state is a direct continuation of the equilibrium liquid state. At still lower temperatures around the so-called thermal glass transition temperature $T_g$ the mass density curve $\rho(T)$ shows a kink-like anomaly (Fig. 3.1a). Depending on the sharpness of this kink the volume expansion coefficient $\alpha_V$ shows a step-like anomaly at $T_g$. Figure 3.1b schematically shows for comparison the temperature behaviour of the mass density of a non-crystallisable liquid (e.g. atactic polymers). The only temperature induced anomaly which remains is the kink-like anomaly of $\rho(T)$ at the glass transition temperature $T_g$. The question marks in Fig. 3.1a,b stress the open question about the origin of this kink: is it purely due to a super-cooling effect (Fig. 3.1b) or to a further super-cooling effect (Fig. 3.1a) or does there exist an intrinsic event which causes this kink-like anomaly of the mass density? Assuming that the density-kink is purely kinetically conditioned ("kinetic hypothesis")

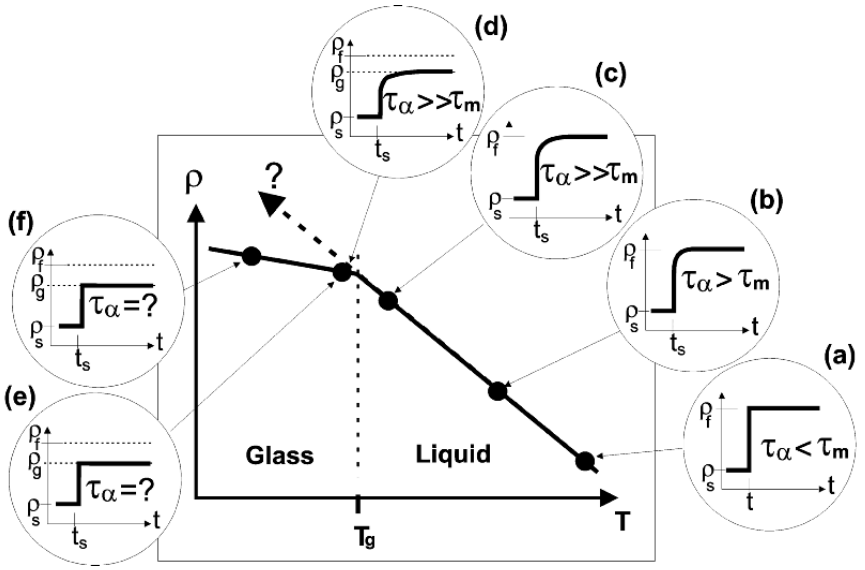


**Fig. 3.2.** Schematic drawing of the evolution of a structural glass transition. Mass density $\rho = \rho(T)$: the graphics (a) to (f) show the temporal evolution of the mass density $\rho$ at fixed temperature $T$

the temperature position of this kink should shift to lower temperatures if the cooling rate is slowed down. Time-domain investigations, as schematically drawn in Fig. 3.2a–d, help to elucidate the validity of the "kinetic hypothesis".

For the thought (time-domain) experiment of Fig. 3.2 we assume that the mass density $\rho$ is measured in a static way by determining at every temperature $T$ the mass and the volume of the sample. At high temperatures, far above the freezing temperature $T_g$, mass-density and volume-changes equilibrate as fast as the temperature of the sample does. After a temperature step $-\Delta T$ the mass density responds almost instantaneously (Fig. 3.2a). As a matter of fact, on approaching the glass transition temperature $T_g$ from above by temperature steps $-\Delta T$, the recovery of the mass density $\rho$ takes more and more time $t$, i.e. $\rho(t)$ is less and less able to follow a temperature step $-\Delta T$ (Fig. 3.2b,c). This is due to the fact that glass-forming liquids exhibit internal degrees of freedom with relaxation times $\tau_\alpha$, which become very large on approaching $T_g$ from above and which even show a certain tendency to diverge in a temperature interval below $T_g$ (Fig. 3.2e–f). The experimental time needed to equilibrate the new temperature after a temperature jump $-\Delta T$ is assumed to be $\tau_m$. If at sufficiently high temperatures $\tau_m \gg \tau_\alpha$ then the mass density $\rho$ is in internal equilibrium. If the recovery time of the mass density $\tau_\alpha$ becomes larger than the experimental time constant of the temperature adjustment $\tau_m$, the mass density $\rho(t)$ shows relaxation behaviour (Fig. 3.2a–d). This relaxation behaviour has been interpreted as the result of cooperative

interaction of the molecules close the glass transition (e.g. [2]) and is called the $\alpha$-relaxation process.

In order to bring the mass density $\rho(T)$ still to equilibrium the experimental time constant $\tau_m$ has to be increased sufficiently in order to realize $\tau_m \gg \tau_\alpha$ or at least $\tau_m > \tau_\alpha$. For the understanding of the thermal glass transition the exciting question arises how the process develops in an equilibrium experiment when decreasing the temperature as slowly as possible (Fig. 3.2a–f). If on cooling, at a certain temperature $T_g$ the $\alpha$-relaxation time $\tau_\alpha$ increases so strongly that $\tau_\alpha$ becomes comparable to $\tau_m$ and even exceeds $\tau_m$ in that case the "bending temperature" $T_g$ is indicative for the fact that the mass density $\rho(T)$ falls out of "equilibrium" (Fig. 3.2a–3.2d–f). In the following this will be denoted as time trap [15]. If on the other hand, the mass density curve shows a kink at $T_g$ although the time trap could be avoided, in that case $T_g$ represents an intrinsic transition temperature (Fig. 3.2a–3.2c,e,f). The $\alpha$-relaxation phenomenon is typical for the glass transition in liquids and will be discussed in Sect. 3.4 of this article as the dynamical aspect of the thermal glass transition.

Thus, as a consequence of the strongly increasing $\alpha$-relaxation times in the vicinity of $T_g$, there exists an inherent risk for every experiment performed to measure non-equilibrium properties close to $T_g$. If the time for temperature equilibration and/or for the equilibration of the measured quantity exceeds the "patience of the experimentalist", non-equilibrium properties are measured. If, as argued in literature ( see any text book on glasses, e.g. [2]), the relaxation time $\tau_\alpha$ of the $\alpha$-relaxation process diverges at a temperature $T_0 \cong (T_g - 40)$ K then the cross-over between $\tau_\alpha$ and the experimental time scale is unavoidable. If the experiment of interest was driven too fast and as a consequence captivated in the "time-trap" a so-called ageing process is possible on a long time scale. This process brings eventually the physical quantity of interest to its equilibrium value. This specific "kinetic" face of the glass transition and the question under which conditions quenched physical properties will age towards their equilibrium values will be discussed in Sect. 3.3. Whether $\tau_\alpha(T)$ really diverges at a temperature $T_0$ is rather questionable.

Section 3.5 deals with the problem whether static or quasi-static properties can be measured in principal around $T_g$, and what they can tell us about the mechanisms behind the TGT. Experimental tools are presented which are at the same time sensitive to large and very small relaxation times and which are therefore sensitive to test the "time-trap" argument. Another experimental approach which has the potential to give some insight into the nature of the thermal glass transition deals with the transition from the dynamically frozen to the solid state. The fact, that this transition is experimentally observable gives a strong hint for the existence of an intrinsic glass or ideal glass transition possibly hidden behind dynamic and kinetic features. Non-linear elastic properties measured at $T_g$ yield a hint to the development of unexpected structural changes at the thermal glass transition. An intrinsic glass transition would be iso-structural and solid in nature and is for fixed external

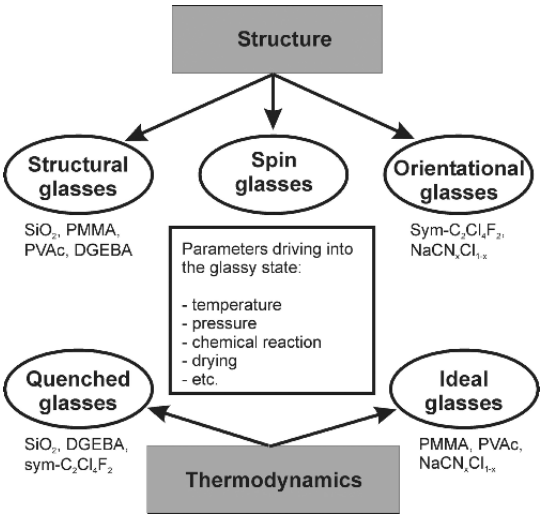


**Fig. 3.3.** Scheme of the most important glass-forming materials as classified by structure and thermodynamics. $SiO_2$ silicon dioxide, PMMA polymethylmethacrylate, PVAc polyvinylacetate, DGEBA diglycidilether of bisphenol A, $C_2Cl_4F_2$ difluorotetrachloroethane, $NaCN_xCl_{1-x}$ sodium cyanide chloride mixed crystal

thermodynamic variables a property of the material. In agreement with daily observations, the static shear modulus is expected to be larger than zero.

An alternative approach to the understanding of the nature of the glass transition is to avoid in principle the time trap by choosing a type of glass transition where no external variables are involved in the transition process. In Sect. 3.6 the scenario of the "chemical glass transition" is proposed as a scientific vehicle to get an alternative view on the glass transition.

In recent years, in addition to structural glasses further classes of materials with inherent freezing features have been discovered. Figure 3.3 gives a schematic drawing about the most important classes of glass forming materials currently discussed in physics.

Structural glasses are glasses like polymethylmethacrylate (PMMA) or silicon dioxide ($SiO_2$) which are completely amorphous but behave mechanically like a solid. Spin glasses are usually crystals where the magnetic spins are randomly oriented but dynamically frozen. Orientational glasses are crystalline materials with frozen orientational disorder. Classifying glasses from the thermodynamic point of view, we distinguish between quenched and ideal glass-formers. Quenched glasses are glassy systems where the disorder of the liquid state is conserved due to fast cooling. The fast cooling prevents the system from crystallization. On the contrary ideal glasses are systems which have no crystalline reference state with lower free energy.

As a matter of fact, the mechanisms which result in spin glass and/or orientational glass transitions are much more evident than those leading to

the glassy state of structural glass formers [27] as there is only one well-known internal degree of freedom provoking the glass transition. For some time it was therefore believed that spin glasses and orientational glasses could be used as rather simple but elucidating model systems for the *thermal glass transition* (TGT) in structural glass formers. However, the results met only in part the expectations [28, 29], but they lead to a better insight into the main ingredients provoking the freezing process, which are: (i) disorder, (ii) frustration and (iii) non-linear molecular interactions [27, 30]. Therefore it makes sense to elucidate the open problems of the thermal glass transition in structural glasses on the background of those occurring in much simpler systems like orientational glass-formers.

Hence prior to the discussion of the nature of glass transitions in structural glasses, three introductory educational examples of orientational glass formers together with some shortcomings will be discussed: mixed crystals of the type $Na(CN)_xCl_{1-x}$, single crystals of sym-$C_2Cl_4F_2$ (difluorotetrachloroethane, DFTCE) and poly-siloxane side-chain liquid crystals.

Cyanide mixed crystals are molecular crystals of the type $M(CN)_xZ_{1-x}$ and $M_xX_{1-x}(CN)$ (where M and X stand for alkali metals and Z for halogenide ions). They are obtained by mixing different pure alkali cyanides or pure alkali cyanides with alkali halogenides. The concentration $x$ very strongly influences the structural phase transition behaviour compared with the pure alkali cyanides. In the following we deal with $Z = Cl$ and $M = Na$. With decreasing temperature pure NaCN undergoes a strong first-order ferroelastic phase transition at $T_c \sim 285\,K$ from cubic to rhomboedric symmetry. Usually, the crystal does not mechanically survive this transition and breaks into pieces. Brillouin spectroscopy (see Sect. 3.2), however, is able to measure in the temperature regime below $T_c$ by focussing the scattering volume into one of the intact domains. Figure 3.4 shows a decrease of the shear elastic stiffness on approaching $T_c$ from higher temperatures followed by a huge jump into the low-temperature phase. Obviously $c_{44}$ is the order parameter susceptibility related to this transition. By decreasing the CN-concentration $x$ the transition temperature $T_c$ from the cubic to the rhomboedric phase can be shifted continuously to lower temperatures.

In the case of $M(CN)_xZ_{1-x}$ crystals the average cubic symmetry observed in the high temperature phase remains unchanged for all temperatures if the concentration $x$ is lower than a critical value $x_c$ [28]. In this concentration range ($x < x_c$) there is no more structural phase transition observed in the temperature dependence of different physical parameters, but the system is believed to undergo an orientational glass transition [27,28,31–36] at a definite temperature characterized by the existence of a minimum value of the shear elastic stiffness $c_{44}(T)$.

Figure 3.5 demonstrates this behaviour for the critical concentration $x_c \sim 0.65$. Compared with pure NaCN (Fig. 3.4) the strong softening of $c_{44} = c_{44}(T)$ is maintained but the first-order character of the $c_{44}$-anomaly is completely lost. The transition temperature largely shifts from $T_c = 287\,K$

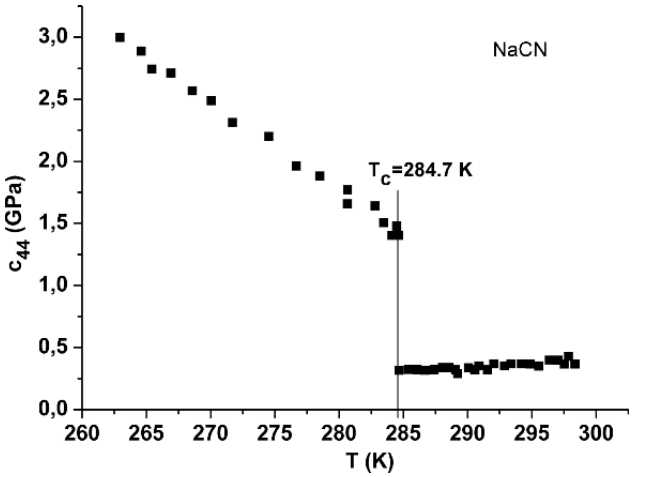


**Fig. 3.4.** Temperature dependence of the elastic shear stiffness $c_{44}$ of NaCN around the phase transition from the cubic ($T > T_c$) to the rhomboedric phase ($T < T_c$)

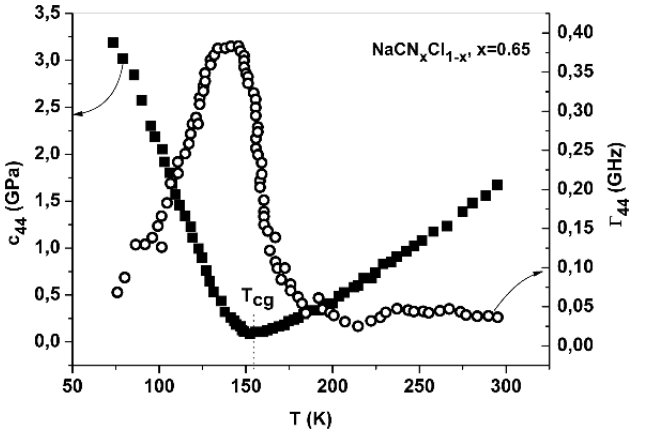


**Fig. 3.5.** Temperature dependence of $c_{44}$ and the related acoustic attenuation $\Gamma_{44}$ of the mixed molecular crystal $NaCN_xCl_{(1-x)}$ with $x = x_c \sim 0.65$

to $T_{cg} = 153\,\mathrm{K}$. The identification of $T_{cg}$ as the glass transition temperature originates from the fact that there is a continuous approach of the first-order phase transition anomaly with increasing Cl-concentration to this minimum of $c_{44} = c_{44}(T)$. In other words this orientational or quadrupolar glass transition emerges from a first order transition due to an increase of positional disorder (CN→Cl) and due to orientational frustration. This interpretation is in clear contradiction to the observations in "quenched structural glasses". In the latter glasses the glass transition temperature $T_g$ is always well below the melting point $T_m$.

A striking feature of Fig. 3.5 is the observation that the $c_{44}$-minimum is accompanied by a maximum of hypersonic loss. This behaviour recalls a dynamic glass transition of structural glass formers rather than that of a static glass transition. That objection against the current interpretation [32] is supported by the fact that the temperature where this minimum takes place is frequency dependent, that also indicates its dynamical character.

The nature of this glass transition seems to be spin glass-like [27,30,37,38]. It is well known that pure NaCl does not show any glass-like behaviour. In so far it is interesting to know to which extent the glassy behaviour imposed by the disorder of the CN-dipoles is still active. According to Fig. 3.6 the minimum within the $c_{44} = c_{44}(T)$ curve is still present at the rather low CN-concentration of $x = 0.2$ which indicates that some relaxation processes are still present at hypersonic frequencies below $T = 150\,\mathrm{K}$ [37].

This result raises the question, whether the earlier interpretation of the orientational glass transition in alkali halides was not wrong and whether eventually a quasi-static glass transition does exist at even lower temperatures. If this view of this kind of "spin glass transition" was correct in that case, the similarities to the TGT of structural glass formers would be much more intimate.

The theoretical description of $c_{44}(T, x)$ has been subject of numerous papers [e.g.] [27, 31, 39, 40]. A consistent application of theoretical models to the experimental data has not given a satisfactory description of the behaviour, as a function of temperature and concentration, in the range $x < x_c$. The consistency of the theory requires that the concentration- and temperature-dependent properties of $c_{44}$ should be described with a unique

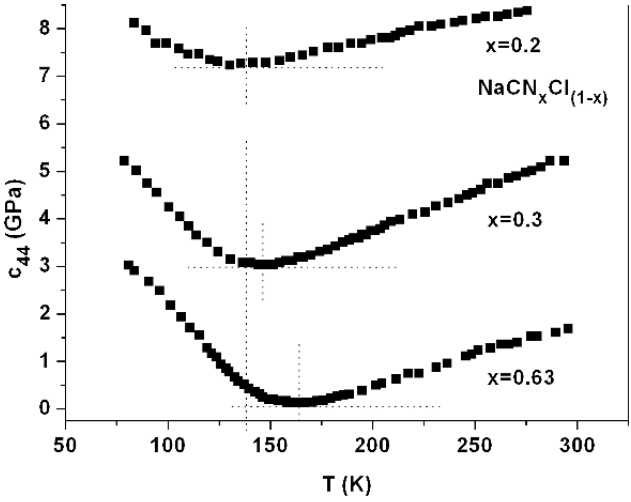


**Fig. 3.6.** Temperature dependence of the elastic shear stiffness $c_{44}$ of $NaCN_xCl_{1-x}$ as a function of the concentration $x$ of CN-dipoles

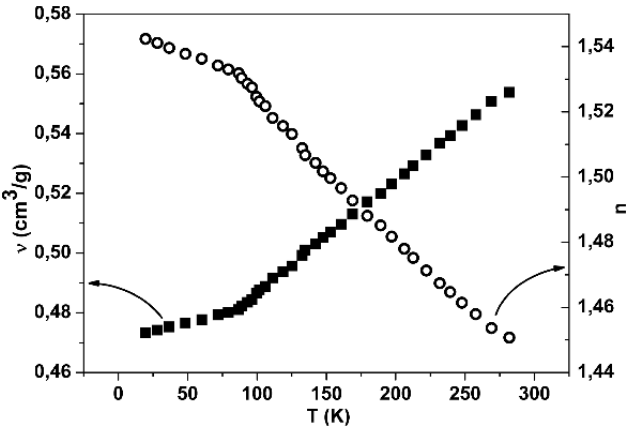


**Fig. 3.7.** Temperature dependence of the specific volume $v$ and the refractive index $n$ of DFTCE

set of parameters independent of concentration and temperature in both concentration ranges $x > x_c$ and $x < x_c$.

An orientational glass transition (spin glass transition) which is much more similar to the one in structural glass formers was found for symmetric difluorotetrachloroethane ($C_2Cl_4F_2$ = DFTCE) [41,42]. This material is at ambient temperature a plastic crystal with cubic symmetry (bcc) [29], which, even in the polycrystalline state, doesn't show optically any grain boundaries. Moreover the DFTCE molecules rotate and undergo permanently trans-gauche transitions according to Boltzmann statistics. Both dynamics interfere but are compatible with the bcc-symmetry. With decreasing temperature the molecular rotations slow down and freeze below the actual structural phase transition ($T_c = 130\,\mathrm{K}$) [42]. The trans-gauche transitions are still present and lead to some molecular disorder and frustration. At the glass transition temperature slightly below 90 K (Fig. 3.7) the super-cooled cubic DFTCE transforms from the dynamically disordered cubic state to the statically disordered cubic state. Therefore, the frozen disorder is predominantly an intramolecular disorder.

DFTCE single crystals have been grown on ultrathin mono-crystalline films of polytetrafluoroethylene (PTFE) [43, 44]. Figure 3.8 shows the elastic indicatrix of a thin DFTCE crystal plate with a thickness of 50 µm as measured with Brillouin spectroscopy (see next section) at ambient temperature. The crystal orientation is believed to be such that the large faces of the crystal plate correspond to cubic faces.

Figure 3.7 shows the temperature dependence of the specific volume and of the refractive index of this DFTCE sample. Both curves show the typical kink-like behaviour usually observed at the TGT of structural glass formers. The specific volume $v$ was measured by x-ray analysis of the cubic lattice. The refractive index $n$ was calculated using the Lorentz-Lorenz relation [45, 46] (see Eq. (3.2)) and calibrating the specific refractivity by $n$-measurements on

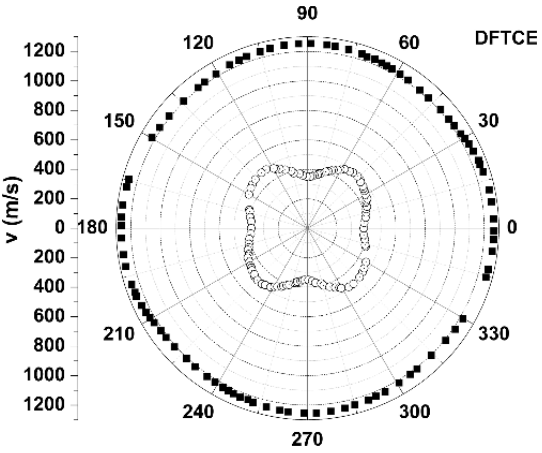


**Fig. 3.8.** Elastic indicatrix of an arbitrary crystal cut of cubic DFTCE. The *filled squares* represent the quasi-longitudinally polarized acoustic phonon branch and the *open circles* represent the quasi transversely polarized acoustic phonon branch

DFTCE at ambient temperature using an Abbé refractometer. The specific refractivity was taken as temperature independent. It should be stressed that the specific volume measurements based on x-ray analysis are much more reliable than dilatometer and pyknometer measurements as used for polymers. Of course the refractive index data depend on the chosen model of Lorenz-Lorentz. The kink-like behaviour of the specific volume curve around the TGT signifies a step-like behaviour of the thermal expansion coefficient at $T_g$ whereby the specific volume is lower in the frozen than in the dynamically disordered state of the sym-$C_2Cl_4F_2$ molecules. For structural glass formers usually $T_g$ is interpreted as the temperature at which the free volume becomes minimal [11,12]. Below $T_g$ the glass forming material behaves solid-like. Since DFTCE is already a solid above $T_g$, the latter interpretation of the step-like change of the thermal expansion coefficient cannot be used. In other words, in a dense single crystal of cubic symmetry the classical concept of free volume becomes meaningless. For single crystals the concept of anharmonicity of the elastic interaction potential rather than the concept of free volume has to be taken into account. Applying this argument to the thermal glass transition of DFTCE it has to be concluded that the intermolecular interaction potential changes discontinuously at its TGT (s. a. below).

Using Brillouin spectroscopy (see Sect. 3.2) we have also studied the temperature dependence of the longitudinal hypersound velocity. It turns out (Fig. 3.9) that the hypersonic velocity also behaves kink-like at the glass transition temperature $T_g \sim 87\,\mathrm{K}$. Thus, at hypersonic frequencies the sound velocity is frequency-clamped near $T_g$ and behaves qualitatively like the density and the refractive index. In contrast to the orientational glass transition in alkali halide mixed systems any elastic softening or elastic discontinuity

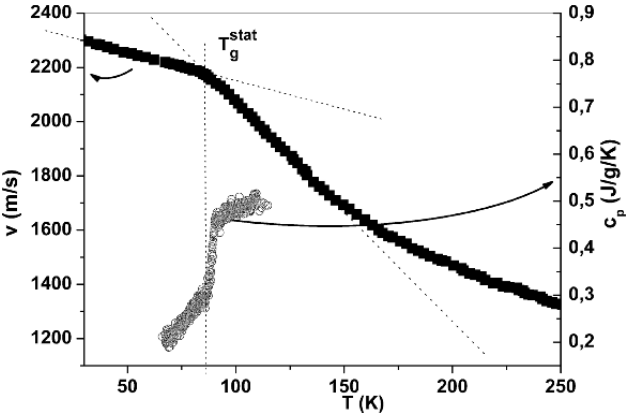


**Fig. 3.9.** Temperature dependence of the longitudinal sound velocity $v$ and of the specific heat capacity $c_p$ of DFTCE

is absent. Moreover, there is no pronounced acoustic attenuation in the vicinity of the TGT. Therefore the phenomenological properties of DFTCE at its thermal glass transition are much more similar to those of structural glass-formers than to those of orientational glasses as discussed above for $M(CN)_xZ_{1-x}$.

This point of view becomes strengthened by the temperature dependence of the specific heat capacity of DFTCE at $T_g$ (Fig. 3.9). The specific heat capacity grows step-like with $T$ at the TGT as it is characteristic for structural glass-formers. It has to be stressed that the specific heat capacity anomaly does not show the typical "Landau-behaviour" [47] usually observed at phase transitions of second order. Hence we conclude that the phenomenological properties of cubic DFTCE behave at about 87 K exactly in the same way as it is observed for structural glass formers at their TGT.

As already mentioned above, the kink-like anomaly observed for the specific volume and the sound velocity at $T_g$ of DFTCE suggests a sudden change of the elastic interaction potential. For cubic crystals such changes can be probed by the so-called mode-Grüneisen parameters $\gamma$ (s. a. Sect. 3.6) introduced by Mie and Grüneisen [48–51]. These parameters depict the relative change of the acoustic phonon frequency of a given acoustic phonon mode with the relative change of the density of the cubic crystal.

$$\gamma(\boldsymbol{p},\boldsymbol{q}) = \frac{\rho}{\omega(\boldsymbol{p},\boldsymbol{q})}\frac{\partial\omega(\boldsymbol{p},\boldsymbol{q})}{\partial\rho} \tag{3.1}$$

where $\omega = 2\pi f$ is the phonon frequency, $\boldsymbol{p}$ is the polarisation of the phonon, $\boldsymbol{q}$ is the phonon wave vector and $\rho$ is the mass density. It is worth noting that Brillouin spectroscopy meets exactly the measuring conditions for mode-Grüneisen parameters provided the specific volume of the crystal of interest is known: how do the phonon mode frequencies change if the crystal expands or shrinks? The origin of the expansion or shrinkage is not defined in Eq. (3.1),

but one can think of pressure or temperature or any other parameter which can make a crystal expand or shrink. It is obvious that a kink in the sound velocity (or sound frequency) curve does not necessarily imply a discontinuity in the mode-Grüneisen parameters. At least in principle, the kink in the specific volume curve could compensate the effect in the acoustic phonon frequency (sound velocity).

For cubic DFTCE a very comfortable situation exists since precise acoustic phonon frequencies as well as precise specific volume data are available. Consequently, the longitudinal mode-Grüneisen parameter can be determined unambiguously. Figure 3.10 shows for DFTCE the longitudinal acoustic phonon frequency $f_L$ as measured by Brillouin spectroscopy and the longitudinal mode-Grüneisen parameter $\gamma_L$. The mode-Grüneisen parameter shows a strong discontinuity at the thermal glass transition. Slightly below $T_g$ the parameter $\gamma_L$ is smaller than just above $T_g$. $\gamma_L \sim 4$ is a reasonable value for a frozen plastic crystal [52]. This discontinuity of $\gamma_L$ at $T_g$ signifies an abrupt change of the elastic interaction potential at the glass transition of cubic DFTCE (see Sect. 3.6). Such a discontinuous change of the elastic interaction potential in a crystal strongly suggests the existence of a phase transition. Taking into account that DFTCE remains cubic in average, this phase transition should be isostructural in nature. It should be stressed again that the kink-like behaviour of the longitudinal acoustic phonon frequency and of the specific volume data has nothing to do with a simple loss of free volume as it is found for liquids and structural glass formers. It is obvious, that the role of free volume will play a crucial role in the interpretation of the TGT of structural glass formers.

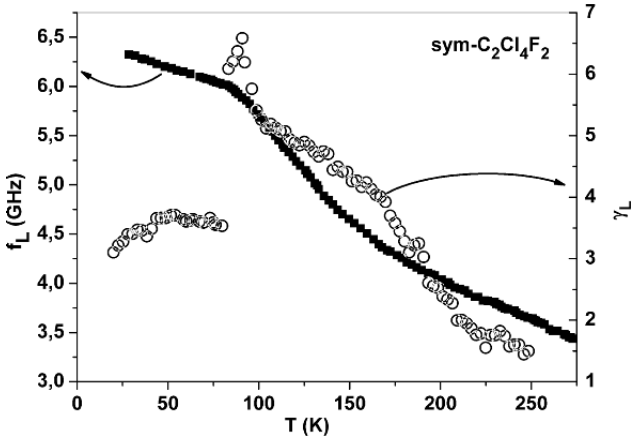


**Fig. 3.10.** Temperature dependence of the longitudinal sound frequency $f_L$ and the longitudinal mode-Grüneisen parameter $\gamma_L$ around the thermal glass transition of DFTCE

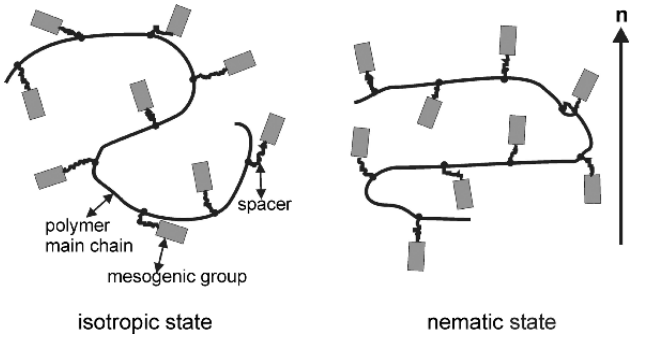


**Fig. 3.11.** Schematic drawing of a polymer side-chain liquid crystal in its isotropic and its nematic state

Whereas the main feature of crystals is their translational order, the main feature of classical liquid crystals like 4-methoxybenzylidene-4'-butylaniline (MBBA) is their orientational order. Similar to crystals, for liquid crystals there exists a hierarchy of order which ranges from the nematic state to the different smectic states [53–56]. Classical liquid crystals are difficult to vitrify. The situation is different for polymer side-chain liquid crystals (PLC) [56–58]. Figure 3.11 shows schematically the isotropic and the nematic structure of PLC's. The polymer backbone is even in the nematic state distributed at random (random coil) provided the spacer molecules, usually n-alkane chains, are sufficiently long. In the so-called isotropic state the mesogenic groups also show random orientational order. In the nematic state an orientational order of the mesogenic groups forms along the director axis **n**. The transition from the isotropic to the nematic state is usually of weak first-order. This holds true e.g. for the refractive index. The material remains "liquid" in the isotropic as well as in the nematic state. Because of the continuously broken orientational symmetry the director can point in any direction of space [59]. Therefore liquid crystals are usually in a polydomain state. For our measurements we have homogeneously oriented the PLC on an ultrathin film of monocrystalline PTFE.

Figure 3.13 shows the sound velocity indicatrix of a poly-siloxane side-chain liquid crystal (Fig. 3.12) measured at ambient temperature which means in the nematic state. It is worth noting, that the nematic state has fibre-symmetry. In contrast to the elastic behaviour of classical nematic liquids,

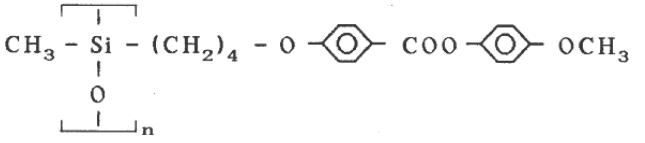


**Fig. 3.12.** Structural formula of poly-siloxane

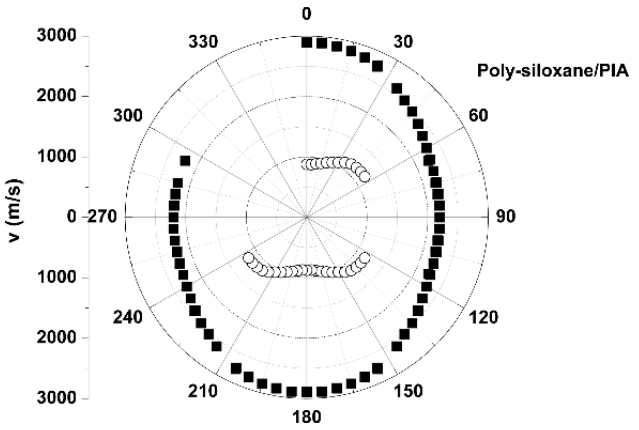


**Fig. 3.13.** Sound velocity $v$ indicatrix (longitudinal: solid squares, transverse: open circles) of a poly-siloxane polymer side-chain liquid crystal measured within the nematic state. 0 degree indicates the direction of the director **n**

PLC's show a pronounced elastic anisotropy. The longitudiual sound velocity is maximal along the direction of the director **n** which indicates that in PLC's there exists a coupling between the nematic order parameter and the elastic deformation. This coupling is obviously provided by the randomly oriented polymer main chain when a solid-like behaviour, indicated by the existence of an acoustic shear mode, sets in (Fig. 3.13).

Figure 3.14 shows the temperature dependence of the sound velocities of the main acoustic modes propagating in the (3, 1)-plane. The 3-axis was chosen to be directed along the director **n** and the 1-axis is orthogonal to the 3-axis. As expected, within the high temperature phase, i.e. the isotropic phase, there is only the longitudinal acoustic mode. At the isotropic $\rightarrow$ nematic transition temperature $T_{ni}$ the longitudinal phonon splits up into two modes displaying the change of symmetry. The acoustic shear mode is still not detectable. The reasons for that behaviour are the liquid nature of the material and its low viscosity at $T_{ni}$. So the shear mode is believed to be overdamped (no acoustic shear mode propagation).

The sound velocity curve $v_{3L}$ shows an inflection point at about 325 K. At this inflection point a hypersonic loss maximum is absent. Therefore the inflection point cannot be interpreted in terms of a dynamical glass transition. In consequence the increase in slope below the inflection point needs an alternative explanation. Between $T_{ni}$ and the inflection point the splitting of the longitudinal modes is probably dominated by the temperature evolution of the nematic order parameter (degree of alignment of the mesogenic side-groups along the director). Since the order parameter has to level with decreasing temperature, the ongoing freezing of the molecular ensemble starts to dominate the acoustic behaviour below the inflection point. The increasing elastic hardening of the polymer matrix emerges in the appearance of the

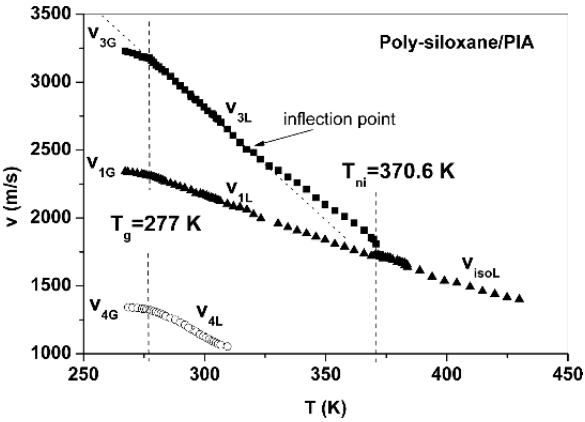


**Fig. 3.14.** Sound velocities $v$ of the principle sound modes of poly-siloxane side-chain liquid crystals as a function of temperature

intrinsic stiffness of the oriented mesogenic side groups. This interpretation is based on the idea that the mechanical behaviour of the two component system (mesogenic groups and polymer matrix) can be approximated by the Reuss-model [57]. This view is supported by the appearance of the acoustic shear mode $v_{4L}$.

Thus Fig. 3.14 clearly shows the influence of anisotropy of the isotropic polymer main chain matrix on the hypersonic velocities. The dynamical freezing process influences predominantly the longitudinal acoustic mode propagating along the direction of the order parameter rather than orthogonal to this direction. That means, that similar to the freezing behaviour of the quadrupolar glass $NaCN_xCl_{(1-x)}$ and in contrast to the behaviour of DFTCE there is an intimate coupling between the order parameter of the nematic state and the dynamic mechanical properties of the matrix on approaching the thermal glass transition.

The common kink at $T_g = 277\,\mathrm{K}$ in all three acoustic modes indicates the static glass transition. Below $T_g = 277\,\mathrm{K}$ the poly-siloxane becomes an orientationally ordered solid. The elastic properties have to be described with an elastic tensor of full fibre symmetry now. Within the glassy state the sound velocities change only moderately with temperature. As in the case of DFTCE and in contrast to the transition behaviour of $NaCN_xCl_{1-x}$ the glass transition in PLC's is well below the structural phase transition. It is worth noting that the hypersonic velocities behave again kink-like at the static glass transition. Since the kinetic view of the glass transition does not know an intrinsic static transition temperature the $v_{3L}$ branch of the liquid phase could be extrapolated to much lower temperatures if infinitely slow cooling is assumed. Because of the strong slope of $v_{3L}$ this would lead to an unreasonably high elastic stiffness $c_{33}$. Therefore the appearance of the TGT is expected in order to reduce the strong slope of the acoustic mode $v_{3L}$. This glass transition is

again accompanied by a step-like behaviour of the mode-Grüneisen parameters. The argument for that statement will become clear in Sect. 3.6, but bases on the fact that the change in slope for both longitudinal acoustic modes is different, whereas the one for mass density is the same for both modes.

In the following we shall definitively leave the ordered state and concentrate on purely amorphous, i.e. structural, glass formers but we shall use the concepts introduced above. In order to understand the nature of canonical glasses and of the TGT we shall concentrate our interest on structural glasses of the "quenched" and the "ideal type".

*Quenched glasses* are formed by freezing supercooled liquids. Thus quenched glasses usually exhibit a crystalline reference state and suffer the risk of recrystallization. In this respect this kind of glasses might be bad candidates for investigations of the relaxation behaviour in the long time limit at the TGT as the glassy state is metastable. However, the usefulness of quenched glasses for the investigation of the TGT depends on the rate of recrystallization.

In order to be sure that only glass transition properties are probed at the TGT *ideal glass formers* should be chosen as model substances. Ideal glasses are characterized by the fact that they do not exhibit a crystalline or any other reference state which is more stable than the liquid phase. Therefore these materials transform necessarily from the stable liquid state into the glassy state, which stability is the matter of debate.

Figure 3.15 shows for atactic polymer chains in a schematic way the frustration mechanism preventing these systems from crystallization. Allowing the monomers of type A and B to polymerize in an atactic, i.e. statistically disordered, manner, it is obvious that these macromolecules can hardly form a crystal with translational symmetry.

With increasing molecular chain length due to the chemical reaction, the molecular dynamics will slow down and may even result in a glassy state at

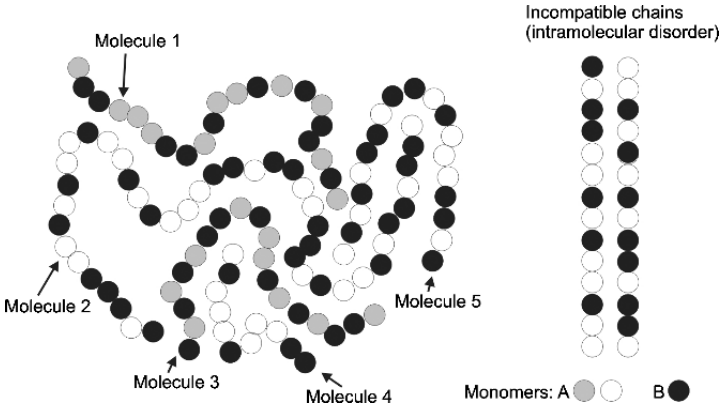


**Fig. 3.15.** Schematic drawing of an ideal glass-former based on the concept of atactic polymers

a given temperature (chemical glass transition see Sect. 3.6). The same effect can be observed for a molecular system of given chain length by decreasing the temperature of this system. In both cases the molecular translation diffusion, a basic feature of a liquid, will be hindered. Whereas there exists no debate on chemical freezing, thermal freezing is usually interpreted as the competition of the intrinsic time scale ($\alpha$-relaxation process) with the patience of the experimentalist [21,60]. This means that the experimentalist does not wait long enough after a temperature perturbation for the relaxed equilibrium value of the measured susceptibility to be reached. This cross-over problem, sometimes called "time trap" [49, 50], is complicated by the fact that the $\alpha$-relaxation time does not behave Arrhenius-like but increases stronger than exponential with decreasing temperature. It even seems that the $\alpha$-relaxation time diverges at a finite temperature $T_0$, called the *Vogel-Fulcher-Tammann* (VFT) temperature [61, 62]. Equation (3.2) displays the phenomenological relation between temperature and the related $\alpha$-relaxation time $\tau_\alpha$

$$\tau_\alpha = \omega_\alpha^{-1} = \tau_{\alpha 0} \cdot \exp\left[\Delta G / \left(R\left(T - T_o\right)\right)\right] \tag{3.2}$$

$\omega_\alpha$ is the relaxation frequency of the $\alpha$-relaxation process, $\tau_{\alpha 0}^{-1}$ is the so-called attempt frequency. $\Delta G$ is the free activation enthalpy and $R$ is the general gas constant.

However, this relation has never been verified experimentally close to the VFT-temperature $T_0$. Keeping in mind that $T_0$ indicates the existence of an intrinsic glass transition at which all relevant relaxations are frozen, it is clear that the above-mentioned cross-over of the $\alpha$-relaxation with any experimental time scale cannot be avoided. This is a strong argument of the kinetic view of the TGT. However this view is based on the divergence of the $\alpha$-relaxation time which has never been proven experimentally.

The experimentally found thermal glass transition temperature is usually about 30–40 K above $T_0$. At such a distance from the temperature $T_0$ where the time constant diverges it should be at least in principle possible to verify to which extent the operative glass transition temperature can be shifted or whether there is a definite low-temperature boundary for this transition [15].

Thus the main questions concerning the understanding of the TGT are whether there exists, at sufficiently slow cooling, an underlying phase transition [15] to an ideal glassy state, or whether the TGT simply signifies the cross-over of the $\alpha$-process with typical time constraints of the experimental technique (including the patience of the scientist) [15].

If the TGT is a purely kinetic effect, there will be only limited interest in this event. If on the other hand there is an underlying phase transition, in that case the question will arise about the nature of the glassy state of matter. In the latter case it will be necessary to introduce in addition to the three classical states of matter (gaseous, fluid and crystalline solid state) a forth state of matter: the structural glassy state. The importance of the problem makes it necessary not only to present and discuss new results but also to

reconsider some older data which are often used as witnesses for the kinetic view of the TGT.

The $\alpha$-process discussed here should not be confused with the high temperature $\alpha$-process discussed in mode-coupling theories [3]. Mode-coupling theory predicts the possibility of an ideal glass transition at temperatures typically 30–40 K above the TGT. This glass transition is believed to be prevented due to so-called hopping processes which finally die out at the TGT.

## 3.2 The Method of Brillouin Spectroscopy

For the present work *Brillouin spectroscopy* (BS) is the central experimental technique. Although this technique is well-established [63–65], its power is not sufficiently known. Moreover, in recent years BS has been not only applied in new fields of physics but it has been developed further in order to give new physical information in addition to the hypersonic properties. Therefore, this method deserves an introduction.

BS is an optical technique which is predominantly used to investigate acoustic properties at hypersonic frequencies. Hence, BS can be applied only to transparent materials, at best to translucent materials. The acoustic wavelengths involved are in the range of 200 nm to several μm. Figure. 3.16 shows a modern Brillouin set-up being able to measure simultaneously at different scattering vectors or in other words in different scattering geometries. For the

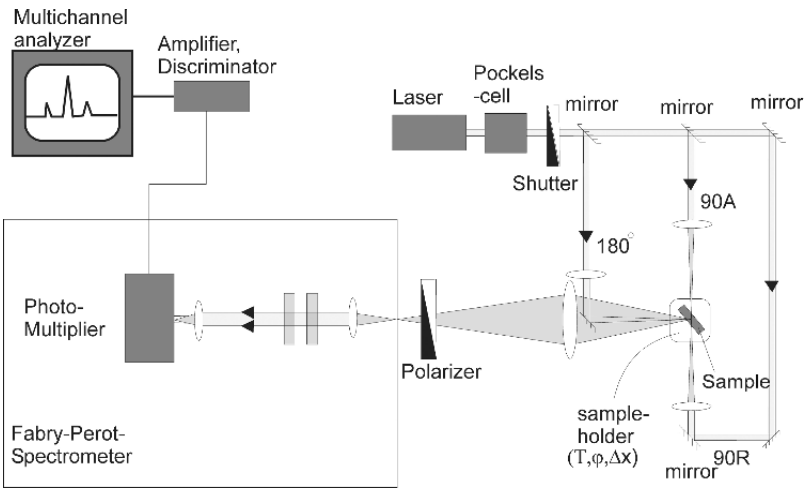


**Fig. 3.16.** Schematic presentation of a Brillouin spectrometer which can be used to measure within three different scattering geometries (even simultaneously): backscattering (180°), 90R-scattering and 90A-scattering (see Fig. 3.18). The sample holder allows for change of temperature ($T$), translational movement of the sample ($\Delta x$) and rotation of the sample ($\varphi$)

sake of simplicity, the sketched Fabry-Pérot interferometer is of the single-pass type. In modern BS multi-pass instruments or even Tandem spectrometers are used [66].

The spectral light intensity distribution measured by the Fabry-Pérot interferometer is converted by a photomultiplier into a suitable electronic pulse sequence which is then accumulated with a photon-counting system, usually an amplifier and discriminator combined with a so-called *multichannel analyzer* (MCA) (see Fig. 3.16). An example for a typical Brillouin spectrum is shown on the screen of the MCA.

Generally the scattering intensity $I(\boldsymbol{q}, \omega)$ per solid angle and frequency interval is proportional to the space and time Fourier transform $\mathbb{F}_{r,t}\{A\}$ of the autocorrelation function $A$ [67, 68]

$$A_{\mathrm{klmn}} = \langle \delta\alpha^*_{kl}(\boldsymbol{r}, t) \cdot \delta\alpha_{kl}(\boldsymbol{r}', t') \rangle \tag{3.3}$$

of the optical polarisability fluctuations $\delta\alpha_{kl}(\boldsymbol{r}, t)$ in the scattering volume [67]

$$I_{si}\left(\boldsymbol{q}, \omega\right) \propto F_{r,t}\left\{A\right\} \tag{3.4}$$

The subscripts $s$ and $i$ mean scattered and incident respectively, and refer to the appropriate polarization directions of the light waves here. Omitting, for simplicity, the tensor properties of $\delta\alpha$ we see that the spectral power density $I_{si}(\boldsymbol{q}, \omega)$ is proportional to the mean square fluctuation component at frequency $\omega$:

$$I_{si}\left(\boldsymbol{q}, \omega\right) \propto \overline{\left(\delta\alpha\left(\boldsymbol{q}\right)\right)^2_{\omega}} \tag{3.5}$$

All kind of excitations like phonons, excitons, spin waves and so on may contribute to the spectral power density. Also higher-order processes as multiphonon interactions may be included formally in this phenomenological treatment by expanding $\delta\alpha(\boldsymbol{q})$ into a power series in terms of symmetry coordinates [69].

Assuming a certain excitation mode characterized by an extensive parameter $\Psi(\boldsymbol{q}, \omega)$ a conjugated force $F(\boldsymbol{q}, \omega)$ and susceptibility $\chi(\boldsymbol{q}, \omega)$, the linear law reads

$$\psi\left(\boldsymbol{q}, \omega\right) = \chi^*\left(\boldsymbol{q}, \omega\right) \cdot F\left(\boldsymbol{q}, \omega\right) \tag{3.6}$$

The spectral power density $I(\boldsymbol{q}, \omega)$ can be related to the imaginary part of $\chi^*(\boldsymbol{q}, \omega)$ by the fluctuation-dissipation theorem [68]

$$I\left(\boldsymbol{q}, \omega\right) \propto \left(n\left(\omega\right) + 1\right) Im\left(\chi^*\left(\boldsymbol{q}, \omega\right)\right) \tag{3.7}$$

where

$$\frac{1}{n\left(\omega\right)} = \exp\left(\frac{\hbar\omega}{kT}\right) - 1 \tag{3.8}$$

The relation may be extended to include several, say $s$, coupled modes $\Psi_j$. To obtain the resulting field of generalized forces one has to add the contributions of the $s$ modes

$$F_i = \sum_{j=1}^{s} \gamma_{ij} \cdot \psi_j \tag{3.9}$$

Where the diagonal elements of the matrix $\gamma$ represent the inverse complex susceptibilities of the uncoupled modes, the off diagonal elements characterize the complex mode-mode coupling strength. Inverting Eq. (3.9) one gets the mode amplitudes

$$\psi_k^* = \sum_{i=1}^{s} \chi_{ki}^* \cdot F_i \tag{3.10}$$

The susceptibilities $\chi_{ki}^*$ determine the scattered light spectrum

$$I(\boldsymbol{q}, \omega) \propto (n(\omega) + 1)\, Im \left[ \sum_{i,j=1}^{s} p_i p_j \chi_{ij}^* (\boldsymbol{q}, \omega) \right] \tag{3.11}$$

The coefficients $p_i$ are related to the light scattering cross sections of the various modes and can be described for example by appropriate components of the elasto-optic tensor [70].

Considering only two modes and abbreviating the sum in Eq. (3.11) by $\overline{\chi*}(\boldsymbol{q}, \omega)$ the result is

$$\overline{\chi}^* (\boldsymbol{q}, \omega) = \frac{\gamma_{22}^* p_1^2 - 2\gamma_{12}^* p_1 p_2 + \gamma_{11}^* p_2^2}{\gamma_{11}^* \gamma_{22}^* - (\gamma_{11}^*)^2} \tag{3.12}$$

or

$$\overline{\chi}^* (\boldsymbol{q}, \omega) = \frac{p_1^2}{\gamma_{11}^* - (\gamma_{12}^*)^2 \chi_2^{0*}} + \frac{p_2^2}{\gamma_{22}^* - (\gamma_{12}^*)^2 \chi_1^{0*}} - \frac{2p_1 p_2}{\gamma_{11}^* \gamma_{22}^* - (\gamma_{12}^*)^2} \tag{3.13}$$

Here $\chi_i^{0*} = \gamma_{ii}^{*-1}$ means the susceptibility of the uncoupled mode $i$ and $(\gamma_{12}^*)^2 \chi_i^{0*}$ is related to its self energy. It may happen that the mode $\Psi_j$ does not produce any change of the polarizability, so $p_j = 0$ and only one term of Eq. (3.13) will be left. In order to give an example, the elasto-optic coupling for transversely polarized acoustic phonons is often extremely small.

The specific form of the light scattering spectrum will depend mainly on the characteristics of the inverse susceptibilities $\gamma_{jj}^*$ of the uncoupled modes. Taking for a damped harmonic oscillator with the damping constant $\Gamma$ and an oscillator strength $\gamma_{j0}$

$$\gamma_{jj}^* = \gamma_{j0} \left( \omega_j^2 - \omega^2 + i \cdot \omega \cdot \Gamma_j \right) \tag{3.14}$$

and for a relaxator with a relaxation time $\tau$

$$\gamma_{jj}^* = \gamma_{j0} (1 + i \cdot \omega \cdot \tau_j) \tag{3.15}$$

it is easy to predict the form of the scattering spectra. However, experiments do not give sufficient information for an unambiguous analysis. Already in the

two-mode case the complex factor $\gamma_{12}$ cannot be deduced definitely if coupling appears.

From (3.14), (3.15) together with (3.11) the spectral power density of one relaxator and one oscillator being uncoupled can be deduced. The imaginary part of the inverse of (3.14) is:

$$Im\left[\chi*\right]_{Osc} = \left(\gamma_0^{-1}\right)_{Osc} \frac{\omega \cdot \Gamma_{Osc}}{\left(\omega_{Osc}^2 - \omega^2\right)^2 + \omega^2 \cdot \Gamma_{Osc}^2} \tag{3.16}$$

For the relaxator the imaginary part of the inverse of (3.15) is:

$$Im\left[\chi^*\right]_{Rel} = Im\left[\gamma^{*-1}\right]_{Rel} = \left(\gamma_0^{-1}\right)_{Rel} \frac{\omega \cdot \Gamma_{Rel}}{\omega^2 + \Gamma_{Rel}^2} \tag{3.17}$$

with $\Gamma_{Rel} = \frac{1}{\tau_{Rel}}$.

Combining (3.16) and (3.17) with (3.11) and ignoring the coupling yields:

$$I\left(\boldsymbol{q},\omega\right) \propto \left(n\left(\omega\right)+1\right)\left[\left(\gamma_0^{-1}\right)_{Rel} \cdot \frac{p_1 \cdot \omega \cdot \Gamma_{Rel}}{\omega^2 + \Gamma_{Rel}^2} + \left(\gamma_0^{-1}\right)_{Osc} \cdot \frac{p_2 \cdot \omega \cdot \Gamma_{Osc}}{\left(\omega_{Osc}^2 - \omega^2\right)^2 + \omega^2 \cdot \Gamma_{Osc}^2}\right]. \tag{3.18}$$

Equation (3.18) gives the shape of a spectrum typical for a liquid of small viscosity consisting of a central peak due to entropy fluctuations and frequency shifted Stokes- and anti-Stokes lines related to density fluctuations resulting in a longitudinally polarized bulk phonon. It is worth noting that Eq. (3.18) gives the physical spectrum of the scattering processes involved, it does not contain the filter properties of the spectrometer. In order to get the information of Eq. (3.18) from a measured spectrum the latter one has to be deconvoluted. Generally, the deconvolution is a difficult task and is done by numerical techniques.

### The Kinematic View of Brillouin Spectroscopy

The kinematic view of BS couples energy and momentum of the interacting photons and phonons involved in the scattering process. As usual in inelastic scattering processes energy and momentum conservation holds [63, 64]:

$$\hbar\omega_s = \hbar\omega_i \pm \hbar\Omega \tag{3.19}$$

$$\hbar\boldsymbol{k}_s = \hbar\boldsymbol{k}_i \pm \hbar\boldsymbol{k} \tag{3.20}$$

where $\omega_i, \omega_s$ and $\Omega$ are the frequencies of the incident light, of the scattered light and of the phonon, $\boldsymbol{k}_i$, $\boldsymbol{k}_s$ and $\boldsymbol{q}$ are the respective wave vectors and $\Theta$ is the scattering angle within the sample (see Fig. 3.17).

Focussing still on a simple liquid and taking into account, that the energy transfer between photons and phonons is in BS extremely small

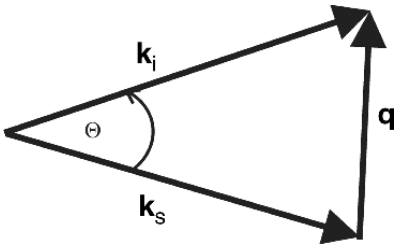


**Fig. 3.17.** Typical scattering diagram for wave vectors: $\boldsymbol{k}_i$ wave vector of the incident light, $\boldsymbol{k}_s$ wave vector of the scattered light, $\boldsymbol{q}$ scattering vector, $\Theta$ scattering angle

$(5 \cdot 10^9/5 \cdot 10^{14} = 10^{-5})$ the vectors $\boldsymbol{k}_i$ and $\boldsymbol{k}_s$ have almost the same length. Provided, acoustic attenuation is negligible ($\Gamma_{Osc} \ll \Omega$) the phase sound velocity can simply be calculated from geometric arguments. Using Eq. (3.19) and Eq. (3.20), and considering the refractive index $n$ of the sample one can easily determine the sound velocity $v$ related to a specific mode (longitudinal, transverse, etc.):

$$v = \frac{\Omega}{q} = \frac{\Omega}{2\pi} \frac{\lambda_{\text{Laser}}}{2n \sin\left[\frac{\theta}{2}\right]} \tag{3.21}$$

Knowing the mass density $\rho$ of the sample under investigation, the elastic modulus related to the wave vector $\boldsymbol{q}$ can be calculated:

$$c\,(\boldsymbol{q}) = \rho \cdot v^2\,(\boldsymbol{q}) \tag{3.22}$$

### Scattering Geometries and Pitfalls

As is seen from Eq. (3.21) the acoustic wavelength

$$\Lambda = \frac{2\pi}{q} = \frac{\lambda_{\text{Laser}}}{2n \sin\left[\frac{\theta}{2}\right]} \tag{3.23}$$

depends on the vacuum wavelength $\lambda$ of the laser, on the scattering angle $\theta$ within the sample and on the refractive index $n$ of the sample. As a consequence of latter influence the acoustic wavelength is e.g. not invariant under changes of temperature which may be a real problem in interpreting Brillouin data.

Fortunately, one of the scattering geometries shown in Fig. 3.18 yields an acoustic wave vector which is independent of the refractive index: the 90A-scattering geometry.

The relations between sound velocity, sound frequency and sound wavelength are as follows for the different scattering geometries [66, 71]:

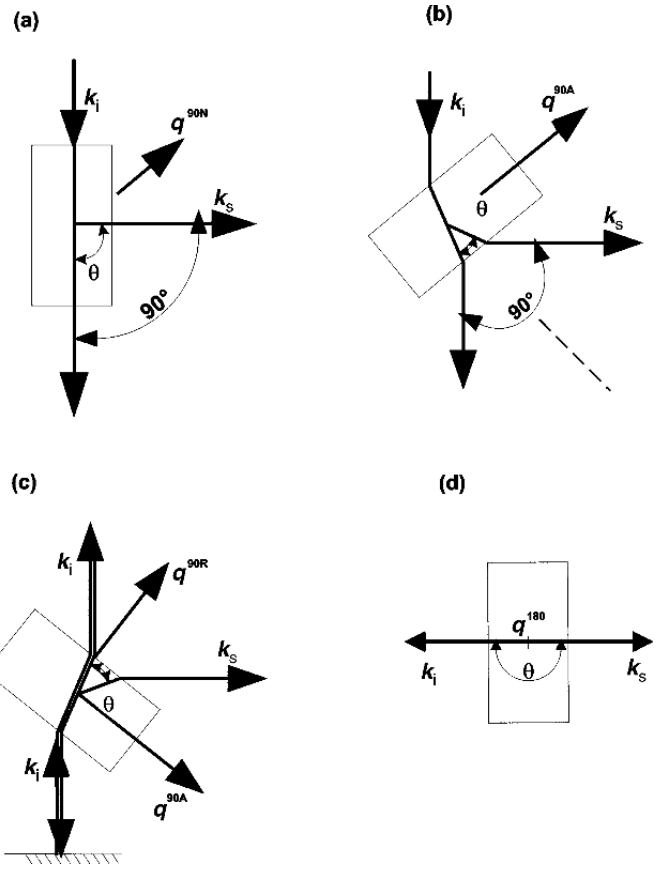


**Fig. 3.18.** Typical scattering geometries used for Brillouin spectroscopy. (**a**) 90N-scattering geometry, (**b**) 90A-scattering geometry, (**c**) combination of 90A- and 90R-scattering geometry, (**d**) back scattering geometry

$$v^{90N}(T) = \frac{\Omega^{90N}(T)}{2\pi} \frac{\lambda_{\text{Laser}}}{2n(T)\sin\left(\frac{90°}{2}\right)} \tag{3.24}$$

$$v^{90A}(T) = \frac{\Omega^{90A}(T)}{2\pi} \frac{\lambda_{\text{Laser}}}{2\sin\left(\frac{90°}{2}\right)} \tag{3.25}$$

$$v^{90R}(T) = \frac{\Omega^{90R}(T)}{2\pi} \frac{\lambda_{\text{Laser}}}{2n(T)\sin\left(\frac{90°}{2}\right)} \tag{3.26}$$

and

$$v^{180}(T) = \frac{\Omega^{180}(T)}{2\pi} \frac{\lambda_{\text{Laser}}}{2n(T)} \tag{3.27}$$

Besides Eq. (3.25) all other equations depend on the refractive index $n$ of the sample, which means, that the acoustic wavelength depends on the

refractive index $n$. In the case of Eq. (3.25) the refractive index enters the refraction process and the phase velocity in a compensating manner and therefore the sound wavelength becomes independent of $n$.

Provided sound dispersion is absent, Eq. (3.25) in combination with Eqs. (2.22, 2.24) and (3.27) can be used to calculate the refractive index from Brillouin data

$$n(T) = \frac{1}{\sqrt{2}} \frac{\Omega^{180}(T)}{\Omega^{90A}(T)} \tag{3.28}$$

$$n(T) = \frac{\Omega^{90N}(T)}{\Omega^{90A}(T)} \tag{3.29}$$

If the samples have an isotropic symmetry Eqs. (3.28) and (3.29) can be used to determine the refractive index of the samples.

If for the frequencies of interest acoustic relaxation processes are active, the right-hand sides of Eqs. (3.28) and (3.29) no more represent the refractive index but the so-called opto-acoustic dispersion functions ($D$-function) [66,72]. The difference $D(T) - n(T)$ gives a measure for dispersion respectively the relaxation strength if present. Further information can be found in Sect. 3.5.

In the case of film- or plate-like samples which have reflecting substrates on one side there exists an alternative scattering geometry, which we call the $RI\theta A$-scattering geometry [72]. It measures the scattered light from the laser beam at the substrate and combines the advantages of the 90A- and the backscattering technique. Figure 3.19 shows schematically the specific properties of this scattering technique.

The $RI\theta A$-scattering geometry [72] is not restricted to an outer scattering angle of 90° but can be applied for any outer scattering angle $\theta$. Thus the $RI\theta A$-scattering geometry results in an a priori backscattering situation with

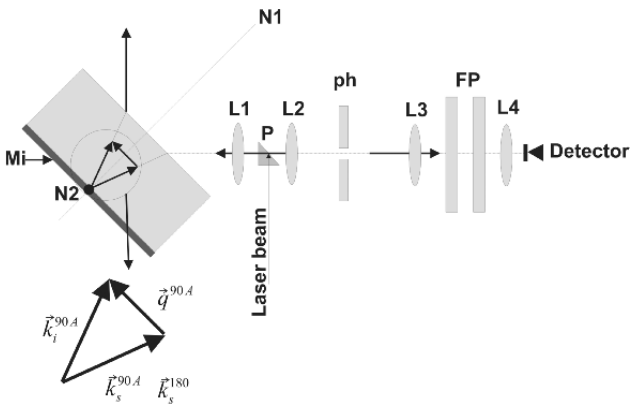


**Fig. 3.19.** Schematic drawing of the so-called $RI\theta A$-scattering geometry. N1, N2 rotation axes, L1–L4 lenses, P prism, ph pinhole, Mi mirror, FP Fabry-Pérot-Interferometer

the possibility to measure in addition a $\theta A$-phonon with a wave vector $\boldsymbol{q}^{\theta A}$, which, because of the optical reflection law, is oriented in the film plane. Rotation around the N2-axis changes the magnitude of $\boldsymbol{q}^{\theta A}$ but maintains its direction. Rotation of the sample around the N1-axis probes the in-plane acoustic symmetry.

## 3.3 The "Kinetic Face" of the Structural Glass Transition

In this section we will review some generally accepted results from literature on kinetic features of the glass transition and discuss some new decisive experimental data. By "kinetic aspects" we mean the influence of the cooling or heating procedure of the sample on the glass transition. So we will analyse the loss of thermodynamic equilibrium of the sample due to those temperature changes which are necessary to bring the sample closer to the glass transition. As already discussed briefly in the introduction, the main unsolved problem about the glass transition concerns the possibility of the existence of a phase transition possibly hidden by kinetic effects.

It is clear, that glasses are solid in the glassy state from an empirical point of view. From the structural point of view they are amorphous as confirmed by x-ray diffraction. Thus the symmetry of the glassy state is isotropic, which is obviously the same as for the liquid state. Consequently, if the TGT was a structural phase transition this transition would be of the iso-structural type.

In literature on glasses (e.g. [73–83]) the TGT is often discussed in terms of the temperature dependence of the shear viscosity $\eta_{44}$ (we use the Voigt notation [84]). Figure 3.20a shows schematically the increase of this viscosity around the thermal glass transition temperature $T_g$. In literature on glasses one usually finds the argument that very close to $T_g$ the shear viscosity takes

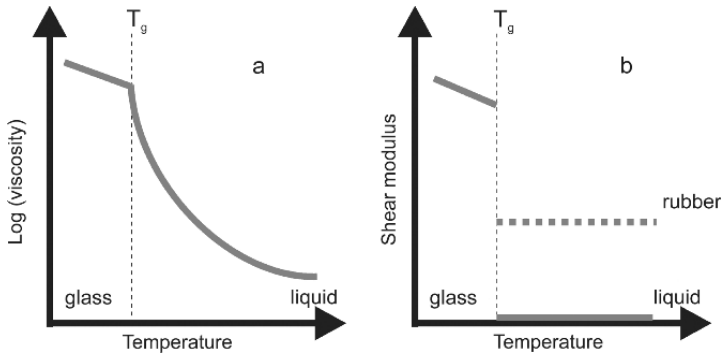


**Fig. 3.20.** Schematics of the temperature-dependence of (**a**) the visocisity and (**b**) the static shear modulus at the glass transition

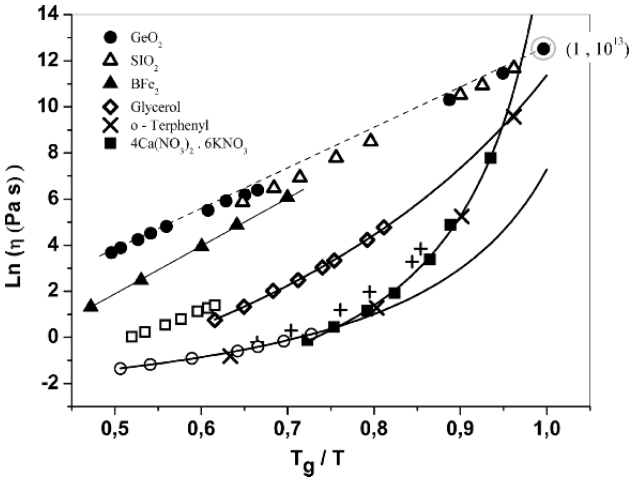


**Fig. 3.21.** Logarithmic viscosity versus the renormalized temperature $T_g/T$ for several typical glass formers

values up to about $10^{12}$ Pa s. Sometimes a viscosity of $10^{12.3}$ Pa s [73,78,79,85] is used as a definition for the glass transition.

However, the temperature dependence of $\eta_{44}$ is not the same for different glass-formers. *Strong glass-formers* (c.f. Fig. 3.21, data from [85]) show an Arrhenius-like temperature behaviour of $\eta_{44}$ whereas *fragile glass-formers* behave VFT-like (c.f. Eq. (3.32)). In order to test the degree of fragility we have fitted some of the data (straight lines in Fig. 3.21) to the VFT-law using the Maxwell relation:

$$\eta_{44} = c_{44}^{\infty} \cdot \tau_{\alpha} \tag{3.30}$$

In Eq. (3.30) $c_{44}^{\infty}$ is the dynamically clamped shear modulus which is assumed to show only a slight temperature dependence and $\tau_{\alpha}(T)$ is the relaxation time of the $\alpha$-relaxation process according to Eq. (3.32). The fitted curves in Fig. 3.21 show, that different glass formers tend to very different viscosities close to $T_g$ and that a limiting value for the shear viscosity of $10^{12}$ Pas is only a rough estimate. Thus, $\eta_{44}(T)$ seems not to be a good quantity in order to describe the TGT. In addition, the viscosity is a transport coefficient, usually defined for liquids. It seems that a susceptibility, like a mechanical modulus, defined for the liquid and the solid state, is more appropriate.

At least for fragile glass-formers the static shear stiffness seems to be more suitable to describe the transition from the liquid to the glassy state. By definition the static shear stiffness $c_{44}^{s}$ is zero in the liquid state. Glasses, on the other hand, show a static shear stiffness $c_{44}^{s} > 0$ (at least on all accessible time scales) indicating an elastic stability comparable to that of crystals. The expected jump-like behaviour of the static shear modulus at $T_g$ is schematically drawn in Fig. 3.20b.

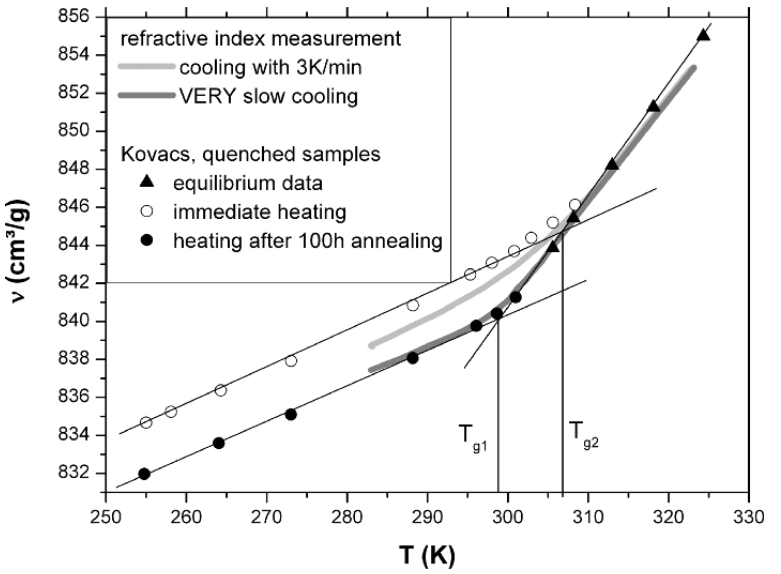


**Fig. 3.22.** Temperature dependence of the specific volume $v$ of PVAc (dots taken from Kovacs [86]) around the glass transition after different cooling procedures

The kinetic face of the TGT in structural glasses is usually shown by demonstrating the ageing behaviour of volume data in the glassy state. In Fig. 3.22 specific volume data of polyvinylacetate (PVAc) given by Kovacs [86] are reconsidered and compared to recent data gained from refractive index measurements by means of the Lorenz-Lorentz equation

$$r \cdot \rho = \frac{n^2 - 1}{n^2 + 2} \tag{3.31}$$

where $\rho$ is the mass density, $r$ the specific refractivity (assumed to be constant) and $n$ the refractive index. This equation is well established for polymers [87].

The dots in Fig. 3.22 denote data from Kovacs, the lines denote the new data. Both data sets agree very well in the high temperature branch ($T > 310\,\mathrm{K}$). The different behaviour below 310 K is due to different thermal treatments of the samples as explained in the following. The triangles represent equilibrium values ($T > T_g$), the circles represent specific volume data obtained on heating after quenching the sample. The values measured almost immediately after the quenching (open circles) are higher than those measured after annealing the sample for 100 h at $T = 255\,\mathrm{K}$ (filled circles). The dark gray line was measured on cooling with a rate of 3 K/min, the light gray line on extremely slow cooling (step-wise with $\Delta T = 1\,\mathrm{K}$ and an average rate of ca. 0.4 mK/min).

The smooth kink in the specific volume curves at the transition from the glassy to the liquid state is interpreted as the operative glass transition due to

the cross-over of the intrinsic time scale of the $\alpha$-relaxation process of PVAc with a time scale related to the thermal history of the sample. As indicated in Fig. 3.22 the intersection of the extrapolated high temperature straight line with those of the two glassy states are used to fix the operative glass transition temperatures $T_{g1}$ and $T_{g2}$. This $T_g$ shift, also reflected in the new data, is typical for the rate dependence of the TGT.

With the Kovacs data the annealing effect leads to a reduction of the specific volume of about $-0.5\%$ for 100 h annealing at $T \approx (T_g - 40\,\mathrm{K})$ with $T_g \approx 300\,\mathrm{K}$. This ageing has been attributed by Kovacs to the metastability of the glass with respect to its fluid phase after quenching. Apparently this annealed state coincides with that of our new data on extremely slow cooling, although the duration of our measurement exceeds the annealing time by at least a factor of 10. Accordingly this state seems not to be arbitrary at all, as different but slow thermal histories lead to the same state. This gives rise to the question: If the system is clearly out of equilibrium (due to a crossing of time scales) and if it relaxes even well below $T_g$ towards its equilibrium, i.e. from the point of view of kinetics towards the extrapolated liquid branch, why should it stop relaxing at a certain point?

Indeed, the absolute values of the specific volume within the glassy state depend on the cooling history of the sample but the slope, which corresponds to the thermal expansion coefficient $\alpha$, does not. So if the glassy state was metastable and strongly dependent on the thermal history, why should its temperature dependence be unique?

Figure 3.23 shows the effect of fast cooling as a source for metastability for the longitudinal elastic stiffness coefficient $c_{11}$ (Voigt notation [84]) of polystyrene (PS) as obtained by Brillouin spectroscopy at sound frequencies in the GHz range. Both $c_{11}$-curves have been measured on step-wise heating with an average heating rate of 0.1 K/min. The curve of open circles was measured on a sample quenched in ice water from 400 K to 300 K. The black curve was also measured in the same way but after extremely slow cooling from above $T_g$ to 300 K. The cooling was performed on step-wise cooling using the time domain method (see Sect. 3.4). The average cooling rate was extremely low (ca. 0.5 mK/min).

As shown before for the specific volume data (Fig. 3.22) the absolute values of the elastic stiffness modulus of the glassy state depend on the thermal history of the sample whereas the slopes of these curves do not. This result is not new but surprising from a physical point of view and will therefore be discussed in Sect. 3.5. The stiffness anomaly of the black curve in Fig. 3.23 around the TGT reflects an overheating effect: Since the sample was extremely slowly cooled to the glassy state, we may expect that the segment packing arrangement became so dense, that the random closed packed (rcp) state [78] was attained. Even on slow heating with +0.1 K/min the time needed for "liquifying" the glassy state was significantly larger than provided by that heating rate. The observed overheating temperature $\Delta T^{oh}$ is about $\Delta T^{oh} \approx 10\,\mathrm{K}$.

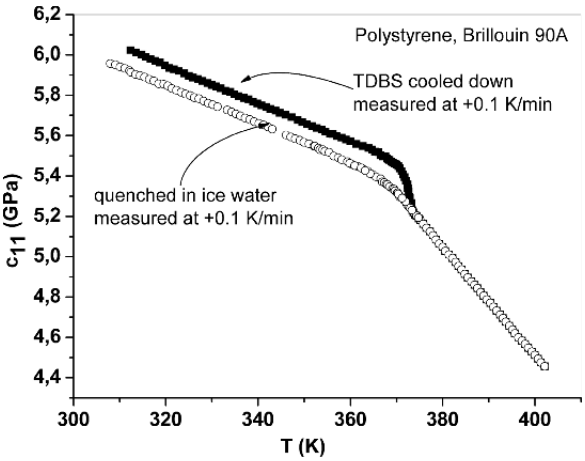


**Fig. 3.23.** Overheating effect at the glass transition temperature of polystyrene induced by strongly differing cooling and heating rates

The physical origin of the metastability demonstrated in Fig. 3.22 and Fig. 3.23 can be twofold at least:

1. Internal degrees of freedom which may be described in terms of irreversible thermodynamics by spatially homogeneous internal variables [88]. The equilibration of these internal variables is retarded on fast cooling or heating.
2. Spatial heterogeneities because of quenching.

The second effect is usually neglected in the discussion about the TGT but it deserves attention for the following reasons.

These spatial heterogeneities result from the low thermal conductivity which is typical for many glasses. Since usual heating and cooling processes transfer heat across the outer surface of the sample, specific volume gradients develop according to the temperature gradient. As an example one may think of a long polymer cylinder (Fig. 3.24) which is rapidly cooled down from high temperatures to below $T_g$. This quenching will freeze at first the outer skin of the sample (Fig. 3.24). Then this outer skin becomes a sort of rigid container which is filled with the same material in the fluid state. With ongoing quenching, the remaining fluid vitrifies layer by layer but with varying cooling rate and under the mechanical stress exerted by the outer solidified part. In the final state the sample consists of a layered structure with an inhomogeneous distribution of mechanical stresses and a radial distribution of glass transition temperatures. It is not surprising that such inhomogeneous samples show apparent ageing effects.

Figure 3.25 shows two specific heat curves measured with adiabatic calorimetry of a polymethylmethacrylate (PMMA) sample, which suffered different thermal histories prior to the two heating runs. The open circles were

**Fig. 3.24.** Schematics of a polymer cylinder with shells representing different cooling rates and hence different glass transition temperatures due to fast freezing

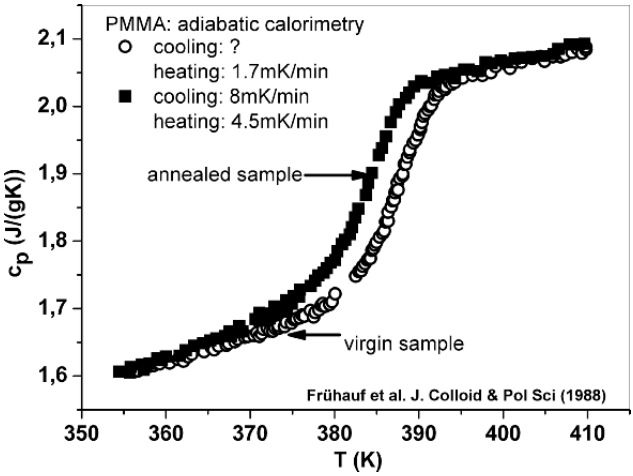


**Fig. 3.25.** Temperature dependence of the specific heat capacity of PMMA after different cooling and heating procedures

measured on a virgin (extruded) sample from ambient temperature to 410 K. Subsequently the sample was slowly cooled down again to ambient temperature by 8 mK/min and then measured again on heating by 4.5 mK/min (black dots). The superior experimental reliability and precision of these data measured with heat-pulse adiabatic calorimetry is illustrated in Fig. 3.26. The margin of error of these specific heat data is smaller than the diameter of data dots. The low- and high-temperature asymptotes of the $c_p(T)$-curve are very well described by straight lines with slightly different slopes being a little bit lower in the liquid state.

Based on this high data quality, the difference in $T_g$ of about 3 K between the virgin and the slowly cooled state of the PMMA sample is real in Fig. 3.25.

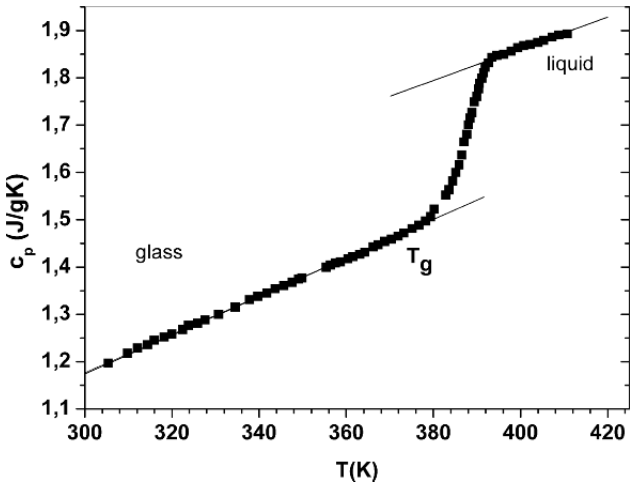


**Fig. 3.26.** Specific heat capacity around the TGT of PMMA, the ordinate is off by roughly 15% due to a calibration error [89]

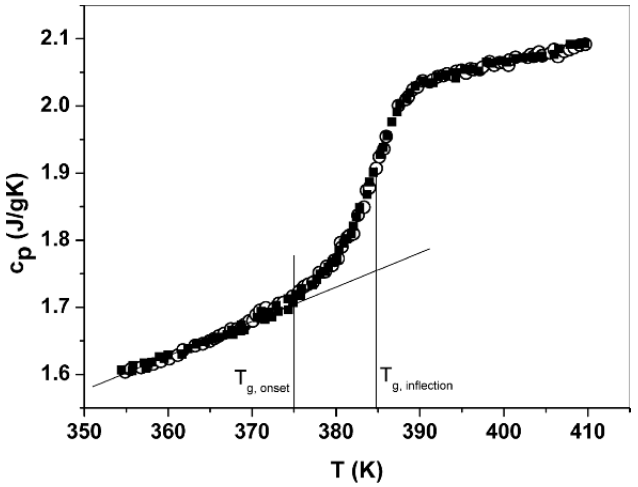


**Fig. 3.27.** Specific heat capacity around the TGT of PMMA for cooling rates differing by a factor of 60 (both of the order of magnitude: mK/min) [89]

Frühauf et al. [89] attributed this shift to the formation of internal stresses and a spatial distribution of glass transition temperatures.

In the following we will discuss data measured on two identical PMMA samples (Fig. 3.27), where very different cooling rates yield the same adiabatic specific heat capacity, indicating that at least in average the same glassy state is produced for both cooling scenarios. The samples have suffered cooling rates differing by a factor of more than 60.

The black curve in Fig. 3.27 was cooled very slowly with 8 mK/min and the circle curve was cooled faster with 519 mK/min which is still slow compared to rates applied in technological processes, however. Both samples were then measured by the same heating rate of about 4.5 mK/min. In the margin of error both curves are identical and show no cooling rate dependence at all. The reason for this complete independence of the TGT on the thermal history is only understood if the rate dependence of $T_g$ can be neglected for the given range of cooling rates. This fact seems to be contradicted by the large change of the cooling rate in combination with the accuracy of the specific heat data.

An alternative interpretation for the observed behaviour could be connected to the observed cut-off of the relaxation frequencies, i.e. the relaxations stop at certain temperature with a finite relaxation frequency. This aspect will be discussed in Sect. 3.4.

If the conclusion can be made that the data of Fig. 3.27 are equilibrium or near equilibrium data, then the step-height of $c_p$ at $T_g$ represents the excess specific heat connected to the "liquefaction" of the glassy state. In physical terms, the precise location of $T_g$ is not obvious. Many authors use the inflection point of the specific heat curve as a good measure to identify $T_g$. Since the temperature width of the thermal glass transition regime is almost 20 K an identification of the inflection point of the $c_p$-curves as a reliable glass transition temperature is questionable. It is more likely, that the onset of the excess specific heat on the background specific heat of the glassy state defines the glass transition temperature. This onset coincides quite well with the kink in the sound velocity and the refractive index.

A completely different view on the kinetic properties of the TGT is obtained having a look at the *"Generalized Cauchy Relation"* (gCR) of amorphous materials [90, 91]. From solid state physics it is well-known that the number of independent coefficients of the elastic stiffness tensor is deduced from the symmetry of the crystal [e.g. [92]]. Additional relations, which further reduce the number of independent elastic stiffness coefficients are known in solid state physics and are called *Cauchy relations* (CR) [93, 94]. Such relations hold only true if the crystal of interest obeys additional constraints about local symmetry (every lattice particle is a centre of inversion), molecular interaction forces (only central forces), and lattice anharmonicity (only harmonic potentials).

For cubic crystals these constraints lead to the relation:

$$c_{12} = c_{44} \tag{3.32}$$

Equation (3.32) reduces the initially three independent elastic coefficients to only two, $c_{11}$ and $c_{44}$ [94]. Imagine now that we were able to produce a ceramic sample made of irregularly oriented cubic nano-crystals which obey a CR according to Eq. (3.32). In that case the ceramic body shows isotropic symmetry on the macroscopic scale. Hence the isotropy condition [92] holds for the orientational average (denoted by the brackets) of the elastic coefficients:

$$\langle c_{12} \rangle = \langle c_{11} \rangle - 2 \cdot \langle c_{44} \rangle \tag{3.33}$$

Combining Eqs. (3.32) and (3.33) we obtain a Cauchy relation for the isotropic state [94]:

$$\langle c_{11} \rangle = 3 \cdot \langle c_{44} \rangle \tag{3.34}$$

Equation (3.34) reduces the number of independent elastic coefficients of the isotropic nano-ceramic from two to one.

If the cubic crystal does not fulfil the requirements of the Cauchy relation, than you can write Eq. (3.32) in a more general way

$$c_{12} = c_{44} + A(T, p, \ldots) \tag{3.35}$$

where $A$ is a term which depends on temperature $T$, pressure $p$, etc.

The orientational average leads then to a generalized Cauchy relation of the isotropic state

$$\langle c_{11} \rangle = 3 \cdot \langle c_{44} \rangle + A(T, p, \ldots) \tag{3.36}$$

According to Eq. (3.36) the deviation from the Cauchy relation of the cubic state measured by A is found as an additive term in the Cauchy relation of the isotropic state Eq. (3.35). This result sheds some interesting light on the possible mechanism leading to the generalized form of the Cauchy relation. Equation (3.35) together with Eq. (3.36) lead to the result that a ceramic based on nano-crystals with cubic symmetry can show an ideal Cauchy relation Eq. (3.35) provided that the cubic crystals follow a Cauchy-Relation ($A = 0$). As a consequence the additive constant $A$ in the generalized Cauchy relation is not caused by the difference in local and global symmetry of the ceramic.

Amorphous glass-formers are not expected to meet the aforementioned conditions about local symmetry, the absence of defects and the absence of anharmonicity. Thus Eq. (3.34) should not apply to these materials.

However, theoretical work [90, 95] proposed a generalized Cauchy relation between the high-frequency elastic shear modulus $G^\infty = c_{44}^\infty$ and the compression modulus $K^\infty$ for dynamically frozen liquid argon:

$$K^\infty = \frac{5}{3} \cdot G^\infty + 2 \cdot (P - n \cdot k_B T) \tag{3.37}$$

where $P$ is the external pressure, $T$ the temperature and $n$ the particle density. Using

$$K^\infty = c_{11}^\infty - \frac{4}{3} c_{44}^\infty \tag{3.38}$$

one finally obtains

$$c_{11}^\infty = 3 \cdot c_{44}^\infty + 2(P - n \cdot k_B T) \tag{3.39}$$

Compared to the CR for the isotropic nano-crystalline case Eq. (3.35), this *"generalized" Cauchy relation* ($g$CR) for the amorphous argon adds a

term, which depends on pressure and temperature and therefore much more equals Eq. (3.36). According to Eq. (3.37) the pre-factor 3 is reproduced for $c_{44,}$ but the relation between $c_{44}$ and $c_{11}$ is not linear for changing pressure or temperature.

To check this point, the TGT of several glass formers (DGEBA, PVAc, Salol, DBP, etc.) were recently studied during slow cooling ($\dot{T} < 0.5\,\mathrm{K}$ /min) by Brillouin spectroscopy at hypersonic frequencies [96]. Due to the high measuring frequency, the method provides the clamped stiffness coefficients $c_{11}^{\infty}(T)$ and $c_{44}^{\infty}(T)$ (Fig. 3.29). As the result, a *linear* relation

$$c_{11}^{\infty}(T) = A^0 + B \cdot c_{44}^{\infty}(T) \tag{3.40}$$

was obtained, $A^0, B$ temperature-independent material constants and $T$ being the temperature. Again, B = 3 was found within the margin of error for all materials under investigation [96]. As shown in Fig. 3.30, the TGT is completely hidden in the elastic data representation described by Eq. (3.40). Accordingly the influence of the TGT has to be identical on both the longitudinal and the transverse acoustic mode.

This observation raises the question whether (i) non-equilibrium processes do not violate the $g$CR at all or whether (ii) the TGT is not necessarily a non-equilibrium process? If hypothesis (i) holds true, the validity of relation (3.40) for the liquid state as well as for the solid state would be less surprising. If on the other hand (ii) holds true, the validity of the $g$CR could turn out to be a versatile tool to discriminate between mechanical equilibrium and non-equilibrium. With respect to this point of view it is highly interesting to elucidate the question whether fast cooling of the liquid to the non-equilibrium glassy states is able to violate the $g$CR. If it happens, whether these non-equilibrium states relax towards their equilibrium and if they do so, on which time scale and to which direction this happens.

All data reported in the following were measured with Brillouin spectroscopy using the 90$A$-scattering geometry (c.f. Fig. 3.18b) detecting simultaneously the longitudinal sound frequency $f_L^{90A}$, and the transverse sound frequency $f_T^{90A}$. It should, however, be stressed that amongst all scattering geometries only the 90$A$-scattering or more general the $\Theta A$–scattering provides a phonon wave vector $q^{\Theta A}$ which is independent of the refractive index $n$ of the sample (Sect. 3.2).

Having determined the sound velocities of the longitudinal and shear polarized phonon modes and assuming that the mass density $\rho$ is known, the elastic constants $c_{11} = c_L$ and $c_{44} = c_T$ are given by

$$c_{ii}^{90A} = c_{L,T}^{90A} = \rho \cdot (V_{L,T}^{90A})^2, \qquad i = 1, 4 \tag{3.41}$$

In order to test whether the $g$CR Eq. (3.40) can be violated by fast quenching we have used the diglycidilether of bisphenol A (DGEBA, Fig. 3.28) as a glass forming organic liquid.

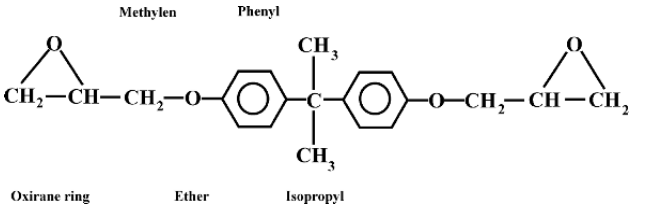


**Fig. 3.28.** Structural formula of DGEBA

It is well-known [96, 97] that bulk DGEBA is a fragile liquid that may crystallize, in special circumstances if nucleation is forced e.g. by rough surfaces, water droplets, etc. DGEBA shows at extremely slow cooling a static (intrinsic) TGT at $T_{gs} = 243$ K [97].

In Fig. 3.29 the elastic stiffness data $c_{11}(T)$ and $c_{44}(T)$ for an extremely slow cooling run are shown ($\sim$0.01K/min). Both elastic moduli versus temperature curves show a kink at about the static glass transition temperature $T_g$ of 243 K [97]. According to the small residuals shown in Fig. 3.29 both frequency curves behave piecewise linearly in the investigated temperature interval.

According to Eq. (3.40) the related $g$CR is depicted in Fig. 3.30. The plot demonstrates that the elastic data measured under these conditions perfectly obey the gCR with $A = 2.6$ GPa and $B = 2.98 \pm 0.2$. Hence within the margin of error $B = 3$ holds true. The distribution of the residuals confirms the linear

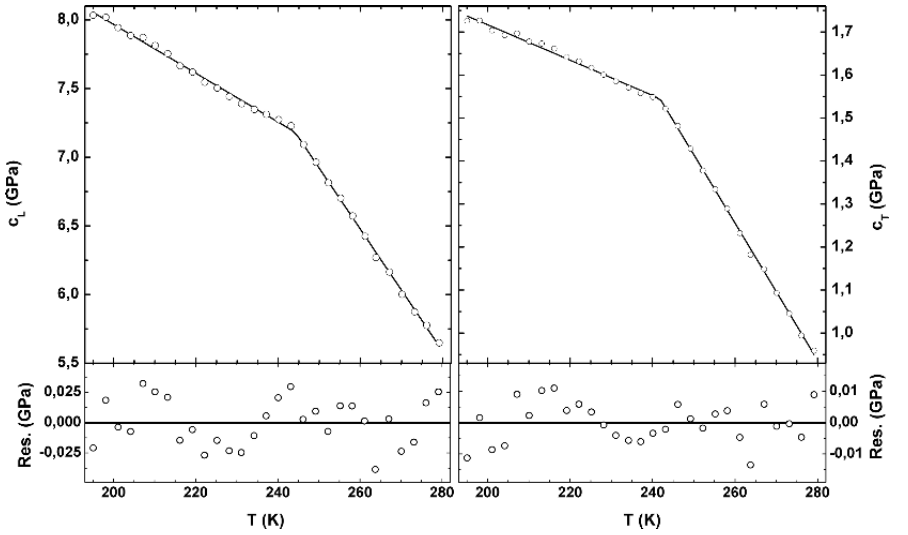


**Fig. 3.29.** $c_L$ and $c_T$ of DGEBA as a function of the temperature $T$. The *straight lines* are fitted curves. The residuals in the lower part demonstrate the agreement of the data with a piece-wise straight line model

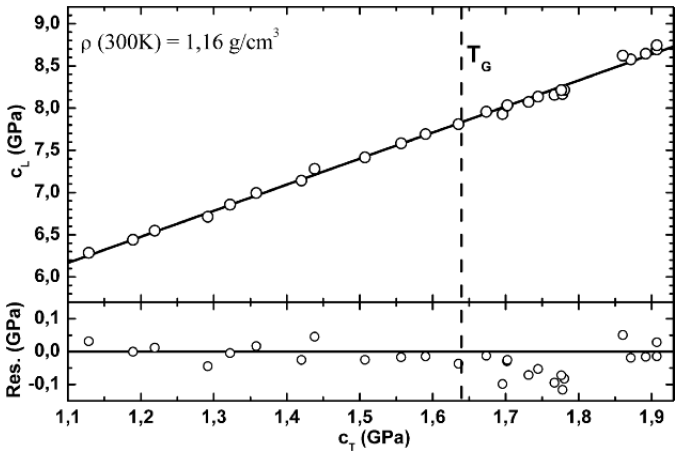


**Fig. 3.30.** $g$CR-representation for the Brillouin data of Fig. 3.29. In the lower part of the figure the corresponding residuals are given. The residuals indicate the good compatibility of the measured data with the $g$CR presented by the *straight line* according to Eq. (3.40)

behaviour of the data representation, and that the TGT is completely hidden in this parametrical representation.

If we tentatively accept a purely kinetic interpretation (see e.g. [98]) of the TGT, we had to assume that $T_g$ could be shifted to higher temperatures, provided the cooling process was speeded up.

In other words, the $g$CR would remain a linear function but would become ambiguous in its physical meaning, i.e. the parameters A and B would have the same values in the equilibrium as in the non-equilibrium state. Consequently, the $g$CR would turn out to be rather insensitive to deviations from equilibrium. If, on the other hand, the slopes of the longitudinal and transverse frequency curves of the new hypothetical glassy state change their relation in comparison to that measured on slow cooling, the $g$CR would become violated for the new glassy state. Keeping in mind that within this approach the slower cooled sample is closer to equilibrium, such behaviour seems not to be very likely. In order to clarify this point we have tested whether the apparent insensitivity of the $g$CR with respect to equilibrium is a general feature of the $g$CR. For this purpose we have used quenching procedures in order to create forced non-equilibrium glassy states. During this fast cooling we are not able to record Brillouin data simultaneously. Therefore we cannot say anything about the evolution of the elastic behaviour during the fast cooling process. As will be shown below (Fig. 3.31c) we were able, however, to measure the sound frequency evolution of samples submitted to intermediate cooling rates (0.05 K/min).

Figure 3.31 shows the $c_{11} = c_{11}(c_{44})$-relation as obtained from Brillouin data derived from different quenching procedures. As indicated above, these

quenching procedures are not really under control. Figures 3.31a,b,d show Brillouin data measured during heating the quenched sample from the glassy to the liquid state. Figure 3.31c shows the Cauchy-representation of Brillouin data measured on intermediate fast cooling of the DGEBA sample. The open circles in Fig. 3.31 give the measured data, the straight lines give the $g$CR. From Fig. 3.31 it is evident that non-equilibrium glassy states produced by quenching lead to a violation of the $g$CR. The quenched samples of Fig. 3.31 show significant positive deviations from the $g$CR. As a matter of fact, this positive deviation is related to a lag of the shear stiffness behind the longitudinal stiffness.

In other words, on quenching the DGEBA sample to low temperatures, the longitudinal modulus develops closer towards the increasing equilibrium value than the transverse modulus does. Moreover, these deviations are able to relax towards the $g$CR during heating and cooling procedures within the glassy state (c.f. Fig. 3.33).

Figure 3.31c demonstrates how the violation of the $g$CR takes place if the BS-measurements are performed during intermediate fast cooling (about 0.05 K/min). It is evident that even if the sample is moderately cooled into the glassy state, significant positive deviations from the $g$CR can be produced. The linear transformation properties implied by the $g$CR and deviations from this linear transformation can be evidenced in a different way. We show in Fig. 3.32 the temperature dependence of the longitudinal and shear phonon corresponding to the Cauchy representation of Fig. 3.31b.

As is seen in Fig. 3.32 we have spread the plot axis for both phonon frequency curves in such a way that the longitudinal and transverse phonon branches coincide within the liquid phase. In the glassy phase the relative slope of the transverse mode becomes smaller in comparison to that of the longitudinal mode, whereas the slope of the longitudinal mode is the same as for slow cooling. According to the related frequency-temperature plots the different ageing processes presented by Figs. 3.31a,b,d meet the "equilibrium glass branches" of the longitudinal and transverse polarized modes defined by Figs. 3.29, 3.30. The low-temperature branch of Fig. 3.31a merges at $T - T_g = 16\,\mathrm{K}$ with the $g$CR. The slope of this low-temperature branch amounts to about $m = 4$ in comparison to $B = 3$. The low-temperature branch of Fig. 3.31b even merges at $T - T_g = 21\,\mathrm{K}$. The slope of this branch amounts to $m = 4.8$. In Fig. 3.31d the onset of the deviation from the $g$CR occurs only at the TGT. No excess of the slope ($m > B = 3$) was ever observed above $T_g$.

In order to elucidate the observed significant ageing behaviour within the glassy state of DGEBA we have performed different cooling and heating cycles within the glassy state of this material. The data are depicted in Fig. 3.33. After quenching the sample to 120 K (cooling rate $\sim -200\,\mathrm{K/min}$) we performed a first heating experiment (run 1) in Fig. 3.33, which we stopped at 195 K. This is more than 40 K below $T_g$.

The slope of the low-temperature branch is $m = 4.15$ in comparison to $B = 3$ in the liquid state. Subsequently we have cooled the sample again

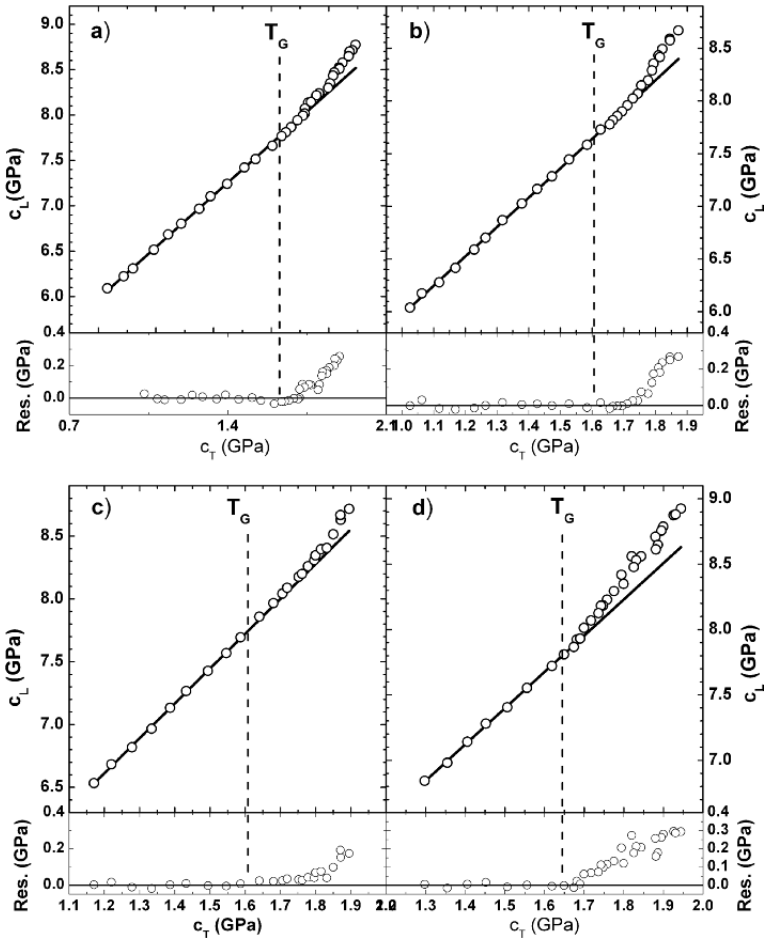


**Fig. 3.31.** *g*CR-representations for different quenching and heating cycles. The residuals indicate the deviations of the measured data from the *g*CR presented by the *straight lines*. Figures a, b, d represent Brillouin data measured on heating after different quenching procedures. Figure c shows a cooling run on intermediate fast cooling. See text for further explanations

to 120 K and then heated the sample to $T_g - 10$ K. The slope of the low temperature branch has now decreased to $m = 3.92$. A further cooling to 137 K and a subsequent heating to ambient temperature yields a slope of $m = 3.48$ for the glassy state. These results confirm the above anticipated ageing process within the glassy state. This thermal relaxation process converges in all our experiments versus a unique glassy state, which we have identified recently on the basis of time domain Brillouin measurements [97] as the equilibrium glassy state of DGEBA (c.f. Sect. 3.4). Definitely, we found no relaxations towards the liquid state, which exceed the sound frequency data

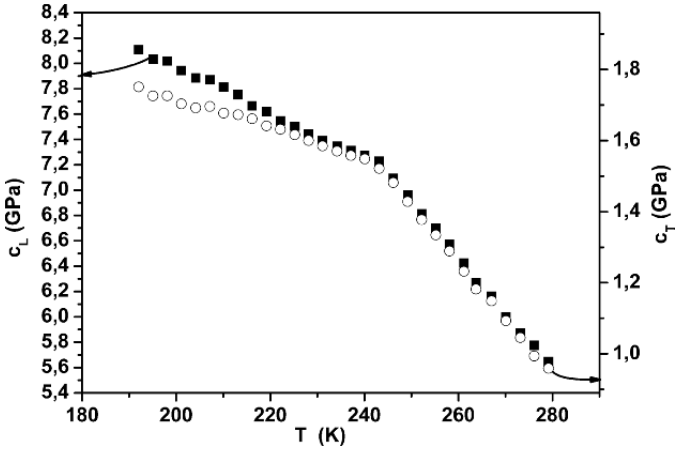


**Fig. 3.32.** Longitudinal and transverse elastic moduli ($c_L$ and $c_T$) for DGEBA as a function of the temperature $T$, measured after quenching to about 77 K

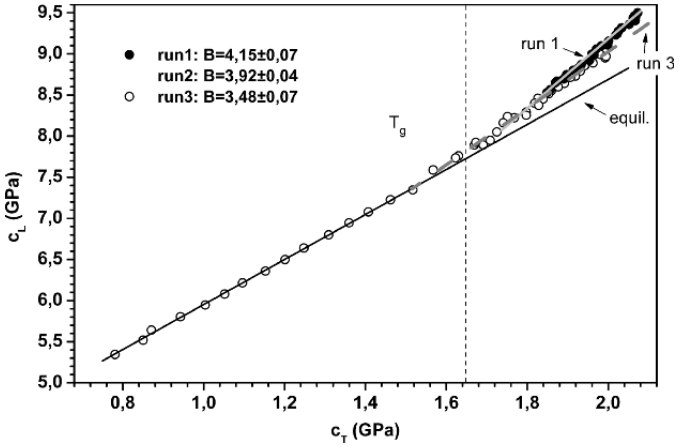


**Fig. 3.33.** $g$CR-representations for different consecutive quenching and heating cycles. All measurements were performed on heating. The full *straight line* represents the $g$CR for the equilibrium state. For further explanations, see text

within the temperature representation of the equilibrium glassy state. This result is based on at least 15 different quenching cycles. According to Ref. [97] the structural $\alpha$-relaxation shows a cut-off at the glass transition temperature (c.f. Sect. 3.4). It is therefore likely that the dynamical processes involved in the ageing process have little in common with the structural $\alpha$-relaxation process. We do not want to compare time constants found in the $g$CR representation during ageing in the glassy state with time constants reported for the hypersound velocities in the liquid state [97]. There is no hint for a direct connection between both processes.

Being convinced that the ageing process within the super-cooled liquid state discussed above has nothing to do with the $\alpha$-relaxation process the question about the reason for the violation of the $g$CR has still to be elucidated. As a matter of fact, the violation of the $g$CR is only observed if the quenching process starts at temperatures more than a hundred Kelvin above $T_g$ and is as fast as than $-200$ K/min. At that cooling speed usual glass structures cannot be formed. In our opinion, the supercooled liquid (with respect to the crystalline state) is driven into a further supercooled state sc2 but this time the super-cooling is related to the glassy state. The state sc2 behaves as a metastable glass. That the glassy state is the related preferential thermodynamic reference state to which the metastable state sc2 relaxes is evident from the experimental facts. The usual local molecular arrest at the intrinsic glass transition is impeded. The experimental data show, that the achieved metastable state sc2 has smaller shear stiffness than the glassy state, whereas the longitudinal modulus is, in comparison to that of the glassy state, not altered. In other words the sc2-state behaves "stiff" on compression but rather "soft" on bending the sample: the state sc2 behaves more liquid-like than a glass. As a matter of fact, heating up to the glass transition temperature erases any memory about the super-cooled state sc2.

In favour of this view are the facts that (i) the temporal evolution of the ageing process is much faster than the hypothetical $\alpha$-process of DGEBA in the temperature range $T_g > T > T_{gs}$, but very close to $T_g$ and that (ii) we found ageing well below the VFT temperature $T_o$. As a consequence, the liquid state of DGEBA seems to be a forbidden state below $T_{gs}$ and the glassy state, which is approached during the thermal ageing appears as an "equilibrium glassy state" of DGEBA for $T < T_g$. Of course we cannot exclude the existence of another energetically more favourable state, but if it exists, this state must be separated from our equilibrium glassy state by such high potential barriers that it is virtually inaccessible. In order to be observable in a Brillouin experiment, the molecular non-equilibrium excitations have to couple to the transverse and longitudinal polarized sound modes and their relaxation times have to be in a time-window accessible to this kind of experiment. It is worth noting that, if this coupling is weak or if the relaxation times are too fast or too slow in comparison to our experimental time scale, Brillouin spectroscopy is ineffective with respect to the test of ageing phenomena.

Studying the experimental results presented in this chapter, we can conclude as follows:

(i) Using appropriate thermal treatments, distinct glassy states with different macroscopic properties, like density or mechanical moduli can be realized.
(ii) In the glassy state there can exist relaxations (due to ageing) which are distinct from $\alpha$-, $\beta$-, $\gamma$-, etc-relaxations (see Sect. 3.4).
(iii) It seems that in structural glass-formers there exists an intrinsic glassy state.

(iv) the ideal glass transition temperature marks the stability boundary for the intrinsic glassy state and the super-cooled glassy states.

## 3.4 The Dynamic View of the Thermal Glass Transition

In this section we will analyse the glass transition and related phenomena which are due to the cross-over of the inverse probe frequency with the intrinsic $\alpha$-relaxation frequency of the glass-forming liquid.

It is usually believed by the glass community that the slowing down of molecular dynamics on approaching the thermal glass transition plays a crucial role for the physical changes appearing at the TGT [99–104], as well as at the glass transition predicted by mode-coupling theory [105, 106] etc. The dynamics associated with those molecular motions which are intimately related to the TGT are usually described by the VFT-law introduced in Sect. 3.1. This primary glass relaxation process is usually called $\alpha$-relaxation process. According to the schematic drawing in Fig. 3.34 the activation plot of the $\alpha$-relaxation frequency is strongly bent towards zero at the so-called VFT-temperature $T_0$ [103, 104, 107]:

$$\omega_\alpha = \tau_\alpha^{-1} = \omega_{\alpha 0} \cdot \exp\left[-\Delta G_\alpha / \left(R\left(T - T_o\right)\right)\right] \tag{3.42}$$

This phenomenological law holds true at least for temperatures $T > T_g > T_0$ and implies a divergence of the $\alpha$-relaxation time $\tau_\alpha$ at $T_0$. In Eq. (3.42) the parameter $\omega_{\alpha 0}$ is the attempt frequency displaying the molecular mobility at high temperatures and $\Delta G_\alpha$ is the activation free energy of the $\alpha$-relaxation process.

It is the trust in this divergence which has stimulated many researchers in the field of glass transition to believe in the kinetic nature of this phenom-

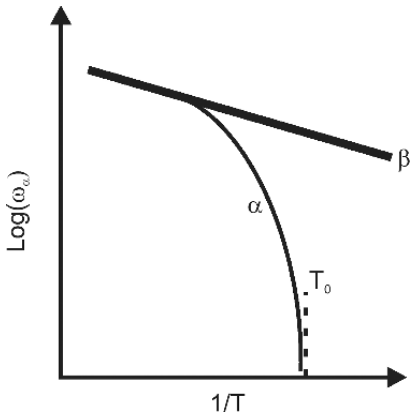


**Fig. 3.34.** Schematic representation of the VFT-law for the $\alpha$-relaxation and the Arrhenius-like behaviour of the $\beta$-relaxation

enon. This belief was supported by manifold observations of ageing processes in the pre- and post-transition temperature intervals of the operative glass transition temperature $T_g$. It should however be stressed, that these observations in favour of a purely kinetic interpretation of the TGT are no proof for any divergence of $\tau_\alpha$ but they are at best a proof for sufficiently large relaxation times in order to compete with usual experimental time constants $\tau_{\exp}$. Thus the real temperature behaviour of the $\alpha$-relaxation time in the limit of large experimental time constants is the fundamental problem. The question, whether $\tau_\alpha$ really diverges or remains finite, decides whether the "cross-over" problematic is unsolvable or just a quantitative problem of the experimentalists patience. This is the reason why it deserves huge interest and is the main topic of this section. Of course, besides the cooperative $\alpha$-relaxation process there may exist other relaxation processes which are thermally activated. In Fig. 3.34 such an Arrhenius-process is designated as $\beta$-process. This kind of relaxation processes is usually not affected by the glass transition.

The deviation of the VFT-law from the Arrhenius behaviour is an experimentally evident precursor of the thermal glass transition not only observed well above $T_g$ but which is found for quenched glass formers even clearly above the melting temperature $T_m$. That means that this precursor of the later TGT is already present in the glass forming material at temperatures at which the material has not decided whether it will densify by crystallization or densify by freezing. In so far the slowing down of the molecular dynamics described by a VFT-behaviour puts the question whether it can be interpreted as a general precursor for a transition into a dense solid state. Independently of the thermodynamic path the primary goal of a cooled liquid seems to be its densification and consequently, to find a state which is as densely packed as possible (close packing). Below the melting point two possibilities exist for this densification. (i) the crystallization and (ii) the thermal freezing. Since crystallization is usually a strong first order transition, the $\alpha$-relaxation is clearly no dynamical precursor for the crystallization process. This argument is supported by the fact that during the undercooling of a glass forming liquid, the crystallisation process is suppressed and the potential melting/crystallization process leaves no mark on the VFT-law. Since in a crystal the average position of the lattice molecules is fixed, the $\alpha$-relaxation process of the related liquid state usually disappears or is quantitatively different from that in the crystalline state. An example of the latter behaviour is DFTCE which has been discussed in the first section. Thus, the first order transition to the crystalline state can be interpreted as one efficient way to achieve the goal of dense packing. The remaining alternative, which is necessarily disordered, is the glassy state with random closed packing (rcp). Then the question occurs, if densification by crystallization changes fundamentally the $\alpha$-relaxation behaviour or even stops it, why should the $\alpha$-process be unaffected by the glass transition and in turn produce the "time-trap" discussed in the first section?

A further comparison between the glass transitions and structural phase transitions might be elucidating. So-called soft mode theories predict that the

lattice instability occurring at a structural phase transition is accompanied by a slowing down of the soft mode frequency to zero [108]. In reality this slowing down of the soft mode frequency to zero never happens, instead the phase transition takes place at a soft mode frequency well above zero. Assigning the experiences with soft modes of structural phase transitions in crystals to the potential behaviour of the $\alpha$-relaxation time the divergence of the $\alpha$-relaxation time $\tau_\alpha = 1/\omega_\alpha$ at the glass transition of a glass forming liquid is little probable. This argument is a further counter-indication against the "cross-over" argument but not a proof yet.

In order to elucidate the true $\alpha$-relaxation behaviour and its influence on phenomenological physical properties at the TGT, the temperature dependence of the latter within the pre-transitional phase close to $T_g$ has to be revisited. It is usually accepted that every liquid can be quenched to the glassy state. According to Sect. 3.1 "quenched glass formers" become supercooled below their melting temperatures whereas ideal glass formers can stay in their thermodynamic equilibrium state until the TGT. Fast cooling (quenching) of a glass forming liquid is accompanied by a decrease of its specific volume $\nu_l(T)$ according to the volume expansion coefficient $\alpha_{lsc}\,(T) = \alpha_l(T)$ (sc supercooled) of the equilibrium liquid. The specific volume in the supercooled liquid state $\nu_{lsc}(T)$ is in general higher than in the crystalline reference state $\nu_{lsc}(T) > \nu_{\mathrm{cryst}}(T)$. Thus, supercooling provides at first a deviation of the specific volume from that of the crystalline reference state but continues that of the thermodynamic equilibrium liquid into the undercooled liquid state. The linear temperature dependence of the specific volume found in the pre-transition temperature interval does not reflect the VFT-behaviour of the main glass relaxations. Only at lower temperatures, in a limited temperature interval, called glass transition interval, the thermal expansion coefficient changes rather abruptly from that of the equilibrium liquid state $\alpha_l\,(T)$ to that of the so-called glassy state $\alpha_g\,(T < T_g) < \alpha_l$ [109–111] (see Sect. 3.3). Ideal glass-formers behave in exactly the same way but transform from the equilibrium liquid state immediately into the glassy state without passing through a metastable pre-transition temperature interval. This means, that from a phenomenological point of view quenched- and ideal glass-formers do not differ from each other although they are in different thermodynamic states.

As a matter of fact, transport properties like the shear viscosity of fragile liquids behave in the same way. Quenched glass forming fragile liquids and ideal glass forming fragile liquids are accompanied by an increase of viscosity stronger than exponential (see Fig. 3.21) and do not reflect the behaviour of the equilibrium liquid at much higher temperatures [112–114].

It appears that the pre-transitional temperature interval as seen by the shear viscosity is much broader than that seen by mass density. From the viewpoint of shear viscosity one has to differentiate between two temperature regions: the rather large pre-transitional temperature interval in the liquid phase and the rather small glass transition zone (kink). The question arises about the reason why the transport of molecules should feel hindered much

more in the pre-transitional temperature interval than by usual thermal activation at much higher temperatures? Geszti [115] has introduced a phenomenological relation between the shear viscosity and the molecular dynamics

$$\eta_{44} = c_{44}^{\infty} \cdot \tau_{\alpha} \tag{3.43}$$

where $\tau_\alpha$ is again the relaxation time related to the TGT (Sects. 3.1, 3.3) and $c_{44}^{\infty}$ is the frequency clamped shear stiffness of a liquid. Equation (3.43) couples in some way the imaginary part ($\sim \eta_{44}$) of the complex shear stiffness of a mechanical continuum to a relaxation time $\tau_\alpha$. In the case of glass forming liquids it couples the solid state like behaviour $c_{44}^{\infty}$ of a liquid observed under frequency clamped conditions to its acoustic attenuation. Keeping in mind, that $c_{44}^{\infty}$ depends linearly on temperature in the pre-transitional liquid phase [116, 117], the more than exponential increase of $\eta_{44}$ with decreasing temperature must be due to molecular dynamics, i.e. the temperature behaviour of $\tau_\alpha$. From a formal point of view the observed saturation (kink) of $\eta_{44}$ at the glass transition might be due to either a saturation of the relaxation time $\tau_\alpha$ and/or to a saturation of $c_{44}^{\infty}$.

Combining Eq. (3.42) with Eq. (3.43) leads to

$$\eta_{44} = c_{44}^{\infty} \cdot \tau_{\alpha 0} \cdot \exp\left[\Delta G_{\alpha} / \left(R\left(T - T_o\right)\right)\right] \tag{3.44}$$

The strong bending of the activation plots of $\tau_\alpha$ and $\eta_{44}$ has been related to an increasing cooperativity [102] of the molecular motions in the pre-transition interval on approaching the TGT. That means, that in order to put one molecule or a molecular group in a better packed environment the molecules in the shell of next neighbours, in the shell of over-next neighbours and so on have to move cooperatively in order to allow for this improved packing. It is this cooperative molecular motion which allows even in the very dense packed state the combined rotational and translational molecular motion necessary for a further densification. Equation (3.44) implies that in a very dense state a further improvement of the density is more time consuming than in a less dense state.

The increases of the bending strength of $\tau_\alpha$ and $\eta_{44}$ also signalize an increase of fragility of the glass former. The magnitude of the temperature difference $|T_g - T_0|$ is a measure for the fragility of the glass former and amounts e.g. to about 40 K for polymers [101, 112, 113].

At this state of discussion the reader is confronted with the situation that the shear viscosity of a fragile glass former increases stronger than exponential on approaching $T_g$ and shows a pronounced kink (saturation) at this temperature. The mass density and the frequency clamped elastic shear stiffness behave linearly in the pre-transitional temperature interval but show a kink at $T_g$. Finally, in contradiction to the temperature dependence of the shear viscosity $\eta_{44}$ the relaxation frequency $\omega_\alpha$ is predicted to follow a VFT-law Eq. (3.42) across the operative glass transition temperature $T_g$ remaining continuous and differentiable at $T_g$ but with a divergence at $T_0 < T_g$. Thus,

a saturation of $\tau_\alpha$ at $T_g$ is not predicted by the VFT-law and obviously, it would contradict the "cross-over argument" given in Sect. 3.1. In other words, the unavoidable "time-trap" introduced in Sect. 3.1 as an argument in favour of the kinetic nature of the glass transition would become redundant if the VFT-law breaks down at $T_g$ (see also the discussion below).

Insisting for the moment on the validity of the VFT-law Eq. (3.42), the only way to force $\eta_{44}$ to saturate at $T_g$ is to saturate $c_{44}^{\infty}$. In this kinetic picture the saturation of $c_{44}^{\infty}$ is synonymous to reaching a non-equilibrium state. But there is also the possibility of structural changes at $T_g$.

The bridge to the "structural changes" eventually might be found in a phenomenological relation between the shear viscosity $\eta_{44}$, the free volume $V_f$ and the occupied volume $V_o$ given by Doolittle [100]

$$\eta_{44} = A \cdot \exp\left[\frac{b \cdot V_o}{V_f}\right] \tag{3.45}$$

where $A$ and $b$ are constants. Following the idea of free volume [118, 119] a volume element $V$ from the glass-forming liquid is then composed of $V = V_f + V_o$. According to Eq. (3.45) the temperature dependence of $\eta_{44}$ stems from the temperature dependencies of $V_f$ and $V_o$. Defining the related volume expansion coefficients $\alpha_f$ and $\alpha_o$ respectively

$$\alpha_f = \frac{1}{V_f}\frac{dV_f}{dT} \tag{3.46a}$$

and

$$\alpha_o = \frac{1}{V_o}\frac{dV_o}{dT} \tag{4.46b}$$

The volume expansion coefficient $\alpha$ and the relative temperature derivative of $\eta_{44}$ can be calculated yielding

$$\alpha = \frac{1}{V}\frac{dV}{dT} = \frac{1}{V}\frac{d\,(V_f + V_o)}{dT} = \frac{V_f}{V}\alpha_f + \frac{V_o}{V}\alpha_o \tag{3.47}$$

and

$$\frac{1}{\eta_{44}} \cdot \frac{d\eta_{44}}{dT} = \frac{b \cdot V_o}{V_f}\left\{\alpha_o - \alpha_f\right\} = \frac{1}{c_{44}}\frac{dc_{44}}{dT} + \frac{1}{\tau_\alpha}\frac{d\tau_\alpha}{dT} = \frac{1}{c_{44}}\frac{dc_{44}}{dT} - \frac{\Delta G}{R}\frac{1}{(T - T_o)^2} \tag{3.48}$$

In Eq. (3.47) the coefficient $\alpha_o$ measures the thermal expansion of the molecules due to thermal molecular excitations in an anharmonic potential and $\alpha_f$ measures the decrease of the free volume with decreasing temperature. Having again a look at the saturation of $\eta_{44}$ at $T_g$ either $\alpha_o$ or $\alpha_f$ or both in Eq. (3.48) have to change at the TGT.

At least for $\alpha_o$ a discontinuous change is only possible, if structural changes, preferably intramolecular structural changes, occur at the TGT. According to the "free volume theory" [118, 119] the free volume $V_f$ goes to a

constant minimum value or even zero at $T^* > 0$ K which means, that the corresponding volume expansion coefficient $\alpha_f$ goes to zero (random closed packing). A spontaneous disappearance of $\alpha_f$ at $T^*$ suggests a volume expansion coefficient $\alpha$ which changes discontinuously at $T^*$. A discontinuous change of the volume expansion coefficient is synonymous to the fact that the molecular interaction potential changes discontinuously at $T^*$. In any case $T^*$ has to be lower than the usual operative glass transition temperature $T_g$. In some theories $T^*$ is brought in connection with $T_{\mathrm{VFT}}$ but without any proof.

In addition, the right hand part of Eq. (3.48) relates the saturation of the shear viscosity to the saturation of the frequency-clamped shear stiffness. It remains the essential question: why does the free volume becomes constant at an operative glass transition temperature $T_g$ while the cooperative motions of the molecules still follow the VFT relation (see Eq. 3.48)? To answer this question a precise reinvestigation of the $\alpha$-relaxation process and of the shear stiffness $c_{44}^{\infty}$ in the pre-transitional temperature interval is imperative. Provided the generalized Cauchy relation (discussed in the previous section) holds true it suffices to investigate the longitudinal elastic modulus instead of the shear stiffness as the latter one is often difficult to measure.

For the sake of simplicity, the following discussion is reserved to ideal or almost ideal glass-formers. The $\alpha$-process can be observed with different experimental techniques. Dielectric-, mechanical- and thermal spectroscopy are amongst the most common techniques, as the complex dielectric susceptibility $\varepsilon^*(\omega)$, the complex elastic stiffness tensor $c_{ij}^*(\omega)$ or the compliance tensor $s_{ij}^*(\omega)$ with $(i, j = 1, 2 \ldots, 6)$ and the complex specific heat capacity $c_p^*(\omega)$ couple to the $\alpha$-process.According to irreversible thermodynamics the $\alpha$-relaxation time $\tau_\alpha$ depends on the thermodynamic boundary conditions and therefore on the measurement technique, at least in principle. In reality these different $\alpha$-relaxation times are often very close to each other.

As indicated in Fig. 3.35 the $\alpha$-relaxation frequency of polymethylmethacrylate (PMMA) follows in the pre-transitional temperature interval a VFT-law [120]. However, according to time domain Brillouin spectroscopy (TDBS, discussed in detail below) close to $T_g$ deviations from the VFT-law occur (open circles in Fig. 3.35) [121]. Just below $T_g$ a strong jump of $\omega_\alpha$ versus $1/T$ is observed (large open circle in Fig. 3.35). The Brillouin results from Fig. 3.35 yield the first relaxation data in a frequency range not attainable so far. Below the temperature related to this jump no further low frequency relaxations are observed even though they should be observable with TDBS if the VFT-law was still applicable. There seems to exist a cut-off of the $\alpha$-relaxation process. A $\beta$-relaxation process accompanying the $\alpha$-process behaves, as expected, Arrhenius-like.

According to the experimental technique in use (TDBS) all relaxation frequencies gathered until the cut-off are equilibrium data. Now there are two possibilities (see Fig. 3.36): (i) No further $\alpha$-relaxations exist. In that case the Brillouin data obtained at lower temperatures are equilibrium data (solid line in Fig. 3.36). (ii) the $\alpha$-relaxation frequency slows down much steeper than

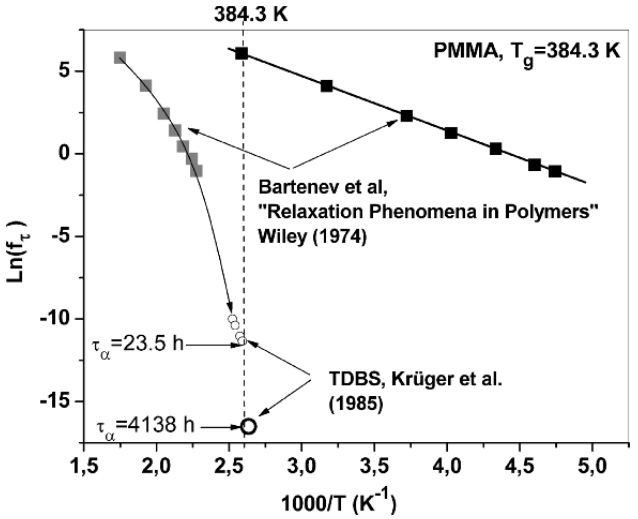


**Fig. 3.35.** Logarithmic $\alpha$- and $\beta$-relaxation frequencies of atactic PMMA as obtained by dielectric spectroscopy and TDBS

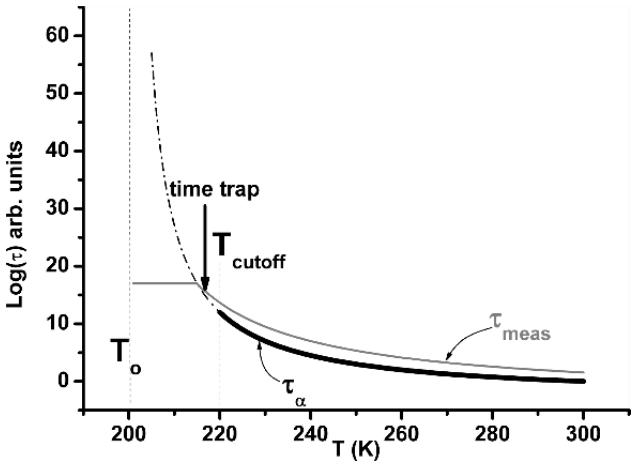


**Fig. 3.36.** Schematics of the evolution of the relaxation time of the $\alpha$-process $\tau_\alpha$ with an assumed cutoff at $T_{\rm cutoff} > T_0$. The time scale of the measurement $\tau_{\rm meas}$ is chosen in such a way that it is always larger than $\tau_\alpha$

predicted by the VFT-law. In that case measurements performed at lower temperatures are performed out of equilibrium not appearing in the figure.

Independently whether the $\alpha$-relaxation time really diverges or just becomes a large quantity, the kinetic view of the TGT implies that the operative thermal glass transition temperature reflects a cross-over between the relaxation time $\tau_\alpha$ with the time constant of the measurement $\tau_{\rm meas}$ (see also

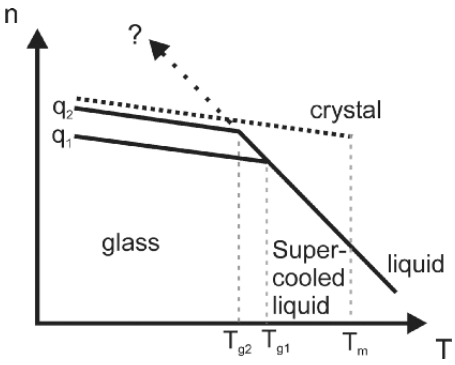


**Fig. 3.37.** Schematics of the cooling rate dependent behaviour of the TGT. $q_1$ $q_2$ cooling rates ($q_1 > q_2$); $T_{g1}$, $T_{g2}$ related glass transition temperatures; $T_m$ melting temperature of the crystalline state

Sect. 3.1). The operative glass transition temperature $T_g$ is defined (Fig. 3.36) implicitly by $\tau_{\text{meas}} \approx \tau_\alpha\,(T_g)$. This cross-over is the "time trap" mentioned in Sect. 3.1. In that case static or high-frequency clamped phenomenological properties like the mass density $\rho\,(T)$ or the refractive index $n\,(T)$ start to deviate from equilibrium (Fig. 3.37). When the cooling/heating rate $q$ of the experiment conflicts with the $\alpha$-relaxation times of the material the operative glass transition temperatures $T_g(q)$ depend on the cooling rate or more generally on the thermal history of the sample. In terms of the refractive index $n$ (Fig. 3.37) the operative glass transition is reached if during cooling with a rate $q_1$ the glass forming material is no more able to realize the equilibrium refractive index. If the cooling process develops too fast in comparison to the time needed to establish the equilibrium, a refractive index *inferior to the latter* is realized. If one even increases the cooling rate from $q_1$ to $q_2$, the operative $T_g$ shifts according to Fig. 3.37 to higher temperatures. It is worth noting that these bending features within the $n(T)$-curve are kinetic in nature.

It should be stressed again that there exist no experimental proofs for a divergence of $\tau_\alpha$. On adjusting $\tau_{\text{meas}}$ always in such a way that $\tau_{\text{meas}} > \tau_\alpha$ it will emerge from the experiment whether an intrinsic glass transition at a temperature $T_{gs}$ occurs or not and whether $T_g$ coincides with $T_0$. Only if the condition $\tau_{\text{meas}} > \tau_\alpha$ is always fulfilled a kinetically induced glass transition is avoided and the *time trap* is under control. In that case, a kinetically induced slope change of the temperature dependent refractive index is avoided and the question appears about the inherent temperature dependence of $n(T)$ below $T_g$.

In order to clarify this situation a convenient experimental scenario has to be chosen to recognize a non-diverging time trap so far it exists. A suitable technique is the above mentioned method of "**time domain Brillouin**

**spectroscopy**" (TDBS) [121, 122]. This technique probes the evolution of the hypersonic velocity stimulated by a step-like change of temperature.

Because of the high probe frequency this technique measures frequency-clamped elastic moduli in the vicinity of the TGT. Using TDBS the only relaxation process which can impose on the sound frequency response can originate in a time lag between the establishment of the sample temperature on one hand and the equilibrium hypersonic velocity on the other. It is worth noting that high-performance TDBS is sufficiently sensitive to resolve temperature jumps $-\Delta T$ as small as 2 K.

Using this technique the two main ingredients necessary to discover an actual cut-off of the $\alpha$-*process* in the glass transition region are: *a.) hypersonic probe frequencies which are sufficiently high in order to yield high-frequency clamped sound velocities in the pre-transitional temperature regime (frequency domain) and b.) the access to extremely low-frequent acoustic relaxations caused by instantaneous temperature changes (time domain).* For clarity Fig. 3.38 shows a schematic diagram displaying the development of the longitudinal elastic stiffness modulus $c_{11}(T)$ on cooling the sample stepwise from the liquid to the glassy state. At high temperatures the elastic properties are determined by the static longitudinal modulus $c_{11}^{s}$. At low temperatures $T < T_g$ the longitudinal modulus of the glassy state $c_{11}^{\text{glass}}$ is measured. Above $T \geq T_g$ adjacent to $T_g$ (the pre-transitional temperature regime) frequency clamped elastic moduli $c_{11}^{\infty}$ are measured.

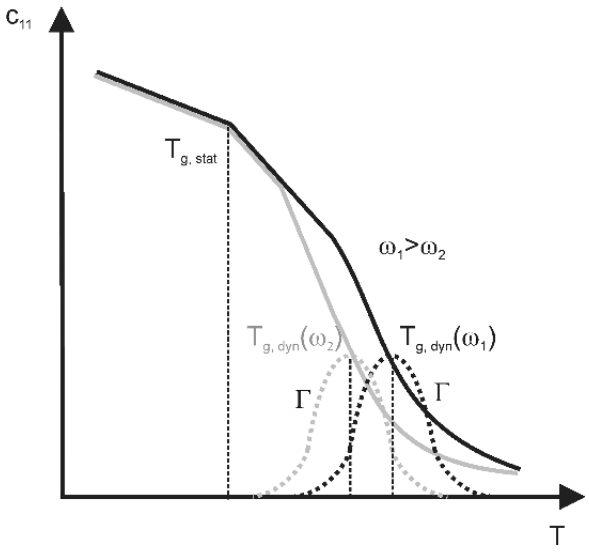


**Fig. 3.38.** Schematic representation of the static and dynamic glass transition. $T_{g,\,\text{stat}}$ static glass transition temperature, $T_{\text{g,dyn}}$ dynamic glass transition temperature (dependent on the measurement frequency $\omega$), $\Gamma$ related acoustic attenuation

The regime of elastic constants between $c_{11}^{s}$ and $c_{11}^{\infty}$ is a dispersion region. Within this region the elastic constant $c_{11}(T)$ is strongly temperature dependent and this is accompanied by strong acoustic attenuation ($\Gamma$). The attenuation maximum at the so-called dynamical glass transition temperature $T_g^{\mathrm{dyn}}$ depends on the probe frequency $\omega = 2\pi f$(e.g. ultrasonics) or alternatively on the acoustic wave vector $\boldsymbol{q}$ (e.g. Brillouin spectroscopy). This maximum determines the $\alpha$-relaxation time $\tau_\alpha$ by the relation

$$\tau_\alpha = 1/\omega \left(T_g^{\mathrm{dyn}}\right) \tag{3.49}$$

At Brillouin frequencies ($f \approx 10\,\mathrm{GHz}$) the hypersonic loss-maximum ($T = T_g^{\mathrm{dyn}}$) is often but not always located about 150 K above the TGT and the lower wing of that maximum ends well above $T_g$. In some cases the low-temperature wing of the hypersonic loss peak shows a cut-off directly at $T_g$ (s.a. Fig. 3.39) which means that hypersonic relaxation processes persist just until $T_g$. The fact that these relaxation processes are stopped by the TGT indicates the close relation with the primary glass transition, since secondary relaxations would not be affected by the TGT. *Therefore it seems that the TGT is not caused by the $\alpha$-process but rather that the TGT stops the freezing dynamics*. From Fig. 3.39 we find that in case of DGEBA the temperature difference between $T_g$ and $T_g^{\mathrm{dyn}}$ is only about 100 K. A further discussion of this feature will be given in the next section.

A central question concerns the temporal behaviour of static or frequency-clamped susceptibilities in the vicinity of the TGT. In terms of high frequency elastic stiffness data the question appears whether the kink in the sound velocity-temperature curves or in the elastic moduli-temperature curves is maintained at extremely slow cooling or whether it can be shifted succes-

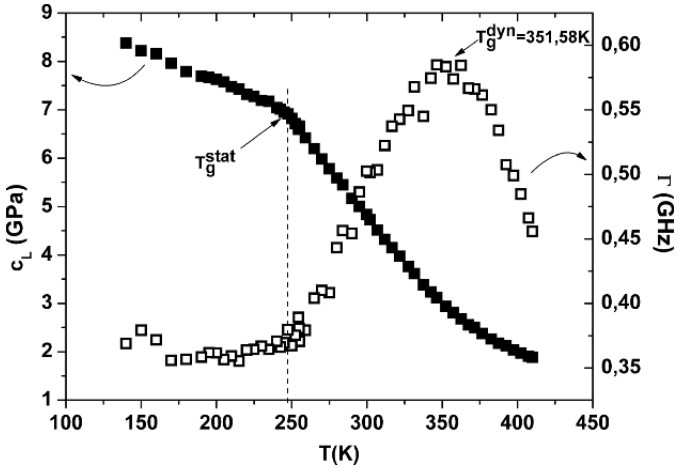


**Fig. 3.39.** Longitudinal elastic modulus $c_L$ and hypersonic attenuation $\Gamma$ versus temperature $T$ for the fragile glass former DGEBA

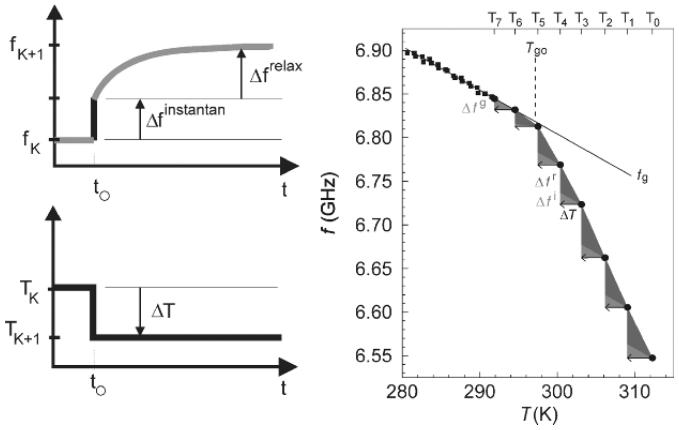


**Fig. 3.40.** Schematic drawing of the time domain BS. Left hand side: temperature step $T_k \rightarrow T_{k+1}$, related sound frequency response $f_k \rightarrow f_{k+1}$, separated in an instantaneous and a relaxing part. Right hand side: sound frequency $f$ vs. temperature $T$, dots representing measured values while the triangles symbolize the instantaneous and the relaxing sound frequency response after each temperature step. Below the operative glass transition temperature $T_{\mathrm{go}}$ only an instantaneous response is measured

sively to lower temperatures with a temperature limit determined only by the patience of the experimentalist.

Figure 3.40 shows schematically the approach of TDBS in case of polyvinylacetate (PVAc) [124–129]. According to Fig. 3.40 a temperature jump of $\Delta T = T_k - T_{k+1}$ is imposed on the sample. Simultaneously the sound frequency response is recorded as a function of time t at the fixed temperature $T_{k+1}$. Every record is performed to that end that the sound frequency response has reached its asymptotic value $f_{k+1}$. As indicated in Fig. 3.40 the complete sound frequency response consists of two parts, an instantaneous response $\Delta f^i$ and a relaxing response $\Delta f^r$. The instantaneous response is almost independent of the temperature $T_{k+1}$ and corresponds to the entire sound frequency response within the glassy state. This result indicates, that the instantaneous response of the liquid state reflects already the temperature coefficient of the longitudinal elastic stiffness of the glassy state. This means that the temperature coefficient of the instantaneous hypersonic response reflects already on the anharmonicity of the frozen state and supports the observation that the temperature coefficient of the longitudinal elastic constant within the glassy state does not depend on the thermal history of the sample.

The following investigations are based on TDBS and dielectric spectroscopy (DES). As usual DES has been performed in the plate condenser geometry at different temperatures in the range of 173 K– 393 K. The dielectric spectra are obtained for a frequency range between $f = 10^2$ Hz and

$10^5$ Hz and were fitted using Havriliak-Negami

$$\hat{\varepsilon}(\omega) = \varepsilon' - i\,\varepsilon'' = -i\,\frac{\sigma_{DC}}{\omega\,\varepsilon_0} + \sum_{k=\alpha}^{\gamma}\left[\frac{\Delta\varepsilon_k}{\left(1+(i\,\omega\,\tau_k)^{\nu_k}\right)^{\mu_k}} + \varepsilon_{\infty k}\right] \tag{3.50}$$

as a model function which in addition to the usual dipole relaxation processes $(\alpha, \beta, \gamma)$ of glass-forming materials includes a dc conductivity term. The quantities $\Delta\varepsilon_k$ designate the relaxation strength and the $\tau_k$ represent the related relaxation times. The $\varepsilon_{\infty k}$ are the frequency-clamped dielectric constants related to the different relaxation processes $k$.

Coming back to the time domain method of BS we need to describe the relaxing part of the frequency response in an analytic way. On approaching the TGT the relaxing part $\Delta f^r$ needs increasingly time to evolve (Figs. 3.41, 3.42). The temporal evolution of the hypersonic $\alpha$-relaxation process can be described by a Kohlrausch-Williams-Watts (KWW) law with a stretched exponential [102]:

$$f(T) = f^{\infty} - \left(f^{\infty} - f^{\text{inst}}\right)\cdot e^{\left\{-\left(\frac{t}{\tau_\alpha}\right)^{\beta}\right\}} \tag{3.51}$$

where $f^{\text{inst}}$ is the instantaneous frequency response, $f^{\infty}$ is the relaxed value and $\beta$ measures the distribution of the $\alpha$-relaxation time ($\beta = 1$ corresponds to monodisperse processes).

The average relaxation time is derived from

$$\langle\tau_\alpha\rangle = \frac{\tau_\alpha}{\beta}\cdot\Gamma\left(\frac{1}{\beta}\right) \tag{3.52}$$

where the Gamma-function yields the time-average of the distribution.

Every fit yields an average relaxation time and a limiting value for the relaxed sound frequency at the related temperature jump. The relaxed sound frequency data are shown in Fig. 3.40. Since the exact location of the intrinsic glass transition temperature, $T_{gs}$, was not known prior to the TDBS experiments, it was not possible to perform a temperature jump ending precisely on $T_{gs}$. In reality a temperature jump was performed which started slightly above $T_{gs}$ $(T_{gs}+\varepsilon)$ and which ended slightly below $T_{gs}$ $(T_{gs}-\varepsilon)$. Astonishingly, at $(T_{gs}-\varepsilon)$, that means already within the glassy state, a final sound frequency relaxation is observed (Fig. 3.43). At still lower temperatures further relaxations are not found. The asymptotic sound frequency value does definitely no more meet the linear extrapolation of the related sound frequency of the liquid state. This result was confirmed by estimating the potential relaxation frequency of the next temperature step within the glassy state. For this purpose the relaxation frequencies have been plotted in an activation diagram (Fig. 3.44). According to this estimation the relaxation frequency should have been observable but was not observed.

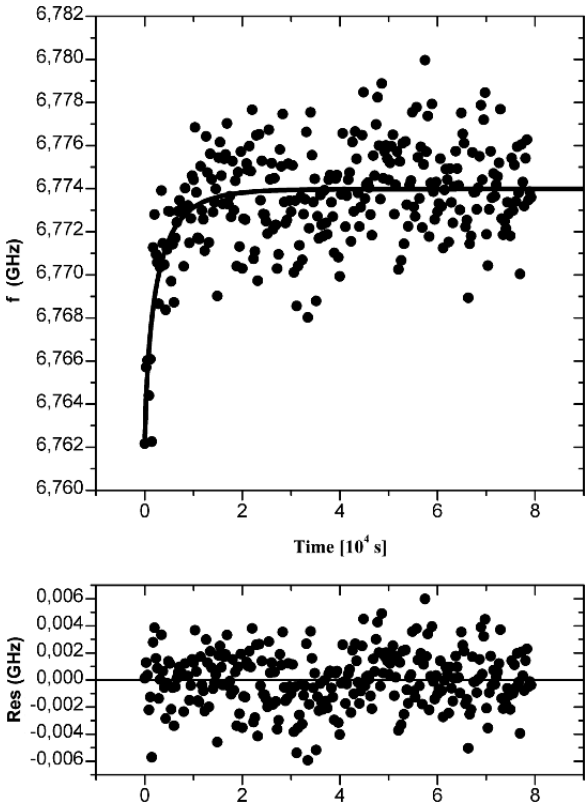


**Fig. 3.41.** Sound frequency response $f$ of PVAc after a temperature step from 307.7 K to 305.7 K. The full line represents a KWW-fit which residuals are shown below

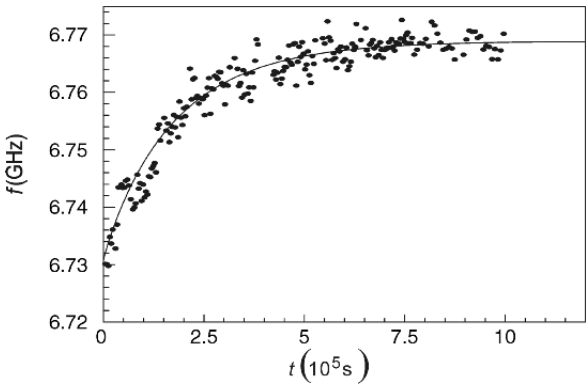


**Fig. 3.42.** Sound frequency response $f$ of PVAc after a temperature step from 303.3 K to 300.4 K. The full line represents the KWW-fit

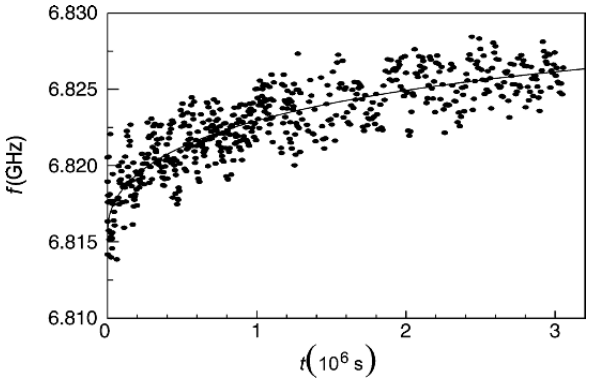


**Fig. 3.43.** Sound frequency response $f$ of PVAc after a temperature step from 297.5 K to 294.6 K. The full line represents the KWW-fit

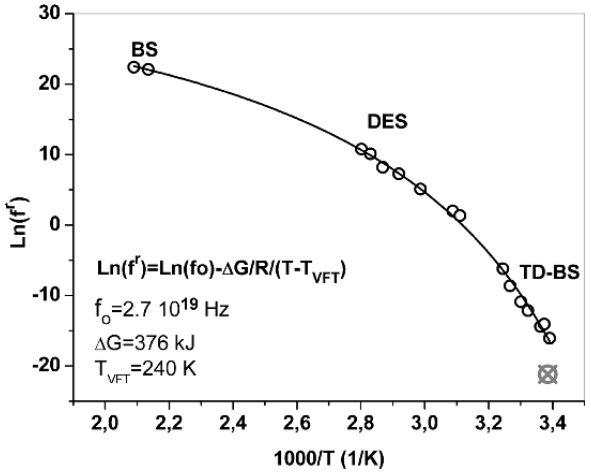


**Fig. 3.44.** Activation-plot ($\alpha$-relaxation frequencies vs. inverse temperature $1000/T$) for PVAc. The frequencies have been determined by BS, dielectric spectroscopy (DES) and time domain (TD) BS

According to these TDBS-data even in the limit of extremely slow cooling there appears a kink in the sound frequency – temperature curve at a temperature $T_{gs}$ (s.a. Fig. 3.40) which is close but slightly below the $T_g$ measured under usual conditions realized in Brillouin experiments. Indeed, the measured $T_{gs}$ is located well above $T_0$ predicted by the VFT representation.

The activation plot of Fig. 3.44 contains, beside dielectric data, Brillouin data measured in the frequency- as well as in the time domain. It seems that these data roughly follow a VFT law; however, a close statistical inspection contradicts this interpretation. Especially the low frequency relaxation frequencies behave Arrhenius- instead of VFT-like. The relaxation

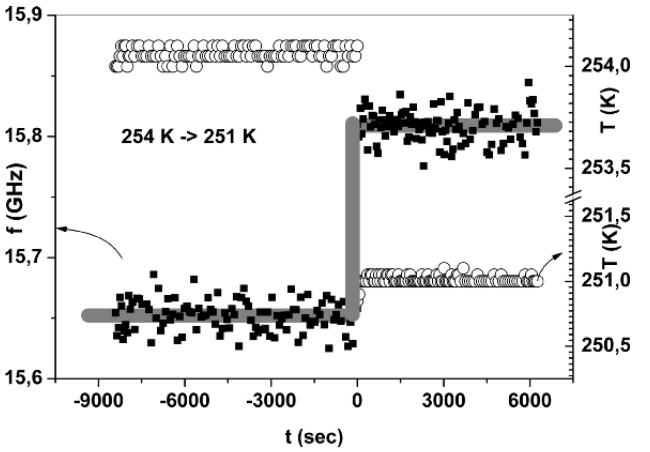


**Fig. 3.45.** Temperature step from 254 K to 251 K (right ordinate) at the reference time for the new temperature step $t = 0$ and the related response of sound frequency of DGEBA. The *horizontal grey lines* are least squares fits

frequency at the lowest temperature doesn't fit at all to the VFT-law. The relaxation frequency of this data point in the glassy state is two orders of magnitude lower than that of the preceding temperature.

The above discussed investigations on the TGT of atactic PVAc suggest the existence of an intrinsic glass transition at a well defined temperature $T_{gs}$. This intrinsic glass transition is evidenced by a strong anomaly of the $\alpha$-relaxation frequency at $T_{gs}$ and by a well defined kink in the sound frequency-temperature diagram.

Recent investigations of glass forming *diglycidyl ether of bisphenol A* (DGEBA) confirm for the primary glass relaxations [122, 123, 130] a strong deviation from the Vogel-Fulcher-Tamman (VFT)-behaviour. In the case of DGEBA the thermal glass transition point is evidenced by a kink in the sound frequency of the longitudinal polarized hypersonic mode and a sudden disappearance of the $\alpha$-relaxation time flattening out as a function of decreasing temperature.

The experimental procedure of TDBS shown schematically in Fig. 3.40 was also used for DGEBA. As for PVAc the temperature-time scenario was started well above the freezing process e.g. at $T \geq T_{gs} + 10$ K and the phonon spectra were accumulated for a sufficiently long time $t$ in order to be sure that the sound velocity (frequency) $v$ ($f$) has relaxed to its equilibrium value $v^{\infty}$ ($\propto f^{\infty}$) of the liquid state.

Figure 3.45 demonstrates that a "temperature step" of $\Delta T = -3$ K at 254 K produces no relaxations of the sound velocity response at all. Consequently, the sound velocity response is as fast as the temperature step experimentally realized. Approaching $T_{gs}$ and making a temperature step from 249 K to 247 K (Fig. 3.46) the sound velocity response is no more instan-

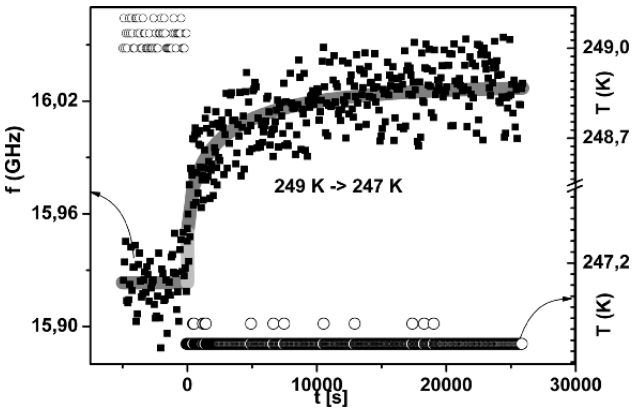


**Fig. 3.46.** Temperature step from 249 K to 247 K (*right scale*) and related sound frequency response of DGEBA (*left scale*). (For further explanations, see text)

taneous but shows a time lag. As for PVAc it was found that close to $T_{gs}$, the sound frequency response can be divided into two parts: an instantaneous response $f^{\text{inst}}$ which responds as fast as the temperature equilibrates and a relaxing part that can be described by the Kohlrausch-Williams-Watts law Eq. (3.51) [101].

The temperature step from 243 K to 241 K (Fig. 3.47) yields a decreased total sound velocity response but no more hint for any relaxation process. From the relaxation times measured at the foregoing temperature steps a hypothetical relaxation time has been estimated for the step from 243 K to 241 K. This estimated sound velocity versus time relaxation curve is also shown in

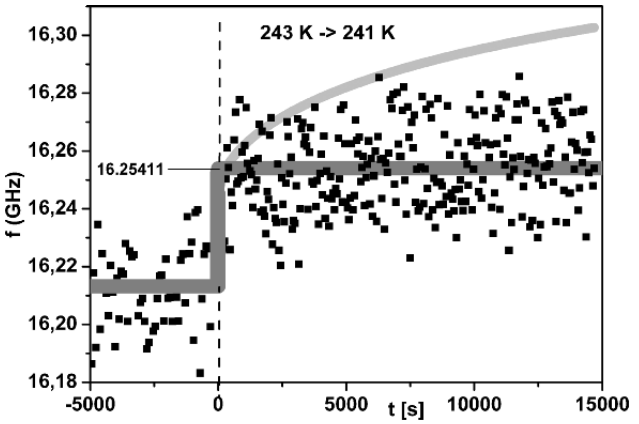


**Fig. 3.47.** Sound frequency response of DGEBA after a temperature step from 243 K to 241 K. The *horizontal dark gray lines* is a linear least-squares fit. The *light gray curve* gives an extrapolation to fluid conditions. (See text for further explanations)

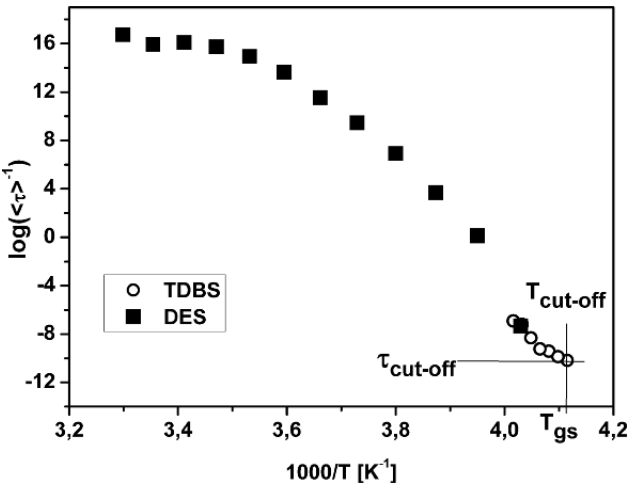


**Fig. 3.48.** Activation-plot of the inverse averaged $\alpha$-relaxation times of DGEBA as measured by DES and TDBS

Fig. 3.47. From this estimate, it can be concluded that at least this kind of relaxation should have been observable if it existed. This result implies that under the given conditions in DGEBA below 243 K, no $\alpha$-relaxation process exists anymore.

The values calculated there for $\langle \tau_\alpha \rangle$ are presented for all measured temperature steps in Fig. 3.48. The step from 245 K to 243 K is the last temperature step still showing a relaxing sound-frequency response as a consequence of the step-wise temperature excitation. Accordingly, the subsequent temperature step from 243 K to 241 K shows only an instantaneous sound velocity response of the glassy state (Fig. 3.36). It is therefore natural to identify $T_{gs} = 243$ K as the intrinsic TGT (see Subsect. 3.5).

Astonishingly, the sets of relaxation times as derived from the DES and TDBS agree quite well with each other, within the margin of error. Taking into account different thermodynamic boundary conditions, irreversible thermodynamics would in principle have predicted different relaxation times for different external variables involved in the relaxation process. As expected at higher temperatures, the $\alpha$-relaxation behaviour as a function of $1/T$ is compatible with the expected VFT-relation. However, on approaching $T_{gs}$ the activation plot flattens out (Fig. 3.48) and shows a cut-off at 243 K indicating a sudden disappearance of the $\alpha$-relaxation process. At the same temperature the $f(T)$-curve shows a kink which, according to the genesis of the sound-frequency data is neither due to the cross-over of the experimental time scale with the $\alpha$-process nor obscured by it.

The main conclusion of the current chapter is that the main glass relaxation process, the $\alpha$-relaxation process, does not follow the VFT-law through the glass transition down to a VFT-temperature $T_0$. TDBS investigations on

three different glass forming liquids show that the $\alpha$-relaxation process exhibits a cut-off well above the VFT-temperature $T_0$. This means, that the "cross-over" argument does not hold for these three materials and that the glass transition temperatures obtained from the TDBS-procedure are intrinsic freezing temperatures specific for each of the three materials.

## 3.5 Static Properties at the Thermal Glass Transition

Taking into account that the TGT in canonical glasses affects predominantly their mechanical properties, one could argue that these properties are suitable probes in order to elucidate the mechanism of the quasi-static glass transition and eventually of the ideal glass transition proposed above [131, 132]. In this context **Brillouin spectroscopy** (BS) is an experimental method of particular interest because BS measures mechanical properties of the glass former in a completely non-destructive manner and without mechanical contact with the sample [7,8,133–136]. Moreover, even some ten degrees above $T_g$, BS measures the instantaneous elastic response in the "slow motion regime" in the sense that $\tau_\alpha \omega \gg 1$ holds ($\tau_\alpha$ structural relaxation time, $\omega$ sound frequency). The latter property provides the possibility to determine, in addition to the hypersonic properties, the refractive indices from pure Brillouin spectroscopic data [137]. Unfortunately, the quasi-static GT is usually only hinted by an undramatic, more or less sharp, kink in the sound frequency vs. temperature curve, which yields no hint for a non-ergodic instability. In addition, this kink depends to a certain extent on the thermal history of the sample, see Sect. 3.1. A main task for the experimentalist is therefore to find experimental scenarios which give answers to the question whether there may exist an intrinsic glass transition and a glass transition temperature which is experimentally accessible and at which some static phenomenological properties change in a well-defined manner.

Static phenomenological properties should be measured either with a static measurement technique in internal thermodynamic equilibrium or with dynamical techniques in frequency-clamped equilibrium. In terms of irreversible thermodynamics, internal equilibrium means that the relevant internal variables $\xi_k$ can be completely expressed by the external thermodynamic variables $\xi_k = \xi(p, T, \vec{E}, \ldots)$. Dynamic measurements of phenomenological properties in internal equilibrium imply

$$\omega \cdot \tau_k \ll 1 \quad \forall \quad k \tag{3.53}$$

where the $\tau_k$ are the structural relaxation times connected to the internal variables $\xi_k$ and where $\omega = 2 \cdot \pi \cdot f$ is the probe frequency of the dynamic experiment [139]. In contrast, clamped equilibrium means that for the probe frequency involved all relevant internal degrees of freedom $\xi_k$ are frequency-clamped, i.e. $\xi_k(\omega) = \text{const}$ for $k = 1, 2, 3 \ldots$. In relation to the relevant

relaxation times $\tau_k$ and the probe frequency $\omega$ the condition of clamped internal variables then means that the system is excited in the so-called "slow motion regime"

$$\omega \cdot \tau_k \gg 1 \quad \forall \quad k \tag{3.54}$$

The measurements of static phenomenological properties like specific volume (mass density) or the properties of the static specific heat capacity are experimentally extremely difficult to realize, especially in the vicinity of the thermal glass transition. Rehage et al. [131], Schwarzl et al. [132] and Kovacs et al. [140, 141] e.g. have demonstrated the experimental difficulties which have to be overcome in order to determine the specific volume across the transition from the liquid to the glassy ("solid") state. One of the problems concerns sticking of the sample to the container walls and accompanying internal stresses. Similar difficulties occur in the course of adiabatic calorimetry measurements [142]. On the other hand this latter technique is the only one which gives reliable information about the static specific heat capacity in the vicinity of the TGT.

Dynamical measurements of clamped phenomenological susceptibilities like dielectric constants measured at optical frequencies, $\varepsilon_{\text{opt}} = n^2$ ($n$ refractive index), or clamped elastic constants, $c_{ii}^{\infty}$, measured at hypersonic frequencies in the vicinity of the glass transition yield equilibrium (frequency-clamped) properties provided the temperature changes necessary in order to reach the thermal glass transition (TGT) are sufficiently small and are performed sufficiently slowly (see Sect. 3.4). Figure 3.49 shows the typical behaviour of the longitudinal and of the shear stiffness of a bisphenol A (I1) [143, 144]. The experimental fact that the shear stiffness $c_{44}^{\infty}$ is observed at Brillouin frequencies above $T_g$ proves that both moduli $c_{44}^{\infty}$ and $c_{11}^{\infty}$ are measured in the "slow motion" regime. They are therefore high frequency-

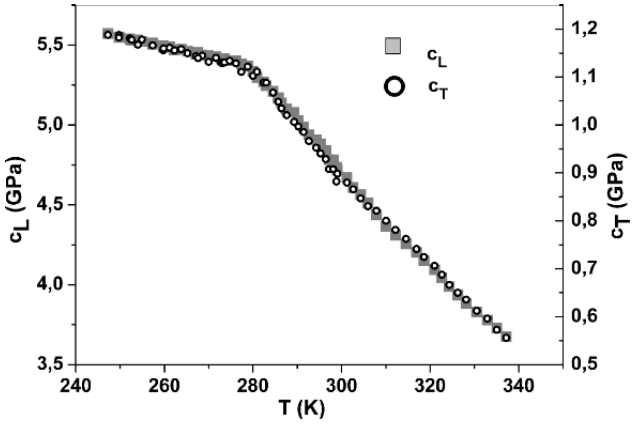


**Fig. 3.49.** Sound velocity of the longitudinal (*full symbols*) and shear (*open symbols*) mode of I1

clamped equilibrium properties with respect to the longitudinal and shear deformation. Both curves show a kink-like temperature dependence at the operative glass transition temperature $T_g$. The question whether the operative kink temperature $T_g$ can be shifted to lower temperatures for infinitely slow cooling decides about the existence of an intrinsic glass transition at a well-defined temperature. The fact that both elastic stiffness curves could be brought to coincidence using an appropriate scaling of the coordinate axes signifies that I1 follows the generalized Cauchy-relation in the whole temperature range, which is an additional proof for the absence of hypersonic relaxations.

The method of time domain Brillouin spectroscopy (TDBS) introduced in Sect. 3.4 is one of the key experimental methods to study the static aspects of the thermal glass transition. TDBS enables us to investigate the elastic constants with respect to the mechanical deformation in the slow motion regime. In the course of Brillouin investigations of the TGT the only remaining external variable is then the temperature $T$. Indeed a sudden temperature change $\Delta T$, necessary in order to approach the TGT at $T_g$, can initiate a relaxation of the sound velocity (sound frequency) with a relaxation time $\tau_\alpha$ which increases on approaching $T_g$ from above. Thus TDBS is able to probe mechanical relaxations with respect to temperature changes $\Delta T$ necessary to investigate the TGT. Particularly, TDBS is able to clarify in which temperature regime above and below $T_g$ thermo-acoustic relaxations are active and especially whether they do persist below $T_g$. The first systematic investigations were reported for polyvinylacetate (PVAc). The investigations on PVAc and other glass-forming materials were performed persuing the following scheme: At some ten Kelvin above $T_g$ hypersonic frequency measurements were started in the slow motion regime $\omega \cdot \tau_\alpha \gg 1$. In order to approach the glassy state small temperature steps -$\Delta T$ (see Fig. 3.50) were performed and the isothermal sound velocity (-frequency) at fixed wave vector was simultaneously recorded until saturation of the velocity/frequency response. Only the fully relaxed sound velocity data were then used for the sound velocity/temperature plot. Figure 3.50 shows the results for PVAc. The most important result of these TDBS investigations is that there exists a well-defined temperature $T_g$ where every $\alpha$-relaxation disappears, or at least spontaneously increases its value by several orders of magnitude. It is worth noting that $T_g$ is well above the hypothetical VFT-temperature $T_0$.

In order to prove that the hypersonic measurements were really performed in the slow-motion regime $\omega \cdot \tau_\alpha \gg 1$ the opto-acoustic dispersion function ($D$-function, Eq. (3.55), s.a. Sect. 3.2) was measured with BS and compared with high performance refractive index measurements. If hypersonic relaxations are present the $D$-function shows a convex deviation from the refractive index curve. The maximal deviation occurs at that temperature where $\omega \cdot \tau_\alpha = 1$.

$$D(T) = \sqrt{\frac{\left(\frac{f^{90R}}{f^{90A}}\right)^2 + 1}{2}} \tag{3.55}$$

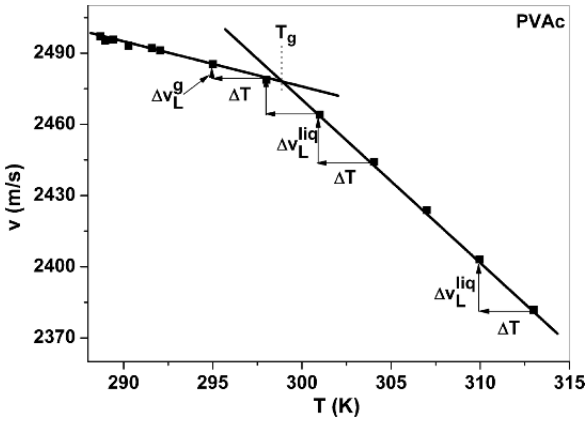


**Fig. 3.50.** Sound velocity of the longitudinally polarized sound mode of PVAc measured with TDBS. $\Delta T$ temperature jump, $\Delta v_L^{\mathrm{lic},\,g}$ relaxed sound velocity response in the liquid (liq) and the glassy (g) state

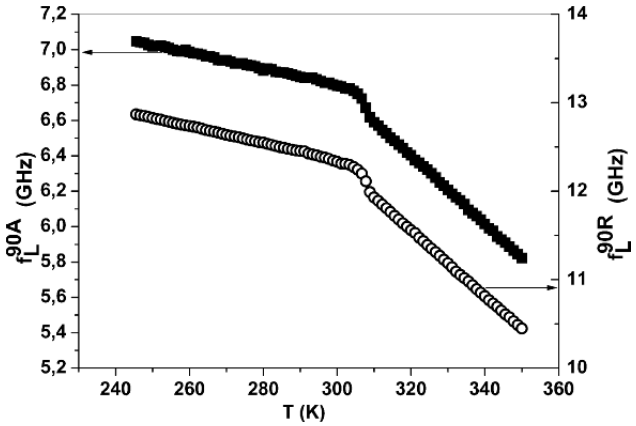


**Fig. 3.51.** Temperature dependence of the hypersonic frequencies of PVAc measured on heating after extremely slow cooling (see Fig. 3.50) using the 90A- and 90R-scattering geometry

The $D$-function was derived from simultaneously determined sound frequencies measured in the 90A- and in the 90R-scattering geometry (Sect. 3.2) and Fig. 3.51.

Since the sound frequencies presented in Fig. 3.51 were measured on heating after an extremely slow cooling of the sample into the glassy state in the course of the TDBS experiment mentioned above, both sound frequency curves show an overshoot (bumper) in the temperature regime of the TGT. This metastability occurs because the material was cooled much more slowly

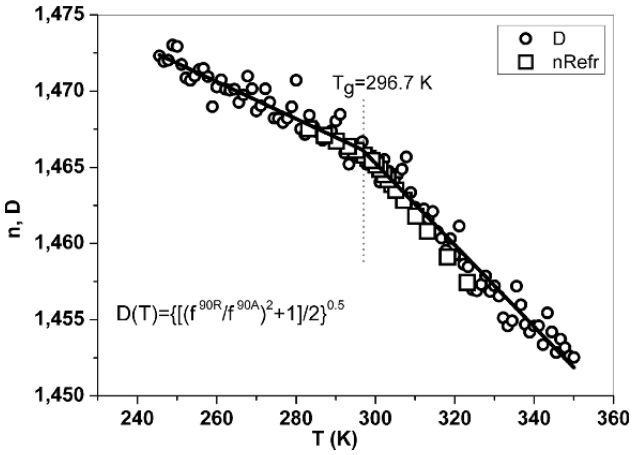


**Fig. 3.52.** Temperature dependence of the opto-acoustic dispersion function ($D$-function) and the refractive index function ($n$-function) of PVAc

to the glassy state (over months) than heated up during the BS measurement (5 days) (see Fig. 3.4).

The refractive indices were measured on step-like cooling over two months using an Abbé refractometer (Fig. 3.52). Within the margin of error the $D$-function coincides with the refractive index function $n(T)$ yielding $D(T) = n(T)$ (Fig. 3.52). Since the $D$-function is derived from two independently but simultaneously measured sound frequency curves the larger data scatter of this curve in comparison to the $n(T)$-curve is comprehensible. In the margin of error the glass transition temperatures measured with both techniques are identical. In consequence in the temperature range of this investigation any hypersonic relaxations or optical relaxations are either absent or act the same way on the two phonons measured in the 90A- and 90R-scattering geometry.

It is extremely important to note that the two "bumpers" at $T_g$ shown in Fig. 3.51 are absent in the $D$-function (Fig. 3.52). These bumpers are of course signs for metastability or even for instability and depend on time and temperature. The reason for the disappearance seems to be a common factor which guides the evolution of $f_L^{90A}(T)$ as well as of $f_L^{90R}(T)$.

Taking into account that the $D$- and the $n$-function are in very good agreement (Fig. 3.52), the disappearance of the overshoot within the $D$-function is not expected to be an artifact of the data-analysis.

Keeping in mind this result, the effect of $q$-vector dependent relaxations on the temperature dependence of the $D$-function has to be investigated. Figure 3.53 shows the temperature dependence of the $D$-function of PVAc up to 530 K. According to Eq. (3.55), $D(T)$ coincides with $n(T)$ outside of relaxation regimes and deviates in a convex manner from the n-function. This is exactly what happens for PVAc above 350 K. The maximum convex deviation

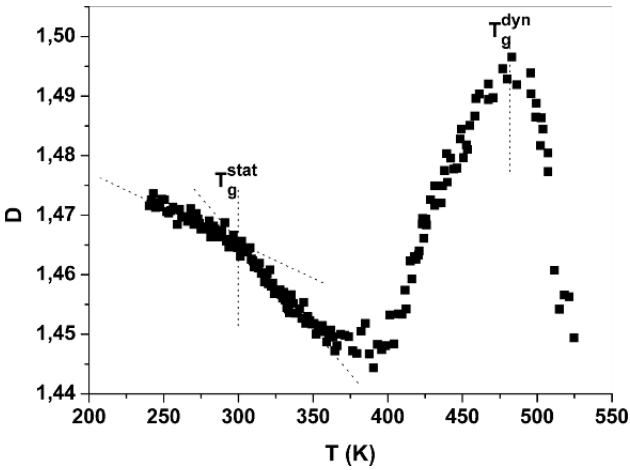


**Fig. 3.53.** Opto-acoustic $D$-function of PVAc measured over a wide temperature range including the range of the dynamical glass transition at hypersonic frequencies

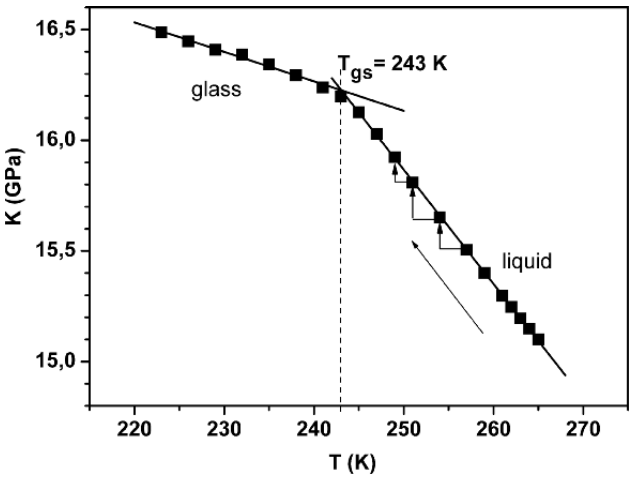


**Fig. 3.54.** Relaxed compressional modulus as a function of temperature for DGEBA. The *straight lines* are fit curves. The *arrow* indicates the cooling regime

from the $n$-function defines the dynamic glass transition temperature at the Brillouin frequencies involved in measurement.

In order to elucidate the nature of the TGT the temperature behaviour of the $D$-function within the glassy state ($T < T_g$) deserves a final discussion: (i) As the $D(T)$- and the $n(T)$-functions coincide totally within the glassy state, $(D(T) - n(T)) = 0$, there is no evidence for acoustically relevant relaxations in the GHz-frequency regime. (ii) The $D(T)$-representation suppresses slowly varying effects of metastability present in the constituting functions,

i.e. the related phonon frequencies. In other words, the $D(T)$-function acts as a filter for changes in acoustic properties due to metastability and displays only equilibrium properties. It is therefore concluded that the $D(T)$-function displays equilibrium properties for the glassy state of PVAc and that in particular the kink at $T_g$ is not due to a cross-over between intrinsic relaxation times and the experimental time scale. Accordingly, the glass branches of the sound frequency (velocity) curves are not metastable.

In literature the TGT is often brought in close relation to the so-called $\alpha$-relaxation process. The $\alpha$-relaxation frequency $f^\alpha$ seems to slow down, according to the VFT-law if the temperature of the glass-forming sample approaches $T_g$ and seems to go to zero if the temperature approaches the so-called VFT-temperature $T_o$ (see Sect. 3.1). Hence it appears that the $\alpha$-relaxation process is in some way the leading process for the glass transition. This holds true for the dynamical glass transition well above the static glass transition when the probe frequency crosses the relaxation frequency. The situation close to the TGT is much more complicated.

At first, the true behaviour of $f^\alpha(T)$ in the vicinity of $T_g$ is an open question and depends evidently on the experimental probe. Moreover, the predicted VFT-behaviour is somewhat similar to the behaviour of a soft mode frequency at a structural phase transition. Keeping in mind that soft-mode frequencies never really go to zero it is thus interesting to know what happens with the $\alpha$-relaxation frequency close to $T_g$.

Secondly, if the $\alpha$-relaxation follows a VFT-behaviour on one hand and if the TGT is investigated with a high frequency probe on the other hand, there should be no probe frequency which could cross the $\alpha$-relaxation frequency. Consequently the only possibility would be that the waiting time between subsequent temperature-changes is too small compared to the thermoelastic relaxation time. Only the latter event could eventually provide a kinetic influence on the glass transition. So the question arises again what happens if this latter kinetic effect is experimentally avoided and what happens in this case with $\alpha$-relaxation processes.

Having established for DGEBA simultaneously the kink-like anomaly in the curve of the frequency clamped sound velocity and the cut-off of the $\alpha$-relaxation process (Sect. 3.4) [145] we conclude that PVAc is not an exception but that also for this material there exists an intrinsic glass transition approximately 20 K above the VFT-temperature $T_o$. Taking into account that the average relaxation time for the temperature jump to $T_{gs} = 243$ K amounts to 5.4 hours and that sound frequency changes in the range of some per mille have to be resolved unambiguously during hours and / or days after a single temperature jump, it is obvious, that the experimental proof of a sample-inherent glass transition process is experimentally not an easy task.

In order to elucidate in addition to the extremely low frequency relaxation behaviour the behaviour at hypersonic frequencies we have simultaneously investigated the sound velocity $v_L$ and the related hypersonic attenuation $\Gamma_L$ of DGEBA over a wide temperature range (Fig. 3.55).

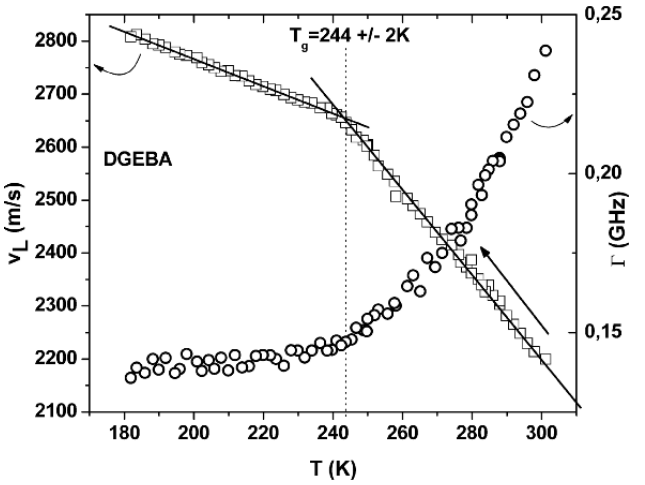


**Fig. 3.55.** Temperature dependence of the longitudinal sound velocity $v_L$ and the hypersonic attenuation $\Gamma_L$ of DGEBA

Astonishingly, and in contrast to the attenuation behaviour of many other glass forming liquids, the hypersonic attenuation maximum comes down directly at the TGT. In other words, for DGEBA until the TGT there exist hypersonic relaxations, which slow down only at $T_g$. For this material it is therefore not true that all $\alpha$-relaxation times are extremely large close to the glass transition. From the TDBS- and the dielectric measurements it is clear that there exist $\alpha$-relaxations which slow down to 5.4 h, but at the same time the hypersonic attenuation behaviour clearly demonstrates the existence of pronounced hypersonic relaxations which only stop at the TGT. So the question arises, why these high frequency relaxations are stopped by the TGT if the TGT itself is believed to be caused by these relaxations?

Taking into account the importance of this observation for the interpretation of the TGT it is interesting to look for further examples, which show a similar relaxation behaviour. A very impressive example for the evolution of the hypersonic dynamics around the TGT was published recently for an epoxy (EPON) [146, 147].

Figure 3.56 shows the hypersonic velocity and the opto-acoustic dispersion function of EPON, both as a function of temperature. The hypersonic velocity behaves as expected in showing a rather sharp kink at the TGT. Really astonishing is the temperature dependence of $D$-function. Within the glassy state $D(T)$ behaves as expected like $n(T)$. Precisely at $T_g$ the $D$-function changes the slope, indicating the onset of hypersonic relaxations. Again this result is in contradiction to the general statement, that close to $T_g$ all relaxations connected to the glass transition should be of very low frequency. Rather, the observed hypersonic relaxation process dies out at the TGT. Whether the existence of this hypersonic relaxation process is without any doubt, its

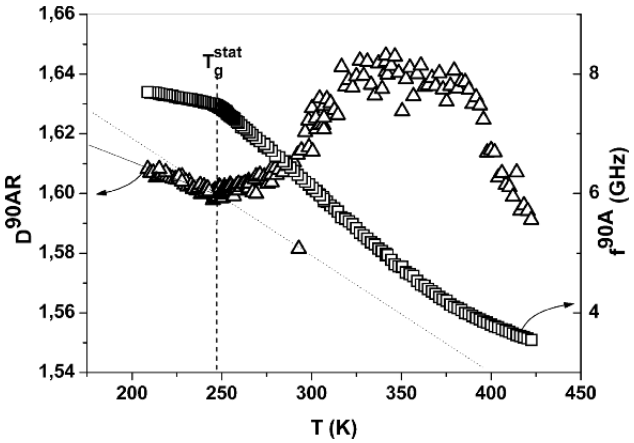


**Fig. 3.56.** Hypersonic velocity and opto-acoustic dispersion function ($D$-function) for EPON, see text for details

origin is not yet clear. From the fact that the $D$-function emerges from two phonon-frequencies related to two acoustic wave vectors of different magnitudes it follows that the convex deviation from the n-function (Fig. 3.56) is due to a relaxation process. The distribution of the relaxation process seems to be either double-valued or alternatively extremely wide.

The complex dendrimer molecule G1 shown in Fig. 3.57 is a model molecule for a glass-forming material, which cannot crystallize [148]. Consequently, the glass transition of the material G1 cannot be masked by a recrystallization process. Whereas the longitudinal sound velocity behaves as expected as a function of temperature (Fig. 3.58), the temperature dependence of the hypersonic attenuation behaves in a strange manner. On approaching the TGT from above the hypersonic attenuation $\Gamma$ increases permanently until $T_g$ and remains constant within the glassy state.

The hypersonic attenuation $\Gamma$ is rather small in the whole temperature regime but shows a minimum at $T \sim 215\,\mathrm{K}$. The attenuation then increases with decreasing temperature towards the TGT. Assuming that the Brillouin measurements are performed in the slow-motion regime this increase can hardly be explained. Another cause for this attenuation could be acoustic scattering on internal stresses, which are built up if the temperature approaches the TGT. Once the dendrimer is frozen, the elastic scattering remains constant. But even if this explanation is not true it is clear that the lack of certain dynamics below the TGT is responsible for the constancy of the sound attenuation.

Having elucidated the relation between the static and the dynamic properties at the TGT a reinvestigation of the relation between kinetic and static properties is reasonable. Taking the temperature and time dependence of the high-frequency longitudinal elastic modulus $c_L^\infty$ as a reference, Fig. 3.59

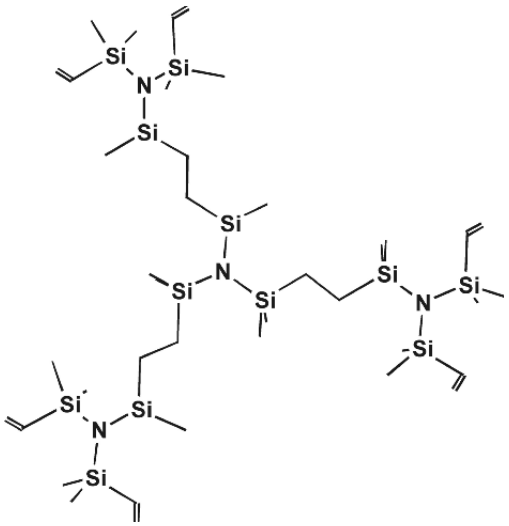


**Fig. 3.57.** Two-dimensional projections of the structure of the Dendrimer G1. The carbon atoms and the hydrogen atoms have been omitted

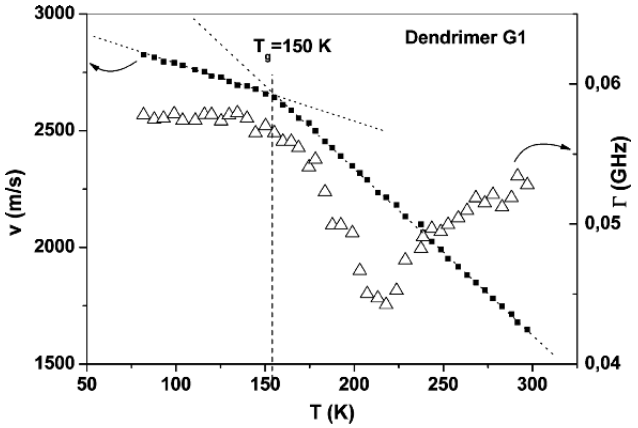


**Fig. 3.58.** Temperature dependence of the sound velocity $v$ and the hypersonic attenuation $\Gamma$ for G1

displays schematically the expectation for this temperature-time dependence from the kinetic point of view on the left side and the experimental observation on the right side. The equilibrium liquid branch of $c_L^\infty$ $(T \geq T_g)$ has a unique tangent

$$m_\ell = \frac{\partial}{\partial T} c_L^\infty \, (T \geq T_g) = \text{const} \, .$$

At sufficiently high temperatures the glass-forming material is in the liquid state. As it is well known [149] the packing of the liquid state is almost solid-

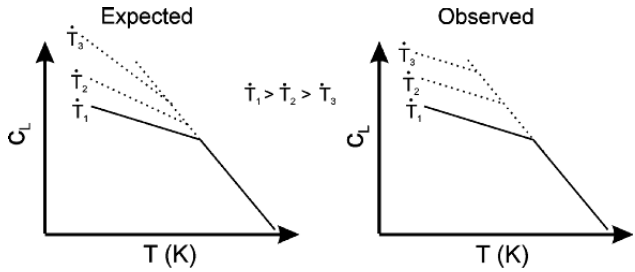


**Fig. 3.59.** *Left*: expected behaviour of the temperature dependence of the elastic modulus $c_L$ around the TGT due to different cooling rates. *Right*: actually observed behaviour of this temperature dependence around the TGT

like, the same holds true for the local order. However, there remains some free volume, which gives space for some random flight of the molecules. Since at the TGT the specific volume behaves continuously (see Sect. 3.3) the liquid and the glassy state have the same specific volume at $T_g$.

Assuming a rather high reference temperature $T$ and a probe frequency $f$ which is sufficiently high providing that still a high frequency clamped elastic modulus is measured, the related $c_L^\infty(T \geq T_g)$-value is located on the equilibrium liquid branch. At slow cooling the measured $c_L^\infty$-data remain on this liquid branch. At a sufficiently large cooling rate $\dot{T}_1$ the $c_L^\infty$-curve bends away from the equilibrium liquid curve (Fig. 3.59). It should be stressed that this bending occurs despite the fact that the molecular dynamics related to the formation of the glassy state is already frequency-clamped. Consequently, what is observed is the temperature-rate dependence of a frequency-clamped quantity $c_L^\infty(\dot{T})$. The question arises then about the tangent of the $c_L^\infty$-curve during fast cooling and its isothermal recovery after quenching. According to all existing experimental data, the change of the tangent $\partial c_L^\infty(T)/\partial T$ behaves continuously as a function of time and of temperature. In the temperature interval between the start of the quenching process and the TGT the absolute value $c_L^\infty(T, \dot{T})$ and the tangent $\partial c_L^\infty(T)/\partial T$ converges versus the related equilibrium values of the liquid state. The relaxation time of this isothermal recovery process increases strongly on approaching the TGT (see Sect. 3.4). The question arises, following a kinetic view of the glass transition, what happens below $T_g$ with $c_L^\infty(T \leq T_g, \dot{T})$ and $\partial c_L^\infty(T \leq T_g)/\partial T$? Intuitively, a smaller cooling rate $\dot{T}$ should bring these values closer to the expected equilibrium data which are located on the extrapolated liquid branch (Fig. 3.59, left).

However, that's not what is observed! A schematic drawing of what actually is observed is given on the right side of Fig. 3.59. Away from the immediate departure from the equilibrium curve, the $c_L^\infty(T < T_g, \dot{T})$-data are located on a straight line with a tangent $m_g = \partial c_L^\infty(T)/\partial T = \text{const}$ which is independent of the cooling rate $-\dot{T}$. It is worth noting that the $y$-axis intercept depends on $-\dot{T}$ and decreases with the increase of the cooling rate. In the other limit,

given by $\dot{T} \to -0$, the kinetic view demands again that the $c_L^{\infty}(T, \dot{T} \to -0)$-values are located on the extrapolated liquid branch. The latter argument demands a discontinuous change from $m_g$ to $m_\ell$ for $T \to T_g$ as well as for $T \to 0$. The independence of $m_g$ from the temperature rate $-\dot{T}$ for $T < T_g$ demands a special structure of the glassy state: Independently from the cooling rate there is formed a glassy state which is randomly closed packed (rcp) where the rcp-state is rigid ($c_{44} > 0$). This rcp-state includes voids (free volume) which are surrounded by the rcp's. The temperature gradient of this state is determined by the temperature gradient of the rcp-matrix which has to be $m_g$. Consequently, there exists a spontaneous transition from the liquid state to a well defined matrix state with a temperature gradient $m_g$ and additional free volume which does not contribute to the thermal expansion of the glassy material but which depends on the cooling rate. This transition from the liquid to the glassy matrix state takes place at the TGT. Therefore, with respect to the free volume the glassy state depends on the cooling rate $-\dot{T}$. With respect to the matrix the glassy state is unique. For very low cooling rates the free volume goes to zero and there remains a well defined glassy state.

The freezing process of glass forming liquids in porous glasses shows a further aspect of the static and dynamic behaviour of the acoustic properties at the TGT. Dibutylphtalate (DBP) is known to be a good glass-forming liquid with a freezing point at about 175 K. Porous glasses with average pore diameters of 20 nm and 2.5 nm were filled with DBP. The glass transition behaviour was investigated with temperature modulated differential scanning calorimetry (TMDSC) and with Brillouin spectroscopy (Fig. 3.60).

First of all there seems to be no $T_g$-shift between DBP-filled porous glasses of 2.5 nm and 20 nm. This result is astonishing for DBP in nanopores of 2.5 nm

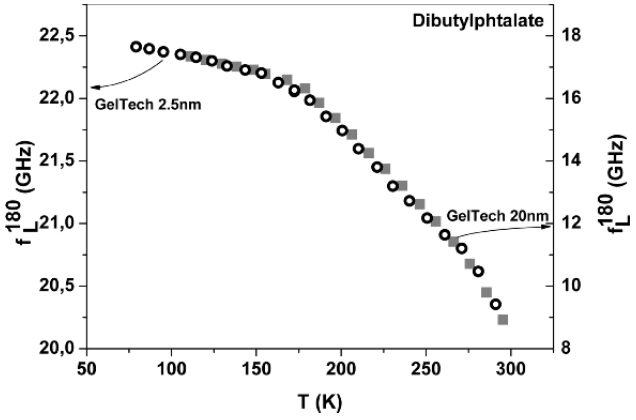


**Fig. 3.60.** Temperature dependence of the hypersonic frequency of DBP in porous glasses with pore diameters of 20 nm and 2.5 nm

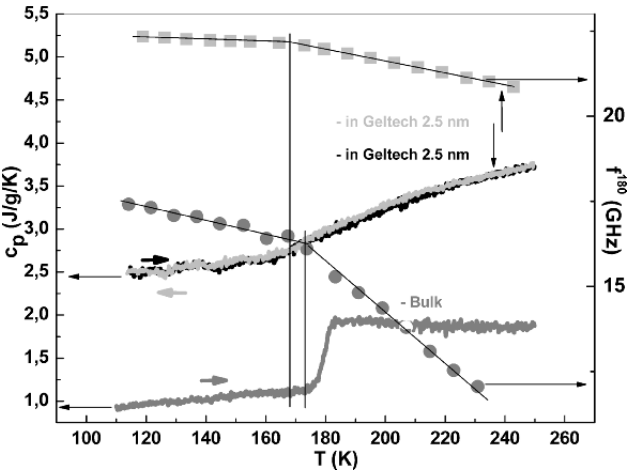


**Fig. 3.61.** Temperature dependence of the specific heat capacity and of the hypersonic velocity of DBP in the bulk and in a porous glass of a pore diameter of 2.5 nm

because there seem to exist mainly DPB molecules which are in direct contact to the wall of the pores. These "DBP-wall molecules" are usually believed to be immobile. Consequently, from a dynamic point of view they should not undergo a glass transition, but they obviously do. Brillouin data as well as specific heat capacity data clearly show a TGT for pore diameters of 2.5 nm. For pore diameters as large as 20 nm there are of course other than "DBP-wall molecules". For this reason a change of the glass transition behaviour is expected between 2.5 nm- and 20 nm diameter pores.

Figure 3.61 shows a comparison of specific heat capacity data and Brillouin data between the bulk DBP and DBP in glass pores of 2.5 nm diameter. For these two extreme situations a clear $T_g$-shift of 5 K and a change in the phenomenological behaviour of the $c_p'$ – curves are observed, whereas the sound frequencies show for both cases the usual kink-like behaviour. Since the amount of DBP per unit-volume in the pore-system is much smaller than in the bulk material the kink in the pore system is much weaker than in the bulk system. The anomaly of the $c_p'$ – curve for DBP in 2.5 nm pores can be interpreted as a kink whereas for the bulk DBP a step rather than a kink is observed.

This step-like behaviour (Fig. 3.61) is usually interpreted as the transition from the fast motion- to the slow motion regime, i.e. the inflection point of the $c_p'$ - curve appears at $2 \cdot \pi \cdot f \cdot \tau \cong 1$. Consequently, steps within the $c_p'$ – curve should be accompanied by a maximal loss, i.e. a $c_p''(T)$– maximum. Figure 3.62 shows that the expected $c_p''(T)$ – maximum is indeed present but does not scale at all with the height of the jump of the $c_p'$ – curve. The jump amounts to about 1 J/g/K whereas the peak height of the $c_p''(T)$– maximum amounts to

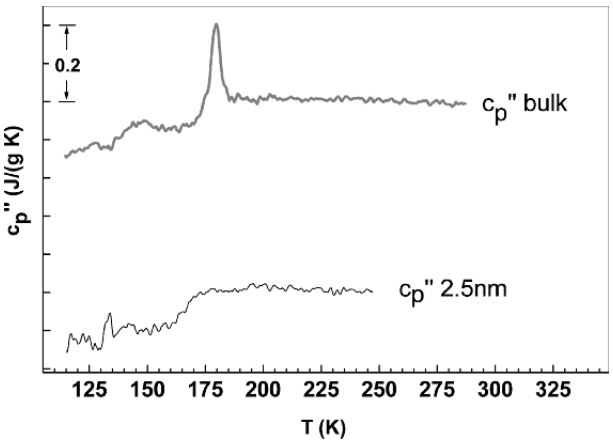


**Fig. 3.62.** Temperature dependence of the imaginary part $c_p''$ for bulk material of DPB and for DBP in a porous glass with pore diameters of 2.5 nm

0.2 J/g/K. On the other hand the width of the peak is rather small so that a broad distribution of relaxation times can be excluded. Consequently, it seems likely that the measured $c_p'$ – curve is composed by a static $c_p$-background and an additional dynamic relaxation anomaly (probe frequency $f = 16.7\,\mathrm{mHz}$).

Comparing the $c_p'$ – and $c_p''(T)$ – data measured for the bulk with those for the nano-pores of 2.5 nm an astonishing result is obtained (Fig. 3.62). The relaxation maximum in $c_p''(T)$ for DBP in 2.5 nm pores has completely disappeared. This result would be in complete agreement with the idea mentioned above that in 2.5 nm pores all molecules are pinned wall-molecules. This idea seems to be in contradiction with the existence of a TGT. If something freezes below $T_g$ it should be allowed to move to some extent above $T_g$. Together these arguments imply that the expected relaxation process lies outside the temperature interval of investigation. If this latter argument holds true, the related TGT has nothing to do with a cross-over between the intrinsic relaxation time and probing time! Consequently the $c_p$-curve measured for DBP in 2.5 nm pores represents static specific heat capacity data. Another consequence concerns the general role of the $\alpha$-relaxation process: the $\alpha$-process is not a prerequisite for the thermal glass transition! It is worth noting that similar behaviours were found for glycerol, I1 and salol in porous glasses of different pore diameters [150].

## 3.6 The Role of Non-Linear Elastic Behaviour at the Thermal and Chemical Glass Transition

In Sect. 3.1 it was shown that orientational glasses, i.e. single crystals with frozen orientational disorder, show the same anomalies within their phenom-

enological properties at their thermal glass transition as structural glass formers do. Above the glass transition of these crystals with orientational disorder the material is dynamically disordered with respect to the molecular orientation [151–155]. However, the positional order is given, at least on average. At the glass transition of these dynamically disordered crystals, the disorder of the molecular orientation freezes but the positional order is maintained. The specific volume, the refractive index and the high-frequency clamped elastic constants show a kink-like behaviour at the glass transition temperature $T_g$ (Figs. 3.6, 3.7). The habitual concept of free volume, which goes to a minimum at $T_g$, in connection with a kind of molecular percolation, becomes meaningless for these orientational glasses. The concept of a molecular interaction potential which changes spontaneously at $T_g$ seems to be more useful [156–162]. Therefore it makes sense to reinvestigate the glass transition in structural glass formers under the aspect of a spontaneously changing molecular interaction potential.

In spin glasses the non-linear behaviour of the order parameter plays a significant role [cf. 163]. Whereas the linear susceptibilities just show a kink, the nonlinear susceptibilities have been found to diverge in the vicinity of the freezing temperature $T_g$. This latter fact yields an additional argument to study non-linear elastic properties around the TGT of structural glasses.

Usually non-linear elastic properties are not easy to measure. This holds especially true for the glass transition zone of structural glasses in which the material transforms from the liquid to the "solid" state. A quantity which reflects non-linear elastic properties on one hand [cf. 157] and which can be determined exclusively from Brillouin spectroscopic data [164, 165] on the other hand are the acoustic **mode-Grüneisen parameters** (MGP) [157]. To our knowledge there exist no theoretical predictions for the temperature behaviour of the MGP's at the glass transition of structural glasses. In an isotropic solid the MGP relates the sound frequency of a $\boldsymbol{p}-$ polarized sound mode of a given wave vector $\boldsymbol{q}$ to its mass density $\rho$ [10].

$$\gamma(\boldsymbol{p},\boldsymbol{q}) = \frac{\partial Ln(f(\boldsymbol{p},\boldsymbol{q}))}{\partial Ln(\rho)} \tag{3.56}$$

Since for isotropic materials there exist only longitudinally and transversely polarized modes ($\boldsymbol{p} = L, T$) we use in the following the notation $L$ and $T$. It is expected that the concept of the MGP can be extended to acoustic waves propagating in liquids, and that within the solid or glassy state, the MGP [166] varies only slightly with temperature. $\gamma_L$ of a liquid still reflects anharmonic properties and structural changes of the liquid state [59,156–158,160,166,167].

There exist only a few Brillouin investigations on the temperature dependence of the MGP at the TGT [156, 164, 165]. Brody et al. [156] investigated polystyrene by Brillouin spectroscopy and reported at $T_g$ a small step of the MGP defined by Eq. (3.56). However, because of their rather large margin of experimental errors they did not arrive at a definitive statement concerning the step-like behaviour of $\gamma_L$. In Ref. [164, 165] the observed discontinuities

of $\gamma_L(T)$ at the glass-transition temperatures $T_g$ of polymethylmethacrylate, polystyrene and polyvinylacetate were related to a change of the molecular interaction forces. The discontinuity of $\gamma_L$ of polystyrene was found to be 4.3 which is by a factor of 3.6 larger than that reported in Ref. [156]. This illustrates some of the difficulties to determine reliable data for MGP's.

In order to determine a MGP, given by Eq. (3.56), one has to study the relative change of the mode frequency $f_{L,T}$ as a function of a relative change of mass density $\rho$. Usually this is realized by changing the pressure $p$ or the temperature $T$ of the sample yielding

$$\gamma_{L,T}(x) = \frac{\rho(x)}{f_{L,T}(x)} \frac{\partial f_{L,T}(x)}{\partial \rho(x)} = \frac{\delta_{L,T}(x)}{\alpha(x)} \tag{3.57}$$

with

$$\delta_{L,T}(x) = \frac{1}{f_{L,T}(x)} \frac{\partial f_{L,T}(x)}{\partial (x)} \tag{3.58}$$

and

$$\alpha(x) = \frac{1}{\rho(x)} \frac{\partial \rho(x)}{\partial (x)} \tag{3.59}$$

with $x$ being the pressure $p$ or the temperature $T$. If $x = T$, then $\alpha$ is the usual thermal volume expansion coefficient. $\alpha(x)$ is a generalized volume expansion coefficient and $\partial_{L,T}(x)$ a generalized frequency coefficient.

It is important to remember that BS probes the acoustic modes at GHz-frequencies. In consequence, BS measures around the TGT predominantly frequency clamped acoustic properties, i.e. the glass forming material under investigation behaves even in the liquid state solid-like with respect to the probe frequency. Modern BS is able to measure acoustic mode frequencies with a relative accuracy of better than 0.1%. This accuracy is sufficient for the determination of MGP's.

More difficult is the determination of sufficiently accurate mass density data. In the context of density measurements around the glass transition the technical problems are significantly increased due to the fact that the sample passes from the liquid to the solid state or vice versa. Of course measurement techniques for these two states need to differ from each other. This problem of accuracy becomes reinforced through the sticking of the sample on the container wall and the accompanying internal stresses. A serious additional problem of accuracy occurs if mode frequencies and mass density data are not measured under precisely the same external conditions. In case that the mode frequencies and mass densities are measured on different samples at different choices of temperatures or pressures an interpolation or curve fitting is needed in order to create values for $f_{L,T}$ and $\rho$ at the same temperatures or pressures. Since the behaviour of MGP's is studied in the vicinity of the TGT, different cooling conditions of the samples in use may destroy the validity of the calculated result. The same holds true for inhomogeneous samples (inhomogeneities may arise from internal stresses). Then the physical information

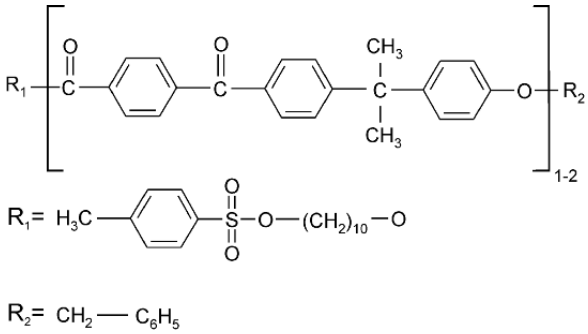


**Fig. 3.63.** Chemical formula of the oligoarylate mixture I2

about the mode frequency and the mass density is obtained from different sample volumes.

A suitable way to overcome most of the problems mentioned above is to obtain the information about the phonon frequencies and the mass density at the same time and temperature or pressure from almost the same sample volume. This is possible using high-performance Brillouin spectroscopy (BS) in the 90A- and the 90R- or 180-scattering geometry. The combination of these scattering techniques provides simultaneously the desired frequencies of the acoustic modes and refractive index data as a function of temperature $T$ [18, 19].

The Lorentz-Lorenz relation

$$\frac{n(T)^2 - 1}{n(T)^2 + 2} = r \cdot \rho(T) \tag{3.60}$$

yields the necessary relation between the refractive index $n$ and the mass density $\rho$. Taking the specific refractivity $r$ as a constant, the generalized expansion coefficient $\alpha(T)$ can be calculated from

$$\alpha(T) = \frac{6 \cdot n(T)}{n(T)^2 - 1)(n(T)^2 + 2)} \cdot \frac{\partial n(T)}{\partial T} \tag{3.61}$$

Calculating the frequency coefficient $\delta_{L,T}(T)$ directly from the measured sound frequencies and using the data given by Eq. (3.54) for the volume expansion coefficient $\alpha(T)$, the MGP's $\gamma_{L,T}(T)$ can be determined according to Eq. (3.57). Whereas the MGP's in the glassy state are clearly connected to anharmonic behaviour, the interpretation in the regime of the clamped fluid is more difficult because of the possible influence of entropic degrees of freedom.

The following analysis of MGP's was made for an oligoarylate mixture which will be called I2 (Fig. 3.63) for convenience. The Brillouin data were measured on slow cooling and the sound frequencies $f_{L,T}^{90A}$ and $f_{L}^{90R}$ were determined simultaneously. Figures 3.64 to 3.66 show the raw data.

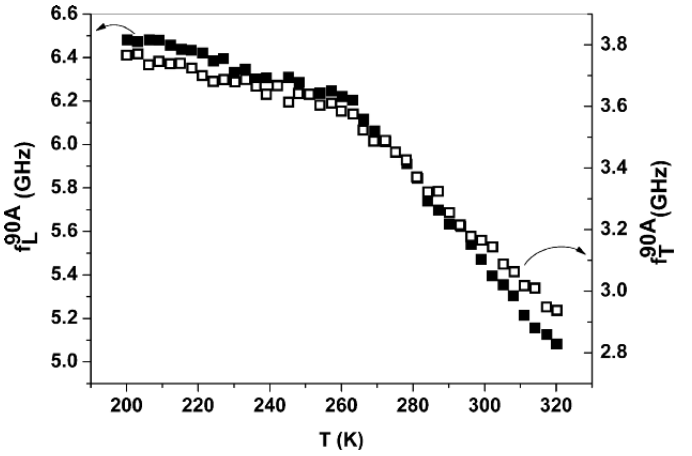


**Fig. 3.64.** Temperature dependence of the longitudinal and transverse 90A-mode of the oligoarylate mixture I2

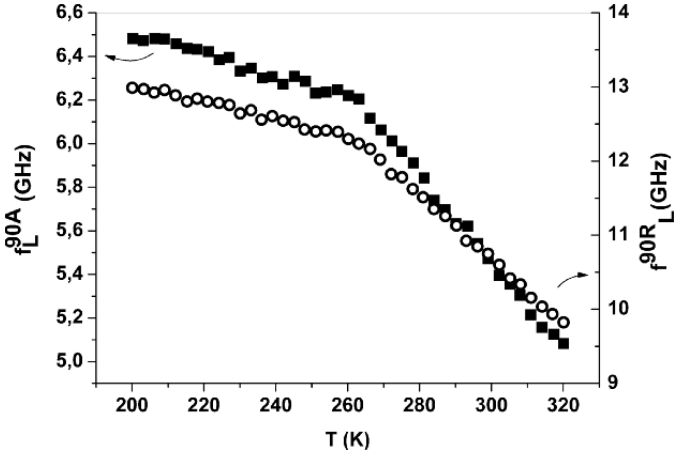


**Fig. 3.65.** Temperature dependence of the longitudinal 90A- and 90R-modes of the oligoarylate mixture I2

The quasi-static TGT is at about 262 K. Up to 320 K the shear phonon could be detected without major difficulties. The opto-acoustic dispersion function ($D$-function) could be derived from the 90A- and the 90R-scattering geometry (Figs. 3.65, 3.66). According to Fig. 3.66 the $D$-data have been interpreted as data for the refractive index. This is reasonable since the refractive index measured with an Abbé refractometer (crossed circle, $nD$) is in accordance with the $D, n$-value obtained from BS.

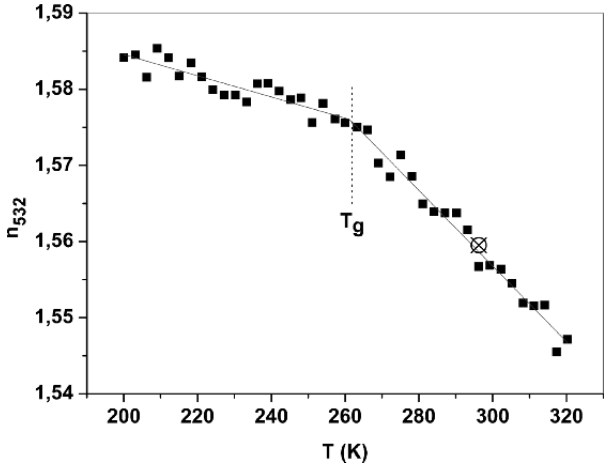


**Fig. 3.66.** Temperature dependence of the refractive index $n$ of I2 as measured by the $D$-function. The crossed circle represents a value measured by Abbé-refractometry

As for other oligomeric glass formers, the square of the acoustic mode frequencies fulfill a generalized Cauchy relation (Fig. 3.67) with a slope of almost 3 as usual (see Sect. 3.3).

The calculation of the longitudinal and transverse mode-Grüneisen parameters poses some numerical problems. Due to the scatter of the measured sound frequency and the refractive index data numerical differentiation gave no reliable results for the frequency coefficient $\delta$ and the volume expansion coefficient $\alpha$. In order to obtain reliable results the measured data were first interpolated and then smoothed (moving average) to a sufficient degree. Figure 3.68 shows the sound frequency data treated in this way.

The immediate vicinity of the TGT has been removed from the numerical treatment because of a possible misleading interpretation of the kink feature. Figure 3.69 displays calculated data for the refractive index and the volume expansion coefficient using the Lorentz-Lorenz relation Eq. (3.53). The data of the immediate vicinity of the TGT have been again removed from the data. The refractive indices obtained from the $D$-function correspond to an optical wavelength of 532 nm and not to $nD$.

Finally, Fig. 3.70 displays the temperature dependence of the longitudinal and transverse acoustic MGP's $\gamma_L(T)$ and $\gamma_T(T)$. In the margin of error both MGP's are identical and behave jump-like at the TGT. The magnitude of the jumps $\Delta\gamma_L$ and $\Delta\gamma_T$ of the mode Grüneisen parameters are of the order of 20%. The tangent of the MGP's is larger in the fluid phase which may be due to the aforementioned entropic influences in the fluid phase.

The question arises about the significance of these results for the nature of the TGT of structural glass formers. If we interpret the TGT as a purely ki-

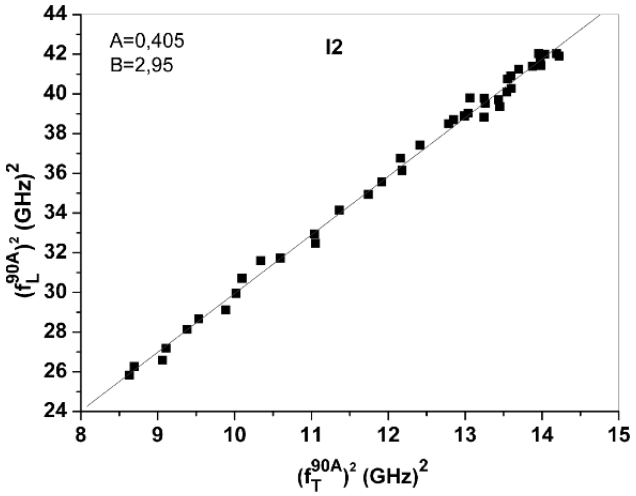


**Fig. 3.67.** Generalized Cauchy relation of I2

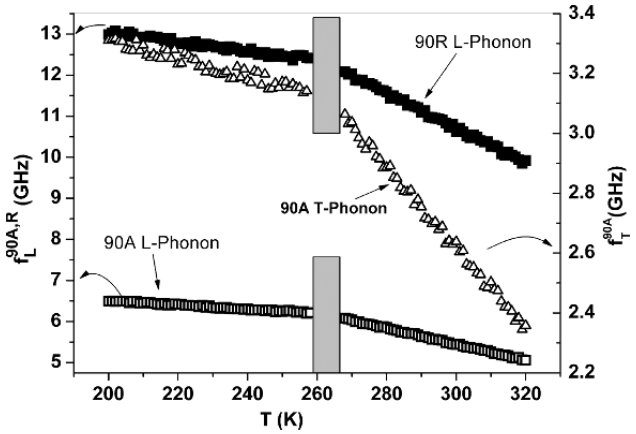


**Fig. 3.68.** Temperature dependence of the longitudinal 90A and 90R phonon frequencies and the transverse 90A phonon frequency

netic phenomenon in the sense that the freezing of the sample can be avoided on an infinitely long experimental time scale, the anomalies $\Delta\gamma_{L,T}$ in the TGT zone would have to disappear. This disappearance has to be discontinuous because on finite experimental time scales $\Delta\gamma_L$ seems to be a conserved quantity, as it shows no explicit dependence on the time scale with the exception of very fast cooling, where $\Delta\gamma_L$ even increases. Consequently, it is hard to believe that $\Delta\gamma_L$ disappears on any experimental time scale.

The jump-like change of the MGP's at the TGT gives a hint on what happens physically at the TGT. In a first approach, the nonlinear elastic be-

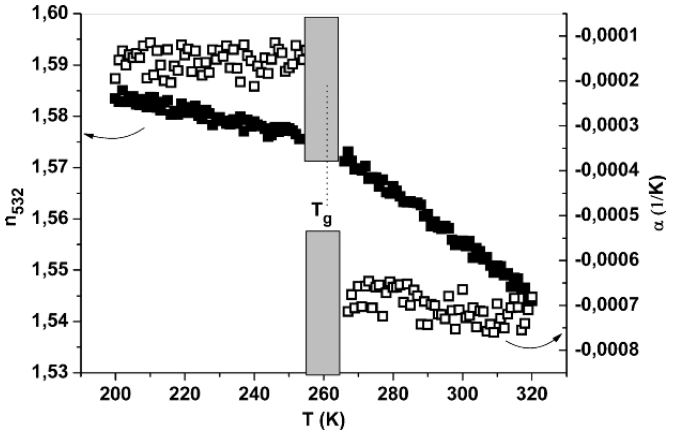


**Fig. 3.69.** Temperature dependence of the thermal expansion coefficient $\alpha$ and of the refractive index $n$ of I2

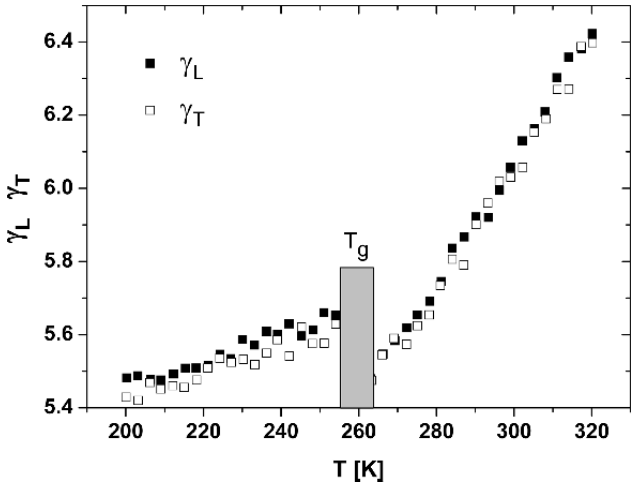


**Fig. 3.70.** Temperature dependence of the longitudinal and transverse MGP's $\gamma_L$ and $\gamma_t$ of I2

haviour of the isotropic state is described by six elastic constants of third order [17,166]: $c_{111}, c_{112}, c_{123}, c_{144}, c_{155}, c_{456}$ together with three isotropy conditions:

$$c_{112} = c_{123} + 2 \cdot c_{144} \tag{3.62a}$$

$$c_{155} = c_{144} + 2 \cdot c_{456} \tag{3.62b}$$

$$c_{111} = c_{123} + 6 \cdot c_{144} + 8 \cdot c_{456} \tag{3.62c}$$

Thus only three independent third order elastic constants remain.

These third-order elastic constants together with the second-order elastic constants can be used to calculate the two acoustic MGP's $\gamma_L$ and $\gamma_T$ [16,20]. The reversal is not true:

$$\gamma_L = \left(\frac{K}{2c_{11}}\right) - \frac{(c_{111} + 2 \cdot c_{112})}{6 \cdot c_{11}} - \frac{1}{3} \tag{3.63a}$$

$$\gamma_T = \left(\frac{K}{2 \cdot c_{44}}\right) - \frac{(c_{144} + 2 \cdot c_{155})}{6 \cdot c_{44}} - \frac{1}{3} \tag{3.63b}$$

with $K$ being the compressional modulus.

Recalling that the second-order elastic constants ($c_{11}$, $c_{44}$ and $K$ behave continuously at the TGT and assuming the temperature difference $\varepsilon$ to be infinitesimally small, at least one of the three third-order elastic constants behaves discontinuously

$$\gamma_L^{T_g+\varepsilon} - \gamma_L^{T_g-\varepsilon} = \frac{1}{6 \cdot c_{11}(T_g)}[(c_{111}(T_g + \varepsilon) - c_{111}(T_g - \varepsilon)) + 2(c_{112}(T_g + \varepsilon) - c_{112}(T_g - \varepsilon))] \tag{3.64a}$$

and

$$\gamma_T^{T_g+\varepsilon} - \gamma_T^{T_g-\varepsilon} = \frac{1}{6 \cdot c_{44}(T_g)}[(c_{144}(T_g + \varepsilon) - c_{144}(T_g - \varepsilon)) + 2(c_{166}(T_g + \varepsilon) - c_{166}(T_g - \varepsilon))] \tag{3.64b}$$

It seems likely that the third-order elastic constants show a jump-like behaviour at the TGT. This latter interpretation suggests the idea that the TGT is accompanied by a jump-like change of the molecular interaction potential.

A structural picture of this jump-like change of the molecular interaction potential has been discussed for the TGT of polyvinylacetate (PVAc) in terms of a percolation of clusters of minimum free volume [171, 172] in the sense of Ref. [162, 173]. Within this hypothesis the jump-like behaviour of $\gamma_L^{90A}(T)$ at $T_g$ is interpreted as a consequence of the spontaneous structural but not symmetry-breaking changes at $T_g$ and that it is therefore unavoidable.

In order to elucidate the nature of the glass transition and in particular to discriminate between the kinetic and the phase transition aspects of the TGT, one of these two aspects should affect the experimental data very little and might even be completely removed from it. As it was shown in the foregoing sections, this can be done by an appropriate choice of experimental conditions. Extremely slow cooling experiments combined with TDBS decreased or even eliminated the influence of kinetics at the TGT. The inspection of the generalized Cauchy relation in combination with fast quenching emphasized the kinetic aspect of the TGT and its connection to ageing phenomena. The study of the non-linear elastic behaviour via the study of thermal MGP's again provided further evidence in favour of our phase transition view of the TGT.

A further approach to the understanding of the glass transition is to leave the thermal version of this phenomenon in order to become completely rid of the kinetics due to the cooling or heating procedures of the sample. Indeed, freezing can proceed in different ways although the thermally induced solidification discussed above is the most frequently investigated process. As discussed above the TGT always suffers from the kinetic restrictions imposed by the strong increase of the structural relaxation time $\tau_\alpha$ above but close to the TGT.

The "cross-over" between the intrinsic structural relaxation time scale $\tau_\alpha$ and the kinetic time scale (cooling rate, probe frequency, etc.) does not exist in an isothermal polymerizing experiment, where the macromolecular structure vitrifies in the course of the chemical reaction (any textbook of polymer chemistry or physics [174–176]). The related **chemical glass transition** (CGT) can be performed without any change of external variables while the internal variables equilibrate due to the chemical reaction.

The structural relaxation time $\tau_\alpha$ increases in the course of the chemical reaction, as new intermolecular bonds hinder the translational motions. In order to visualize such a CGT, an experimental probe is needed that will neither significantly disturb this equilibration process nor is influenced by dynamic effects inside the sample. Provided the probe works in the limit of linear response, the experimental time constants $\tau_{\exp}$ (inverse probe frequencies) have to be chosen in a way, that the relevant internal thermodynamic variables do either move freely, i.e. $\tau_\alpha/\tau_{\exp} \ll 1$, or behave as clamped quantities, $\tau_\alpha/\tau_{\exp} \gg 1$.

The isothermal, isobaric curing of an epoxy resin can be considered as a model for the CGT. The curing process starts from a two-component oligomer. Once started, the polymerization, driven by the related chemical activities, runs under appropriate conditions to the final brittle (glassy) polymer network [174–176]. As a particular feature, the CGT is not dominated by changes in molecular conformations and packing but by changes of the molecular structure due to the chemical conversion. Physical properties like mass density $\rho$, chemical turnover $u$, refractive index $n$, frequency-clamped elastic constants [15] $c_{11}^{\infty}$ and $c_{44}^{\infty}$, etc. behave completely continuously in the course of the polymerization process. Different to the TGT, the CGT does not appear as a distinct anomaly in phenomenological properties (with the exception of the specific heat capacity $c_p$) measured in linear response.

In the following we will study the curing process of our model substance epoxy. The starting ingredients of this epoxy are diglycidylether of bisphenol A (DGEBA, 100 mass parts) and diethylenetriamine (DETA, 14 mass parts). In the curing experiment, temperature ($T \approx 296\,\mathrm{K}$ and pressure (ambient) are set. The gross epoxy group consumption $u$ serves as the leading internal variable.

A suitable probe for the intrinsic glass transition which is little sensitive to kinetic influences is provided by the acoustic MGP discussed before in this section. Discontinuous changes of the MGP's which are indicative for spon-

taneous changes of the molecular interaction potential are only expected at phase transitions (e.g. [158]). As a matter of fact, the strength of the discontinuity is more or less independent of the cooling or heating rate although these rates can slightly modify the temperature position of the discontinuity. Having in mind this discontinuous behaviour of the longitudinal acoustic MGP at the TGT the question appears whether or not acoustic MGP's could provide a clearer picture of the location of the CGT on the scale of the chemical turnover and about the nature of this reaction-driven freezing process.

Accordingly, the role of MGP as a sensitive probe for the glass transition during chemical freezing is the matter of debate.

The basic relation for an acoustic mode-Grüneisen parameter as a function of chemical turnover appears at a first sight strange:

$$\gamma^{p,\boldsymbol{q}}\left(f^{p,q}(u),\rho\left(u\right)\right)=\frac{\frac{1}{f^{p,q}(u)}}{\frac{1}{\rho(u)}}\frac{\frac{df^{p,\boldsymbol{q}}(u)}{du}}{\frac{d\rho(u)}{du}}=\frac{\delta^u}{\alpha^u} \tag{3.65}$$

In Eq. (3.65, $p$ $(=L,T)$ denotes the polarization of the sound mode, $\boldsymbol{q}$ is the wave vector. $\alpha^u$ represents a generalized volume expansion coefficient, and $\delta^u$ is a generalized gradient of sound velocity.

As the chemical reaction changes continuously the system itself, the usual concept of MGP as a measure for anharmonicity is not applicable in this case. Even if the potential was harmonic but dependent on $u$, the MGP would be changed due to the reaction. Therefore to differentiate between the classic MGP and the one defined for a chemical reaction, the latter one is denoted as CMGP. The physical meaning of the CMGP is somewhat clouded.

As for the TGT the CMGP's are best measured with Brillouin spectroscopy or more precisely with Time Domain Brillouin spectroscopy (TDBS) (see Sect. 3.4) using the so-called 90A-scattering geometry [163, 165]. This scattering technique meets exactly the measuring condition for the sound frequency, which is needed to calculate the related CMGP's [156, 158, 159, 165, 166]: a constant phonon wave vector in the course of a changing phonon frequency $f$. A laser wavelength $\lambda_{\text{opt}} = 532\,\text{nm}$ yields an acoustic wave vector:

$$q^{90A}=\left\{\left(4\cdot\pi\cdot\sin\left(\pi/4\right)\right)/532\,\text{nm}\right\} \tag{3.66}$$

The hypersonic velocities are then obtained from the usual dispersion relation

$$v_{L,T}^{90A}\left(t\right)=\frac{2\cdot\pi\cdot f_{L,T}^{90A}\left(t\right)}{q^{90A}} \tag{3.67}$$

The determination of CMGP's at the CGT has to be done at constant temperature. As discussed above, the determination of CMGP's needs the knowledge of the mass density measured under the same conditions under which the related phonon frequencies were determined. Again, the mass density can best be obtained via the optical refractive index with help of Eq. (3.53). At ambient temperature a very precise way to measure refractive index data

is Abbé refractometry. With this technique the temporal evolution of the refractive index of the model epoxy can be determined at the same wavelength, $\lambda_{\mathrm{opt}} = 532\,\mathrm{nm}$ as used for Brillouin spectroscopy. The refractive index $n = \sqrt{\varepsilon^{\infty}(\lambda_{\mathrm{opt}})}$ is directly related to the dielectric constant measured at optical frequencies ($f_{\mathrm{opt}} \approx 5 \cdot 10^{14}\,\mathrm{Hz}$).

Figure 3.71 gives an overview over the temporal evolution of the refractive index $n$, of the longitudinal sound velocity $v_L$ and of the specific heat capacity $c_p$ for a curing process at 296 K. It is obvious from Fig. 3.71 that the apparent anomalies in the three susceptibilities occur at different times and therefore at different degrees of chemical turnover. Consequently there is no unique indication for the location of the CGT.

Whereas for the TGT the natural driving parameter is the temperature $T$, the natural parameter for the CGT is the time $t$. Of course, the time $t$ is not a property of the material under study. A more physical driving parameter would be the amount of chemical conversion (turnover) $u$ (s.a. Fig. 3.72). Attenuated total reflection infrared spectroscopy (IR-ATR) yields the chemical turnover $u$ as a function of curing time $t$. With the intensity $I(1510\ \mathrm{cm}^{-1})$ of the phenylene band as internal standard, the intensity $I(915\ \mathrm{cm}^{-1})$ of the epoxy band is normalized to: $I_{\mathrm{EP}}^{\mathrm{norm}}(t) = I_{915}(t)/I_{1510}(t)$. Then, the IR-spectroscopic degree of epoxy group consumption $u$ is calculated from $u(t) = [1 - \frac{I_{\mathrm{EP}}^{\mathrm{norm}}(t)}{I_{\mathrm{EP}}(0)}]$.

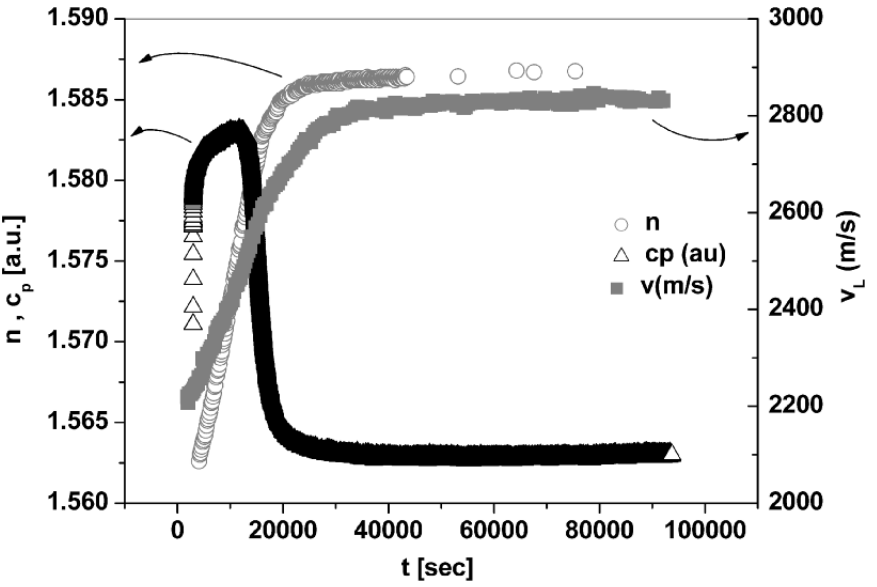


**Fig. 3.71.** Temporal development of the refractive index $n$, the specific heat capacity $c_p$ and the longitudinal sound velocity $v_L$ during the cross-linking of a DGEBA/DETA mixture of 100/14 at $T = 296\,\mathrm{K}$

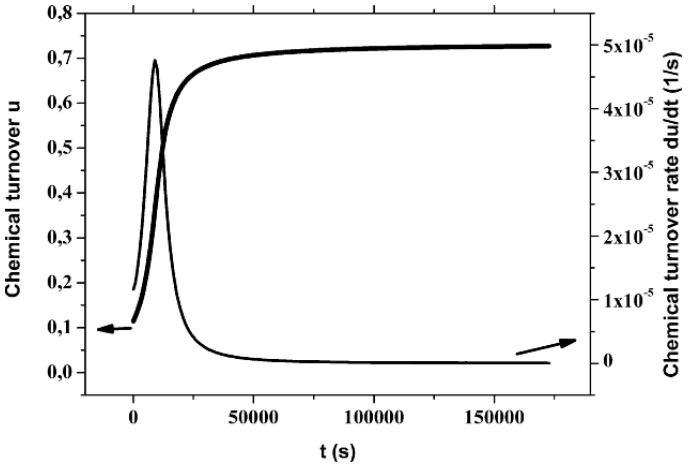


**Fig. 3.72.** Chemical turnover $u$ and chemical turnover rate $\frac{du}{dt}$ as a function of curing time $t$ for the cross-linking of DGEBA/DETA 100/14

Figure 3.72 shows for the model epoxy mentioned above how the chemical turnover $u$ and its rate $\partial_t(u)$ depend on the curing time $t.u = u(t)$ behaves completely smooth and $\partial_{\mathrm{t}}(u)$ shows a peak in the short time regime at about $t = 9000\,\mathrm{s}$. It is evident, that even after differentiation of $u = u(t)$ no discontinuity emerges from the measured data.

As mentioned above, CMGP's are derived from static or frequency-clamped acoustic properties. Therefore it has to be checked whether the sound modes are measured in a relaxation-free time regime.

Figure 3.73 shows the evolution of the structural relaxation time $\tau_\alpha$ as measured by dielectric spectroscopy (DES) within the time interval between roughly $t_{\mathrm{cure}} = 0\,\mathrm{s}$ and $t_{\mathrm{cure}} = 25 \cdot 10^3\,\mathrm{s}$. The relaxation time increases within this time interval from about $\tau_\alpha = 10^{-9}\,\mathrm{s}$ to $\tau_\alpha = 10\,\mathrm{s}$. Following usual conventions the DES data can be used to define an operative glass transition time: $t_g^{\mathrm{op}} = 2.5 \cdot 10^3\,\mathrm{s}$.

According to Fig. 3.73 the CGT is accompanied by a strong increase of $\tau_\alpha$. In the time interval $I_{\mathrm{soft}} = [0, t_g^{\mathrm{op}}]$ the hypersonic frequency $f_L^{90A}$ increases from about 5.5 GHz to 7.5 GHz (Fig. 3.73). As a result, BS as a probe for hypersonic frequencies $f$ offers the possibility to measure clamped mechanical properties in almost the full interval: $2 \cdot \pi \cdot f \cdot \tau_\alpha \gg 1$. As a result, neglecting curing times up to 5000 s the related elastic constants $c_{11}^{\infty}$ and $c_{44}^{\infty}$ are frequency-clamped quantities.

Figure 3.74 gives the frequency clamped sound velocities $v_L^{90A}(t)$ and $v_t^{90A}(t)$ and the refractive index $n = n(t)$ as measured with an Abbé refractometer. All Brillouin data which eventually do not represent the frequency-clamped state have been suppressed. The longitudinal and the transverse

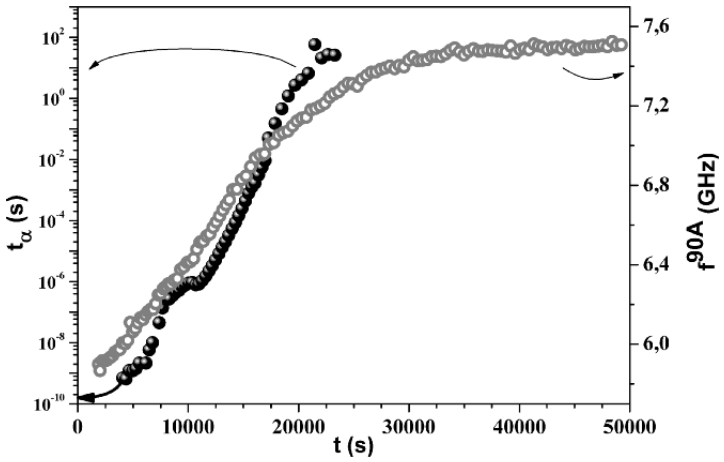


**Fig. 3.73.** Sound frequency $f_L^{90A}$ and structural $\alpha$-relaxation time as a function of curing time $t$ for DGEBA/DETA 100/14

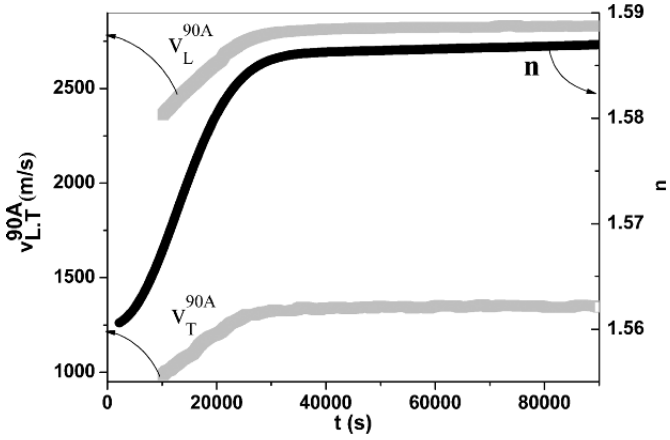


**Fig. 3.74.** Sound velocity (L-mode: $f_L^{90A}$; T-mode: $f_L^{90A}$ and the refractive index, $n_D^{296K}$, as a function of curing time $t$

sound velocities $v_L^{90A}(t)$ and $v_t^{90A}(t)$ behave strongly non-linearly but both show a very similar increase with the curing time.

We have recently shown that the changes of $c_{11}$ and $c_{44}$ in the course of the thermal glass transition usually follow a generalized Cauchy condition [177–179]

$$c_{11}(x) = A + 3 \cdot c_{44}(x) \tag{3.68}$$

with

$$\partial_x c_{11} = 3 \cdot \partial_x c_{44} \tag{3.69}$$

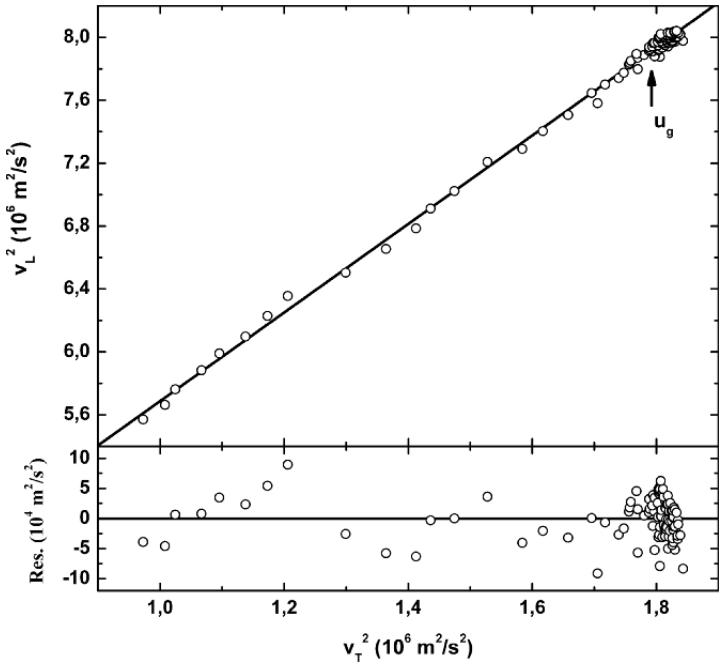


**Fig. 3.75.** Linear fit of the squared hypersound velocities $(v_{\mathrm{L}}^{90A})^2$ vs. $(v_{\mathrm{L}}^{90A})^2$. The residuals of the fit show the validity of the generalized Cauchy condition $(v_{\mathrm{L}}^{90A})^2 = \tilde{A} + 3 \cdot (v_{\mathrm{L}}^{90A})^2$

($x$ = time, temperature, turnover). The same relation is found for our model epoxy during the chemical reaction even across the chemical glass transition.

Figure 3.75 shows the result using the sound velocity representation [178, 179]

$$\left(v_L^{90A}\right)^2 = \tilde{A} + B \cdot \left(v_T^{90A}\right)^2 \tag{3.70}$$

with $\tilde{A} = A/\rho = 2.3 \cdot 10^6$ m$^2$s$^2$ and $B = 3$. This Cauchy relation holds true throughout the whole curing process.

Taking into account that any curing process reflects a succession of non-equilibrium transitions it is really surprising that the generalized Cauchy relation holds true.

This result is even more astonishing if we take into account results on thermally quenched canonical glass formers mentioned in Sect. 3.3: the quenching process has destroyed the Cauchy relation yielding a higher slope of the $c_{11} = c_{11}(c_{44})$-curve. If even the non-equilibrium curing process does not violate the Cauchy relation, one can conclude that the totally hidden CGT represents at least not a strong non-equilibrium process in the sense that the longitudinal and the shear elastic constant get out of equilibrium with respect to each other.

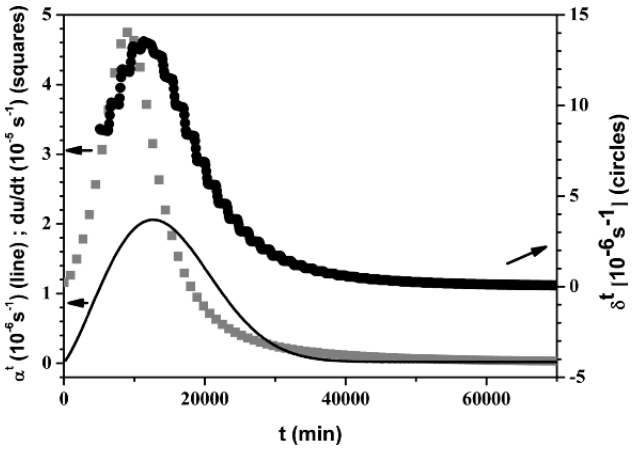


**Fig. 3.76.** Temporal volume expansion coefficient $\alpha^t$, temporal sound frequency gradient $\delta^t$ of the L-mode and the chemical turnover rate $\frac{du}{dt}$ as a function of curing time $t$

It remains the question whether the acoustic CMGP's do respond more sensitively to the CGT than the Cauchy relation does. The acoustic CMGP's $\gamma$ are related to the sound mode frequencies $f$ and to the mass density $\rho$, which in turn are functions of $u$. Since the external parameters like temperature and pressure are kept fixed during the measurement, all time scales relevant for the chemical freezing process are controlled internally by the chemical reaction. Hence, the cross-over problem as observed at the TGT is avoided, the CGT cannot be obscured by kinetic effects.

For the evaluation of the CMGP the quantities $f$, $\rho$ and $u$ are independently measured as a function of curing time $t$ at 296 K but in order to calculate the related

$$\gamma_{L,T}^{90A} = \gamma_{L,T}^{90A} = \frac{\delta_{L,T}^{90A}(u)}{\alpha(u)} \tag{3.71}$$

the $\delta$ and $\alpha$-values have to be provided for the same $u(t)$. Again interpolation between measured data and the application of moving averages solve the numerical problems. Figures 3.75 and 3.76 depict the temporal sound propagation coefficient

$$\left(\delta_{L,T}^{90A}\right)^t = \frac{1}{f_{L,T}^{90A}} \frac{\partial f_{L,T}^{90A}}{\partial t} \tag{3.72}$$

as calculated from $f_{L,T}^{90A}(t)$.

Since the determination of the MGP's needs the generalized volume expansion coefficient $\alpha^u$ this quantity has to be derived from the time dependence of the refractive index $n(t)$ and of the chemical turnover $u(t)$. In a first step $\alpha^t$ is calculated

$$\alpha^t = \frac{1}{\rho} \cdot \frac{\partial \rho}{\partial t} = \frac{6n(t)}{n^4(t) + n^2(t) - 2} \cdot \frac{\partial n}{\partial t} \tag{3.73}$$

Figure 3.76 shows the temporal evolution of this quantity. The refractive index $n = n_D^{296\mathrm{K}}$ was measured with an Abbé refractometer at a temperature of 296 K (black curve in Fig. 3.74). The $n(t)$-data were measured on the same epoxy batch which was splitted for the different experiments after preparation. With the available $\partial_t u$-data (Fig. 3.72), the generalized expansion coefficient $\alpha^t$ can be transformed into

$$\alpha^u = \frac{1}{\rho} \cdot \frac{\partial \rho}{\partial u} = \frac{\alpha^t}{du/dt} \tag{3.74}$$

Having calculated all ingredients, we are able to determine the CMGPs from Eq. (3.70). Figure 3.78 provides the results for $\gamma_L^{90A}$ and $\gamma_T^{90A}$ of these calculations as a function of $u$. The chemical turnover $u_g$ corresponding to the peak position of $\gamma_L^{90A}(u_g)$ and $\gamma_T^{90A}(u_g)$ is interpreted as the degree of chemical conversion for which the ideal glass transition takes place as explained in the following.

Firstly, the peaks of the MGP's occur by far later than those of $\delta^u$ and $\alpha^u$ (Figs. 3.76, 3.77). Secondly $\frac{\delta_{L,T}^u}{\alpha^u}$ remains constant in the region of the strongest variations of these two quantities whereas the peaks of $\gamma_{L,T}^{90A}$ appear far in the almost flat wings of $\delta^u$ and $\alpha^u$ for $u > 0.6$ (Fig. 3.79). Consequently, the appearance of the $\gamma_{L,T}$-peaks results from the different levelling of $\delta^u$ and $\alpha^u$ at high degrees of curing: on approaching the CGT the volume expansion coefficient $\alpha$ slows faster down than the frequency expansion coefficient $\delta$ does and finally levels. This means, that the frequency change per change of density increases on approaching the CGT. If at still higher degrees of chemical

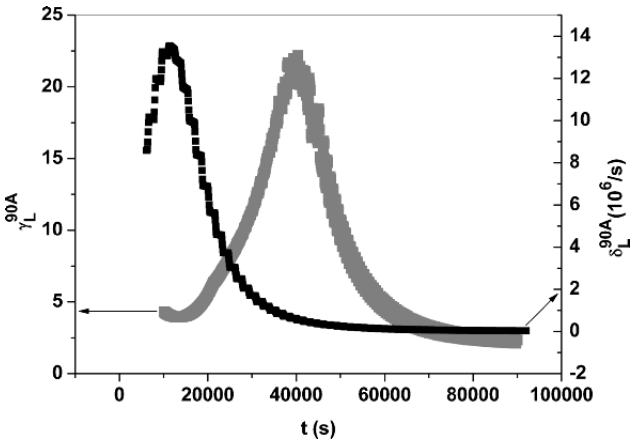


**Fig. 3.77.** Temporal longitudinal frequency coefficient $\delta^t$ and temporal MGP $(\gamma_L^{90A})^t$ of the L-mode as a function of curing time $t$

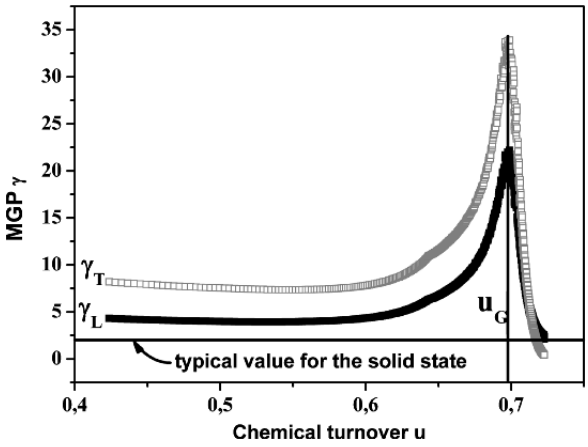


**Fig. 3.78.** Grüneisen parameters $\gamma_L$ and $\gamma_T$ as a function of the degree of chemical conversion $u \cdot u_g$ gives the "critical" degree of chemical conversion at which the ideal glass transition is assumed to take place

turnover the frequency coefficient also starts to level, the CMGP slows down again.

For the epoxy samples of 14 mass percent DETA the DETA concentration is sufficiently high (over-stoichiometric) that, at least in principal, the chemical reaction could be completed. It is therefore interesting to note that the chemical turnover $u$ for the sample of 14 mass percent DETA does not reach the value of 100% but stops at 70% if the curing process takes place

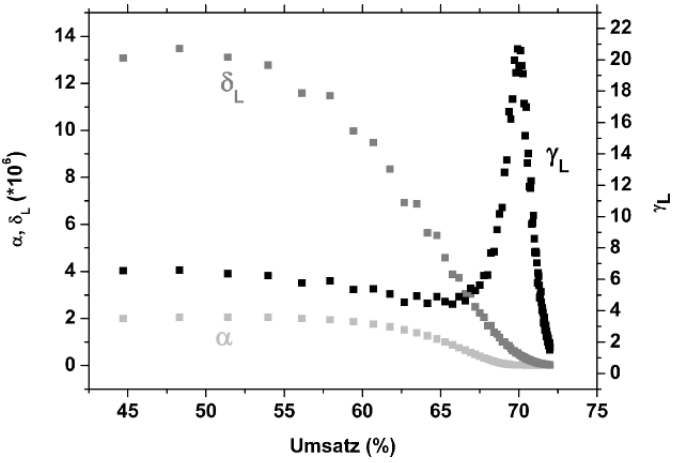


**Fig. 3.79.** Sound frequency coefficient $\delta$, expansion coefficient $\alpha$ and longitudinal mode-Grüneisen parameter $\gamma_L$ spectroscopic chemical conversion $u$ of DGEBA/DETA 100/14

at $T_{\mathrm{cure}} = 296\,\mathrm{K}$. It seems that the CGT stops or at least significantly slows down the curing process. This explains the anomaly of the volume- and the frequency coefficients around the critical concentration $u_g$ (Fig. 3.79). It is therefore expected that the CGT's of reactive epoxy systems depend on the concentration of DETA and shift to shorter times with increasing concentration of the latter. At a sufficiently low amount of DETA the formation of network knots is limited so strongly that no more chemical freezing takes place during polymerization at ambient temperature. The evolution of the CMGP as a sensitive indicator for the CGT should therefore depend on the DETA concentration. Figure 3.80 confirms this interpretation. The sample of 18 mass percent DETA shows its CGT after about 300 min of curing whereas the CGT of the sample of 14 mass percent DETA freezes only after about 500 min. The sample with only 6 mass percent of DETA does not freeze at all at ambient temperature. Of course, these results do not give information about a possible shift of the critical turnover with the concentration of DETA. Recent measurements on polyurethanes show in principal the same behaviour at the CGT [180]. In Fig. 3.80 another feature of the CMGP's at the CGT becomes evident which concerns the long time behaviour. As a matter of fact, after a sufficiently long curing time there should be neither a change of the mass density nor of the phonon frequencies, all quantities should saturate. Consequently, the CMGP's should become constant but that information is by definition inaccessible. An approximative information about the limiting values for the CMGP's can be calculated from $\delta$ and $\alpha$-values reliably larger than zero.

In conclusion, the reactive system DGEBA/DETA (100/14) transforms during the crosslinking process from a two-component liquid via a percolated

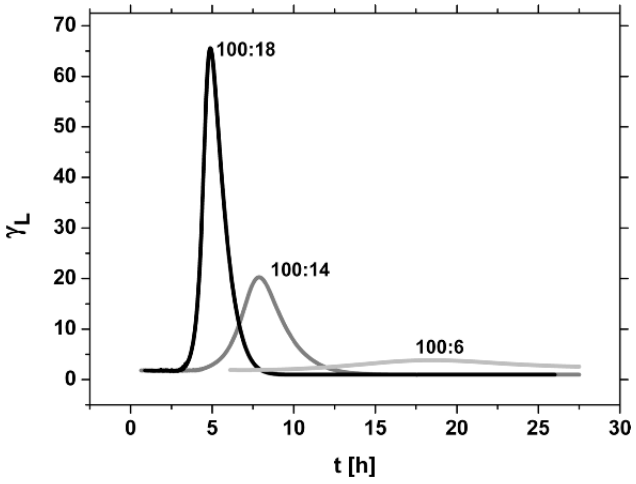


**Fig. 3.80.** Temporal evolution of the longitudinal mode-Grüneisen parameters for the model epoxy system DGEBA/DETA 100/18, 100/14 and 100/6

epoxy network into a chemically induced glass. The most pronounced change of behaviour is the given by the maximum of the CMGP, so that this maximum has to be identified with the chemical glass transition. As kinetic influences are excluded an intrinsic glass transition seems to exist for this model epoxy at the degree of conversion, $u_g \sim 0.70$. In the phase of low chemical conversion, i.e. in the "liquid phase" with $u \ll u_g$, the Grüneisen parameters $\gamma_L$ and $\gamma_T$ exceed those of the glassy state ($u > u_g$) respectively. Although a percolation transition exists below $u_g$, this transition seems not or only weakly coupled to the measured and calculated phenomenological parameters. At $u_g$, the longitudinal as well as the transverse acoustic mode-Grüneisen parameters go through a rather sharp maximum.

It should be stressed that for $u = u_g$ the TGT of the material coincides with the curing temperature $T_g(u_g) = T_{\text{cure}}$. Therefore it exists an inherent correlation between the CGT and the TGT. But in as much as the material can continue to cure in the chemical glassy state the related thermal glass transition temperature will exceed the curing temperature.

To this end it is interesting to clarify the different significances of the MGP's for the thermal and the chemical freezing process. For the TGT it should be kept in mind, that constant MGP's indicate, that the related molecular interaction potential is independent of temperature and a discontinuous change of the MGP's at a definite temperature $T_g$ indicates a discontinuous structural change within the material of interest. This point of view implies that in the liquid and the glassy state of a given canonical glass former respectively two different molecular interaction potentials are responsible for the temperature dependence of phenomenological properties and that these properties at a given temperature correspond to a related thermally excited state within the appropriate potential. In reality the MGP's are not completely independent of temperature. This holds especially true for the liquid state and indicates the appearances of slight but continuous changes of the local structure with changing temperature and/or the influence of entropic degrees of freedom.

During chemical freezing the situation is completely different. With increasing curing time the initially two-component liquid transforms continuously to a molecular network. This formation of a molecular network corresponds to a continuous change of structure and therefore should yield time dependent MGP's. This means that the changes of the CMGP's observed in the course of curing may reflect structural changes rather than pure changes of anharmonicity. This is understandable since all external variables remain constant during the curing process. It is interesting to note that in the early curing regime until the CGT, that is the regime were the formation of network knots is fast, the two acoustic CMGP's $\gamma_{L,T}^{90A}(u)$ remain almost independent of $u$ (Fig. 3.78). Obviously, this behaviour corresponds to a roughly linear dependence of the elastic modulus on mass density, as $\delta = \gamma \cdot \alpha$. Indeed, over a wide range of $\rho$-values the elastic modulus $c_{11}$ behaves linearly as a function of $\rho$. Only in the glass transition region a strong increase of $c_{11}$ followed by

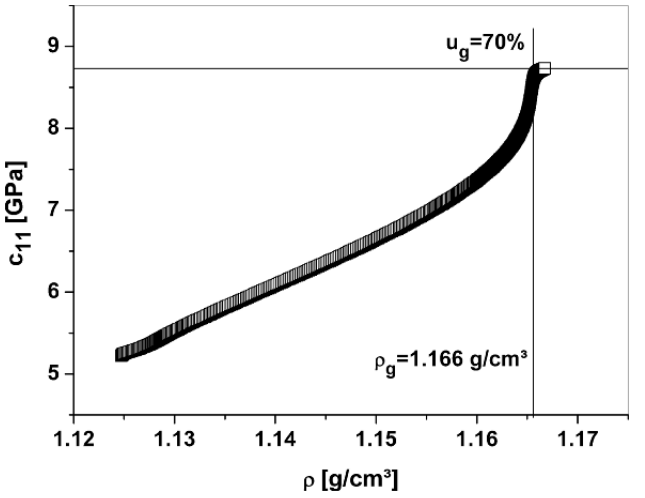


**Fig. 3.81.** Difference in the sum of third-order elastic constants $c_{111}$ and $c_{112}$ between glassy and fluid phase vs. chemical conversion $u$ for DGEBA/DETA 100/14

a levelling of this quantity appears (Fig. 3.81). In other words, the structural changes accompanying the curing process do not affect the relative change of the phonon frequencies induced by the changes of mass density created by the same chemical process. This implies, that all changes in the frequency coefficients $\delta_{L,T}^{90A}(u)$ and the volume expansion coefficient $\alpha(u)$ can be described by the same factor $c(u)$ with

$$\delta_{L,T}^{90A}(u) = \delta_{L,T}^{90A}(u_0) \cdot c_\delta(u) \tag{3.75a}$$

$$\alpha(u) = \alpha(u_0) \cdot c_\alpha(u) \tag{3.75b}$$

with $\mathrm{c}_{\alpha,\delta}(u_0) = 1$.

Dividing Eq. (3.77a) by Eq. (3.77b) yields

$$\frac{c_\delta(u)}{c_\alpha(u)} = \text{const} = \frac{c_\delta(u_0)}{c_\alpha(u_0)} = 1 \tag{3.76}$$

Of course this identity is only approximately fulfilled. Within the peak region representing the CGT the order relation $c_\delta(u_o) \geq c_\alpha(u_o)$ holds true.

It therefore has to be concluded, that from the mechanical point of view the chemical freezing process is much more dominant and effective than the driving polymerization and percolation process. Even in a molecular plastic crystal the same kind of discontinuity was found (see Sect. 3.1, DFTCE).

In the vicinity of the CGT the $\alpha$-relaxation process is slow and the continuation of further curing is in concurrence to the freezing process. At the beginning of the CGT, due to the improved molecular packing, first the changes of the density are slowed down but still some curing can happen in the almost

fixed molecular skeleton. The additional bonds, included in the spatially fixed molecular structure, further stabilize the existing skeleton and thus increase the phonon frequency due to an improved elastic stiffness. This additional stabilization of the given molecular skeleton causes the anomaly of the CMGP. After the CGT the system behaves like a solid, so that further bonds can influence the elastic behaviour only slightly. The glassy state hinders the translational diffusion of oligomers and cross-linked clusters but does not fully stop it, so that further reactions are still possible. These further reactions deprive the system of this potentially swelling molecular groups, so that the density is increased, which leads to a slowing down of the CMGP's.

It is self explaining that mechanical properties which describe mechanical stiffnesses are suitable probes for glass transitions. The stiffening at the transition from the liquid to the glassy state is at least partly caused by an improved molecular packing. But that is only part of the truth. As has been deduced in this chapter from the evolutions of the MGP's around the glass transitions, there exists an additional contribution to elastic stiffness caused by stiffened spring constants not related to density changes. The chemical glass transition demonstrates this effect drastically, because additional chemical bondings can at least in principal increase the mechanical stiffness without changing the mass density. The same observation of an excess stiffness as a function of density holds true at the thermal glass transition, although additional bondings don't play any role. This excess stiffness occurring at glass transitions seems to be one of the central features of glass transitions.

## 3.7 Conclusion

There is no doubt that kinetic phenomena accompany the thermal as well as the chemical glass transition. The leading role of the molecular kinetics for the thermal and the chemical glass transition is not confirmed. Beyond the influence of molecular kinetics there are sufficient proves for the existence of an intrinsic glass transition which nature has to be elucidated furthermore.

The most striking evidences for the existence of such an intrinsic feature are as follows:

The investigation of the generalized Cauchy relation on differently quenched glass forming liquids has shown that there exist two different glassy states: one which follows the generalized Cauchy relation and one which violates it. Significant quenching creates a metastable glass and thus violates the generalized Cauchy relation. Under the latter conditions aging can be observed. However, this aging process does not bring the material to the liquid phase as predicted by the kinetic view but to a stable reference glassy state.

Time Domain Brillouin Spectroscopy shows for different glass forming liquids a definite cut-off for the low-frequency relaxation processes often accompanying the thermal glass transition. As a consequence the move away from

local equilibrium of the reference state due to a cross-over between the experimental time scale and the the $\alpha$-relaxation time can be avoided and a "equilibrium glassy state" is observed.

The inspection of the opto-acoustic dispersion function ($D$-function) proves that in several glass forming liquids relaxation processes within the GHz-range are present which are eliminated only by the quasi-static glass transition. In contrast to the kinetic point of view, close to the quasi-static glass transition there are still very mobile relaxation processes which are cut off by the quasi-static freezing process.

Glass-forming liquids filled-in in nano-porous glasses prove that the quasi-static glass transition can occur without being accompanied by the $\alpha$-relaxation process. As a consequence, the glass transition takes place without any cross-over of the experimental time with $\alpha$-relaxation time.

The quasi-static glass transition in polymer liquid crystals has necessarily to appear in order to avoid unrealistic elastic constants (supplement to the so-called "Kauzmann Paradoxon").

Structural glass formers and orientational glass formers sometimes show identical anomalies at the quasi-static glass transition. The glass transition in orientational glasses doesn't need the ingredient of cooperative rearrangement units.

The analysis of mode-Grüneisen parameters shows that the quasi-static thermal glass transition is accompanied by a discontinuity of the physical property. This result implies a jump-like change of the molecular interaction potential at the glass transition indicating a spontaneous change of structure. This discontinuity creates jump-like changes of the involved third-order elastic constants. The latter observation is a clear hint for a phase transition.

Reactive polymers show a chemically induced freezing process called "chemical glass transition" during the curing process. This type of transition shows again an anomalous behaviour of the mechanical properties during freezing, indicating the existence of an intrinsic transition. The curing process is a completely free running process without any influence of the experimentalist on the ongoing freezing process.

It is therefore time to revise the actual view of the glass transition.

## References

1. K. L. Ngai, "Universal Patterns of Relaxations in Complex Correlated Systems", in "Disorder Effects on Relaxation Processes", Richert/Blumen, Springer-Verlag, Berlin, Heidelberg (1994)
2. E. Donth, "Relaxation and Thermodynamics in Polymers, Glass transition", Akademie-Verlag, Berlin (1992)
3. W. Götze, L. Sjögren, Rep. Prog. Phys. **55**, 241–376 (1992)
4. J. H. Gibbs, E. A. DiMarzio, J. Chem. Phys. **28**, 373 (1958)
5. G. Gee, Contemp. Phys. **11**, 313 (1970)

6. J. J. Prejean, in "Dynamics of Disordered Materials", Ed. by D. Richter, A. J. Dianoux, W. Petry and J. Teixeira, Proceedings in Physics **37**, 242, Springer (1989)
7. J. Jäckle, Rep. Progr. Phys. **49**, 171 (1986)
8. J. Jäckle, J. Phys. Cond. Matter, **1**, 267 (1989)
9. J. K. Krüger, R. Roberts, H.-G. Unruh, K.-P. Frühauf, J. Helwig, H. E. Müser, Progr. in Coll. & Polym. Sci. **71**, 77 (1985)
10. K.-P. Frühauf, J. Helwig, H. E. Müser, J. K. Krüger, R. Roberts, Colloid & Polymer Science **266**, 814 (1988)
11. M. H. Cohen, D. Turnbull, J. Chem. Phys. **31**, 1164 (1959)
12. M. H. Cohen, D. Turnbull, J. Chem. Phys. **34**, 120 (1961)
13. K.-P. Bohn, J. K. Krüger, in "Structure and Properties of Glassy Polymers", ACS Symposium Series 710, ed. by M. R. Tant and A. J. Hill (1998)
14. W. Götze, in "Liquids, Freezing and Glass Transition", edited by J. P. Hansen, D. Levesque and J. Zinn-Justin, Elsevier, Amsterdam (1989)
15. J. K. Krüger, Th. Britz, J. Baller, W. Possart, H. Neurohr, Phys. Rev. Letter **89**, 285701 (2002)
16. S. Brawer, "Relaxation in Viscous Liquids and Glasses", American Ceramic Society (1985)
17. M. D. Ediger, Annu. Rev. Phys. Chem. **51**, 99–128 (1999)
18. S. R. Elliott, "Physics Of Amorphous Materials", Longman (1990)
19. C. A. Angell, K. L. Ngai, G. B. McKenna, P. F. McMillan and S. W. Martin J. Appl. P., **88**, 3113 (2000)
20. I. Gutzow and J. Schmelzer, "The Vitreous State" Berlin: Springer (1995)
21. P. G. Debenedetti "Metastable liquids – concepts and principles", Princeton University Press (1996)
22. D. Richter, A. J. Dianoux, W. Petry and J. Teixeira (eds.) "Dynamics of Disordered Materials", Springer-Verlag (1989)
23. A. J. Kovacs, Journal of Polymer Science **30**, 131 (1958)
24. G. Parisi, F. Zamponi, J. Chem. Phys. **123**, 144501 (2005)
25. T. M. Truskett, V. Ganesan, J. Chem. Phys. **119**(4), 1897 (2003)
26. G. Tarjus, D. Kivelson, in "Jamming and Rheology: Constrained Dynamics on Microscopic and Macroscopic scales", S. Edwards, A. Liu, S. Nagel Eds., Taylor and Francis, London (2001)
27. D. Chowdhury "Spin glasses and other frustrated systems" World scientific (1986)
28. J. K. Krüger, R. Jiménez, K.-P. Bohn, J. Petersson, J. Albers, K. Klöpperpieper, E. Sauerland, H. E. Müser, Phys. Rev. B Cond. Matter, **42**, 8537 (1990)
29. R. Jiménez, B. Jiménez, J. K. Krüger, J. Schreiber, F. Sayetat, F. Mauvy, Ferroelectrics **157**, 141 (1994)
30. Fischer & Hertz, "Spin glasses" Cambridge university press (1991)
31. K. Binder, A. P. Young, Rev. Mod. Phys. **58**, 801 (1986)
32. K. Knorr, A. Loidl, Phys. Rev. B **31**, 5387 (1985)
33. S. K. Satija, C. H. Wang, Solid State Comun. **28**, 617 (1978)
34. S. K. Satija, C. H. Wang, J. Chem. Phys., **69**, 1101 (1978)
35. C. H. Wang, S. K. Satija, Chem. Phys. Lett., **87**, 330 (1982)
36. R. Böhmer, A. Loidl, Phys. Rev. B **42**, 1439–1443 (1990)
37. R. Jiménez, K. P. Bohn, J. K. Krüger, Eur. Phys. J. B, **13**, 643 (2000)

38. J. Hessinger, K. Knorr, Phys. Rev. Letter, **63**, 2749 (1989)
39. K. H. Michel, Phys Rev B, **35**, 1405 (1987)
40. J. M. Rowe et al., Phys. Rev. Letter **53**, 1158 (1973)
41. K. Kishimoto, H. Suga, S. Seki, Bull. Chem. Soc. Japan **51**, 1691 (1978)
42. K. Kishimoto, H. Suga, S. Seki, Cond. Matter., 19 (1978)
43. J. K. Krüger, M. Prechtl, J. C. Wittmann, S. Meyer, P. Smith, J. F. Legrand, J. Pol. Sci. Part B **30**, 1173 (1992)
44. J. K. Krüger, M. Prechtl, J. C. Wittmann, S. Meyer, J. F. Legrand, G. Asseza, J. Pol. Sci. Part B, **31**, 505–512 (1993)
45. H. A. Lorentz, Wied. Ann. Phys., **9**, 641 (1880)
46. L. V. Lorenz, Wied. Ann. Phys., **11**, 70 (1880)
47. M. Goldstein, The Journal of Physical Chemistry, **51**(9), 3728 (1969)
48. M. Born, K. Huang, "Dynamical theory of crystal lattices", Clarendon Press, Oxford (1968)
49. J. K. Krüger, K. P. Bohn, R. Jimenez, Condensed Matter News **5**, 10 (1996)
50. J. K. Krüger, K. P. Bohn, R. Jimenez, J. Schreiber, Colloid & Polymer Science **274**, 490 (1996)
51. J. K. Krüger, K.-P. Bohn, J. Schreiber, Phys. Rev. B **54**, 15767 (1996)
52. J. W. Tucker, V. W. Rampton, "Microwave ultrasonics in solid state physics", North Holland Publishing Co. (1972)
53. P. G. de Gennes, "The physics of liquid crystals", Clarendon Press (1974)
54. S. Chandrasekhar "Liquid crystals", Cambridge monographs on physics (1977)
55. J. K. Krüger, C. Grammes, R. Jiménez, J. Schreiber, K.-P. Bohn, J. Baller, C. Fischer, D. Rogez, C. Schorr, P. Alnot, Phys. Rev. E, **51**(3), 2115 (1994)
56. C. Grammes, J. K. Krüger, K.-P. Bohn, J. Baller, C. Fischer, C. Schorr, D. Rogez, P. Alnot: Phys. Rev E, Vol. **51**(1), 430 (1995)
57. J. K. Krüger, L. Peetz, R. Siems, H.-G. Unruh, M. Eich, O. Herrmann-Schönherr, J. H. Wendorff,, Phys. Rev. A **37**, 2637 (1988)
58. J. K. Krüger, C. Grammes, J. H. Wendorff, in "Dynamics of Disordered Materials", Eds. D. Richter et al., Springer Proceedings in Phys. **37**, 216 (1989)
59. D. Forster "Hydrodynamic fluctuations, broken symmetry, and correlation functions", W. A. Benjamin, Inc. (1975)
60. J. Wong, C. A. Angell "Glass – Structure by spectroscopy" Marcel Dekker, Inc. (1976)
61. G. S. Fulcher, J. Am. Chem. Soc. **8**, 339, 789 (1925)
62. G. Tammann, "Der Glaszustand", Leopold Voss, Leipzig (1933)
63. B. J. Berne, R. Pecora, "Dynamical Light Scattering", John Wiley (1975)
64. B. Chu, "Laser Light Scattering", Academic Press (1974)
65. W. Hayes, R. Loudon, "Scattering of Light By Crystals", John Wiley (1978)
66. J. K. Krüger, in "Optical Techniques to Characterize Polymer Systems", edited by H. Bässler, Elsevier (1989)
67. L. D. Landau, E. M. Lifshitz, "Lehrbuch der Theoretischen Physik", Bd. VIII, "Elektrodynamik der Kontinua", Akademie Verlag Berlin (1966)
68. L. D. Landau, E. M. Lifshitz, "Lehrbuch der Theoretischen Physik", Bd. V, "Statistische Physik", Akademie Verlag Berlin (1966)
69. H.-G. Unruh, J. Krüger, E. Sailer; Ferroelectrics **20**, 3–10 (1978)
70. J. F. Nye, "Physical Properties of Crystals", Oxford Press (1972)
71. J. K. Krüger, A. Marx, L. Peetz, R. Roberts, H.-G. Unruh; Colloid & Polymer Sci., **264**, 403–414 (1986)

72. J. K. Krüger, J. Embs, J. Brierley, R. Jimenez; J. Phys. D – Appl. Phys. **31**, 1913 (1998)
73. C. A. Angell, K. L. Ngai, G. B. McKenna, P. F. McMillan S. W. Martin J. Appl. Phys. **88** 3113 (2000)
74. K. Binder, A. P. Young, Rev. Mod. Phys. **58**, 801 (1986)
75. K.-P. Bohn, J. K. Krüger, in "Structure and Properties of Glassy Polymers", ACS Symposium Series 710, ed. by M. R. Tant and A. J. Hill (1998)
76. M. H. Cohen, D. Turnbull, J. Chem. Phys. **31**, 1164 (1959)
77. M. H. Cohen, D. Turnbull, J. Chem. Phys. **34**, 120 (1961)
78. P. G. Debenedetti, "Metastable liquids – concepts and principles", Princeton University Press (1996)
79. E. Donth, Relaxation and Thermodynamics in Polymers, Glass transition, Akademie-Verlag, Berlin 1992
80. S. R. Elliott, "Physics of Amorphous Materials", Longman (1990)
81. Fischer, Hertz "Spin glasses" Cambridge University Press 1991
82. W. Götze, in "Liquids, Freezing and Glass Transition", edited by J. P. Hansen, D. Levesque and J. Zinn-Justin, Elsevier, Amsterdam, 1989
83. W. Götze, L. Sjögren, Rep. Prog. Phys., **55**, 241–376 (1992)
84. B. A. Auld, "Acoustic Fields and Waves in Solids", John Wiley (1973)
85. J. Jäckle, Models of the glass transition. Rep. Prog. Phys., **49**, 171 (1986)
86. A. J. Kovacs, Journal of Polymer Science **30**, 131 (1958)
87. J. K. Krüger, C. Grammes, J. H. Wendorff, in Dynamics of Disordered Materials, Eds. D. Richter et al., Springer Proceedings in Physics **37**, 216 (1989)
88. H. Baur, "Thermophysics of Polymers, I: Theory", Springer Verlag (1999)
89. K.-P. Frühauf, J. Helwig, H. E. Müser, J. K. Krüger, R. Roberts, Colloid & Polymer Science **266**, 814 (1988)
90. R. Zwanzig, R. D. Mountain, J. Chem. Phys. **43**, 4464 (1965)
91. J. K. Krüger, J. Baller, A. le Coutre, R. Peter, R. Bactavatchalou, J. Schreiber, Physical Review B, **66**, 012206-1/4 (2002)
92. J. F. Nye, "Physical Properties of Crystals", Oxford Press (1972)
93. M. Born, K. Huang, "Dynamical theory of crystal lattices", Clarendon Press, Oxford (1968)
94. G. Grimvall, "Thermophysical properties of materials in Selected topics in solid state physics", Vol. XVIII, ed. by E. P. Wohlfarth, North Holland (1986)
95. J. P. Boon, S. Yip, in "Molecular Hydrodynamics" Mc Graw Hill (1980)
96. J. K. Krüger, J. Baller, A. le Coutre, Th. Britz, R. Peter, R. Bactavatchalou, J. Schreiber, Phys. Rev. B **66**, 12206 (2001)
97. J. K. Krüger, Th. Britz, J. Baller, W. Possart, H. Neurohr, Phys. Rev. Letter **89**, 285701 (2002)
98. S. Brawer, Relaxation in Viscous Liquids and Glasses, American Ceramic Society, (1985)
99. M. D. Ediger, Annu. Rev. Phys. Chem. **51**, 99–128 (1999)
100. A. K. Doolittle, J. Appl. Phys., **22**, 1471 (1951)
101. J. Wong, C. A. Angel, "Glass" Marcel Dekker (1976)
102. W. Williams, D. C. Watts, Trans. Farad. Soc., **66**, 80 (1970)
103. E. Donth, Relaxation and Thermodynamics in Polymers, Glass transition, Akademie-Verlag, Berlin 1992
104. P. G. Debenedetti, "Metastable liquids – concepts and principles", Princeton University Press (1996)

105. W. Götze, in Liquids, Freezing and Glass Transition, edited by J. P. Hansen, D. Levesque and J. Zinn-Justin (Amsterdam)
106. W. Götze, L. Sjögren, Rep. Prog. Phys., **55**, 241–376 (1992)
107. G. S. Fulcher, J. Am. Chem. Soc. **8**, 339, 789 (1925)
108. W. Cochran, "The Dynamics of Atoms in Crystals" in the Structures and Properties of Solids 3, Arnold (1973)
109. J. J. Alkonis, A. J. Kovacs, in "Contemporary Topics in Sciences", Ed. M. Shen, Plenum Press, **3**, 257 (1979)
110. G. Rehage, J. Macromol Sci., Phys., **818**, 423 (1980)
111. F. R. Schwarzl, F. Zahradnik, Rheol. Acta, **19**, 137 (1980)
112. C. A. Angell, "Strong and Fragile Liquids", in "Relaxations in Complex Systems", K. Ngai, G. B. Wright eds., Springfield, VA (1985)
113. C. A. Angell, "Perspectives on the Glass Transition", J. Phys. Chem. Sol. **102**, 205 (1988)
114. The Journal of Chemical Physics, **118**, 1593–1595 (2003)
115. T. Geszti, J. Phys. C. Sol. State. Phys., **16**, 5805 (1983)
116. J. K. Krüger, in "Optical Techniques to Characterize Polymer Systems", edited by H. Bässler, Elsevier (1989)
117. K.-P. Bohn, J. K. Krüger, in "Structure and Properties of Glassy Polymers", ACS Symposium Series 710, ed. by M. R. Tant and A. J. Hill (1998)
118. M. H. Cohen, D. Turnbull, J. Chem. Phys. **31**, 1164 (1959)
119. M. H. Cohen, D. Turnbull, J. Chem. Phys. **34**, 120 (1961)
120. G. M. Bartenev, J. V: Zelenev, "Physik der Polymere", VEB Verlag für Grundstoffindustrie, Leipzig (1979)
121. J. K. Krüger, R. Roberts, H.-G. Unruh, K.-P. Frühauf, J. Helwig, H. Müser Progr. in Coll. & Polym. Sci. **71**, 77 (1985)
122. J. K. Krüger, J. Baller, A. le Coutre, R. Peter, R. Bactavatchalou, J. Schreiber, Physical Review B, **66**, 012206–1/4 (2002)
123. J. K. Krüger, T. Britz, J. Baller, W. Possart, H. Neurohr; Phys. Rev. Letter, **89**(28), 285701 (2002)
124. J. K. Krüger, K.-P. Bohn, R. Jimenez; Condensed Matter News **5**, 10 (1996)
125. J. K. Krüger, K.-P. Bohn, M. Pietralla, J. Schreiber; J. Phys.: Condensed Matter **8**, 10863 (1996)
126. J. K. Krüger, K.-P. Bohn, J. Schreiber; Phys. Rev. **B 54**, 15767 (1996)
127. J. K. Krüger, K.-P. Bohn, R. Jimenez, J. Schreiber; Coll. Polym. Sci. **274**, 490 (1996)
128. K.-P. Bohn, J. K. Krüger; American Chem. Soc., Washington, DC, Developed from a symposium sponsored by the Division of Polymeric Materials: Science and Engineering at the 213th National Meeting of the American Chemical Society, San Francisco, California, April 13–17 (1997)
129. J. K. Krüger, K.-P. Bohn, M. Matsukawa; Phase Transitions **65**, 279–289 (1998)
130. J. K. Krüger, T. Britz, A. le Coutre, J. Baller, W. Possart, P. Alnot, R. Sanctuary, New Journ. Phys, **5**, 80.1–80.11 (2003)
131. G. Rehage, J. Macromol Sci., Phys., **818**, 423 (1980)
132. F. R. Schwarzl, F. Zahradnik, Rheol. Acta, **19**, 137 (1980)
133. W. Hayes, R. Loudon, "Scattering of Light By Crystals", John Wiley (1978)
134. B. Chu, "Laser Light Scattering", Academic Press (1974)
135. B. J. Berne, R. Pecora, "Dynamical Light Scattering", John Wiley (1975)

136. J. K. Krüger, A. Marx, L. Peetz, R. Roberts, H.-G. Unruh, Colloid & Polymer Sci., **264**, 403–414 (1986)
137. J. K. Krüger, in "Optical Techniques to Characterize Polymer Systems", edited by H. Bässler, Elsevier (1989)
138. J. K. Krüger, J. Embs, J. Brierley, R. Jimenez; J. Phys. D – Appl. Phys. **31**, 1913 (1998)
139. H. Baur, "Thermophysics of Polymers, I: Theory", Springer Verlag (1999)
140. A. J. Kovacs, in "Structure and Mobility in Molecular and Atomic Glasses", Ed. By J. M. O'Reilly and M. Goldstein, Ann. N. Y. Acad. Sci. **371**, 38 (1981)
141. A. J. Kovacs, Fortschr. Hochpolym. Forschung, **3**, 394 (1963)
142. K.-P. Frühauf, J. Helwig, H. E. Müser, J. K. Krüger, R. Roberts, Colloid & Polymer Science **266**, 814 (1988)
143. H. Seliger, M. B. Bitar, H. Nguyen-Trong, A. Marx, R. Roberts, J. K. Krüger, H.-G. Unruh; Macromol. Chem. **185**, 1335–1360 (1984)
144. J. K. Krüger, A. Marx, R. Roberts, H.-G. Unruh, M. B. Bitar, H. Nguyen-Trong, H. Seliger; Maromol. Chem. **185**, 1469–1491 (1984)
145. J. K. Krüger, Th. Britz, J. Baller, W. Possart, H. Neurohr, Phys. Rev. Letter **89**, 285701 (2002)
146. M. Matsukawa, N. Ohtori, I. Nagai, K.-P. Bohn, J. K. Krüger, Jap. J. Appl. Phys. **36**, 2976 (1997)
147. J. K. Krüger, K.-P. Bohn, M. Matsukawa, Phase Transitions **65**, 279–289 (1998)
148. J. K. Krüger, M. Veith, R. Elsäßer, W. Manglkammer, A. le Coutre, J. Baller, M. Henkel, Ferroelectrics, **259**, 27–36 (2001)
149. Frenkel, "Kinetic Theory of Liquids", Dover Publications, New York, 1955
150. R. Holtwick, "Niedermolekulare Flüssigkeiten in nano-porigen Trägermaterialien – zur Natur des Glasübergangs", Dissertation Universität des Saarlandes, Saarbrücken (1998)
151. K. Knorr, A. Loidl, Phys. Rev. B **31**, 5387 (1985)
152. J. Hessinger, K. Knorr, Phys. Rev. Letter, **63**, 2749 (1989)
153. R. Böhmer, A. Loidl, Phys. Rev. B **42**, 1439–1443 (1990)
154. J. K. Krüger, R. Jiménez, K.-P. Bohn, J. Petersson, J. Albers, K. Klöpperpieper, E. Sauerland, H. E. Müser, Phys. Rev. B Cond. Matter, **42**, 8537 (1990)
155. R. Jiménez, B. Jiménez, J. K. Krüger, J. Schreiber, F. Sayetat, F. Mauvy, Ferroelectrics **157**, 141 (1994)
156. E. M. Brody, C. J. Lubell, CH. L. Beatty, J. Pol. Sci., Pol. Phys. Ed., **13**, 295 (1975)
157. E. Grüneisen, Ann. d. Physik, **26**, 211 and 393 (1908)
158. W. Ludwig, "*Festkörperphysik*", Akademische Verlagsgesellschaft (1978)
159. G. Leibfried, W. Ludwig, Solid State Physics, 12 (1961)
160. T. H. K. Barron, J. G. Collins, G. K. White, Adv. Phys. **29**, 609 (1980)
161. K. Brugger, T. C. Fritz, Phys. Rev. **157**, 524 (1967)
162. M. H. Cohen, D. Turnbull, J. Chem. Phys. **31**, 1164 (1959)
163. J. J. Prejean, in "*Dynamics of Disordered Materials*", Ed. by D. Richter, A. J. Dianoux, W. Petry and J. Teixeira, Proceedings in Physics **37**, 242, Springer (1989)
164. J. K. Krüger, R. Roberts, H.-G. Unruh, K.-P. Frühauf, J. Helwig, H. E. Müser, Progress in Colloid & Polymer Science **71**, 77 (1985)

165. J. K. Krüger, in "*Optical Techniques to Characterize Polymer Systems*", Ed. by H. Bässler, Elsevier, Amsterdam, Oxford, New York 1989
166. G. Grimvall, "*Thermophysical Properties of Materials*" North-Holland (1986)
167. Frenkel, "Kinetic Theory of Liquids", Dover Publications, New York, 1955
168. H. A. Lorentz, Wied. Ann. Phys., **9**, 641 (1880)
169. L. V. Lorenz, Wied. Ann. Phys., **11**, 70 (1880)
170. J. K. Krüger, K. P. Bohn, R. Jimenez, Condensed Matter News **5**, 10 (1996)
171. J. K. Krüger, K. P. Bohn, R. Jimenez, J. Schreiber, Colloid & Polymer Science **274**, 490 (1996)
172. M. P. Stevens, "Polymer Chemistry an Introduction", Addison-Wesley Publishing Company (1975)
173. M. H. Cohen, D. Turnbull, J. Chem. Phys. **34**, 120 (1961)
174. J. R. Rabek, "Experimental Methods in Polymer Chemistry", John Wiley (1980)
175. B. Wunderlich, "Macromolecular Physics", Vol. **1**–**3**, Academic Press (1973)
176. R. Zwanzig, R. D. Mountain J. Chem. Phys **43**, 4464 (1965)
177. J. K. Krüger, J. Baller, A. le Coutre, R. Peter, R. Bactavatchalou, J. Schreiber, Physical Review B, **66**, 012206–1/4 (2002)
178. J. K. Krüger, T. Britz, A. le Coutre, J. Baller, W. Possart, P. Alnot, R. Sanctuary, New Journ. Phys, **5**, 80.1–80.11 (2003)
179. C. Vergnat, M. Philipp, Diplomarbeiten, Saarbrücken, 2006, to be published
180. C. Truesdell, "Mechanics of Solids", Vol. IV, Waves in Elastic and Viscoelastic Solids" Springer Verlag (1974)